Two strategies to maintain the intestinal homeostasis: anion-exchange resin to avoid antibiotic-induced dysbiosis and mannan-coated antigen nanoparticles for allergy treatment

李, 順怡

Two strategies to maintain the intestinal homeostasis: anion-exchange resin to avoid antibiotic-induced dysbiosis and mannan-coated antigen nanoparticles for allergy treatment

Shunyi Li

Graduate School of Systems Life Sciences

Kyushu University

2023

Abstract

Two strategies to maintain the intestinal homeostasis: anion-exchange resin to avoid antibiotic-induced dysbiosis and mannan-coated antigen nanoparticles for allergy treatment

Shunyi Li

Doctor of Engineering

Graduate School of Systems Life Sciences

Kyushu University

2023

In the intestine, there is the largest lymphoid tissue in the body. At every moment, immune cells are influenced by the commensal microbiota. These immune cells play a key role in maintaining immune homeostasis by inhibiting the response to antigens from commensal bacteria as well as food. At the same time, gut commensal bacteria also modulate the immune system through metabolites. Imbalance of the gut microbiota, termed dysbiosis, can trigger some immune diseases such as allergy by affecting the activities of immune cells near or far from the site of dysbiosis. One risk factor to induce dysbiosis is administration of antibiotics. To prevent dysbiosis, it need to administrate antibiotics without destroying gut microbiota. To treat the allergy which has developed, allergen immunotherapy (AIT) is used to induce antigen-specific immune tolerance. Nanoparticles (NPs) such as emulsions and liposomes have been used into pre-clinical

allergy treatment in recent years, but preparation method of these NPs are complicated. In this thesis, I prevented antibiotic-induced dysbiosis by an anion-exchange resin (AER), and developed two NPs to treat allergy.

In Chapter 2, I used an AER for adsorbing the β-lactam antibiotic cefoperazone (CEF). The AER was used to adsorb CEF through electrostatic and π-π interactions. The AER was specific for CEF over biological molecules in the intestine and protected *Escherichia coli* from CEF *in vitro*. Furthermore, oral administration of the AER reduced the fecal free CEF concentration, and protected the gut microbiota from CEF-induced dysbiosis.

In Chapter 3, I developed a simple approach for preparing disulfide bond crosslinked mannoprotein (MAN)-ovalbumin (OVA) NPs (MDO), in order to induce OVA-specific immune tolerance via dendritic cells (DCs). DCs play a crucial role in the antigen-specific immunotherapy which could induce regulatory T (T_{reg}) cells to maintain tolerance. Mannan on the surface of MDO enhance uptake efficiency of DCs and antigen presentation efficiency of MDO on DCs was high. MDO showed low reactivity with anti-OVA antibodies and did not induce anaphylaxis in allergic mice, which demonstrated high safety of MDO. In mouse allergic asthma model, MDO showed great prevention effect and therapeutic effect through both oral and subcutaneous administration. Thus, based on the therapeutic efficiency and safety of MDO, I believe that MDO could act as a new approach for allergy treatment.

In Chapter 4, I followed the strategy in Chapter 3 which used disulfide bond to crosslink MAN and protein for DC targeting. In this chapter, I used human serum albumin (HSA) as matrix to prepare MAN-coated NP to delivery antigens and drugs which is suitable for precious antigen delivery. HSA-based matrix could delivery antigens which have similar denaturation temperature with HSA and low tendency of self-aggregation. I demonstrated that MAN-coated HSA-OVA NP (MHO) could target DCs, enhanced uptake efficiency, antigen presentation efficiency and inhibited activation of DCs. Thus, antigen-HSA NPs are possible to treat allergy effectively and

safety.

The new approaches in this thesis may provide a fresh perspective into the development of more straightforward methods to utilize the materials to maintain immune homeostasis via the intestine. These approaches maybe more effective, safer and lower cost to treat several diseases.

Contents

Abbreviation

AC	Activated charcoal
AER	Anion exchange resin
AIT	Allergen immunotherapy
APC	Antigen-presenting cell
BAL	Bronchoalveolar lavage
CDI	*Clostridioides difficile* infection
CEF	Cefoperazone
CFU	Colony form units
CLR	C-type lectin receptor
Cry j	Japanese cedar pollen antigen
CX_3CR1^+	CX_3C-chemokine receptor 1^+
DC	Dendritic cell
DC-SIGN	Dendritic cell-specific intercellular adhesion molecule 3-grabbing non-integrin
ELISA	Enzyme-linked immunosorbent assay
FcR	Fragment crystallizable region receptor
FLT-3L	FMS-like tyrosine kinase 3 ligand
GM-CSF	Granulocyte–macrophage colony-stimulating factor
HO	Disulfide bond crosslinked human serum albumin-ovalbumin nanoparticle
HPLC	High performance liquid chromatography
HSA	Human serum albumin
IER	Ion exchange resin
IgA	Immunoglobulin A
IgE	Immunoglobulin E
IgG	Immunoglobulin G

IL-4	Interleukin-4
IL-5	Interleukin-5
IL-6	Interleukin-6
IL-10	Interleukin-10
IL-13	Interleukin-13
ITAM	Immunoreceptor tyrosine-based activation motif
ITIM	Immunoreceptor tyrosine-based inhibitory motif
LPS	Lipopolysaccharide
M cell	Microfold cells
MAN	Mannoprotein
MDO	Disulfide bond crosslinked mannoprotein-ovalbumin nanoparticle
MFI	Mean fluorescence intensity
MGO	Glutaraldehyde crosslinked mannoprotein-ovalbumin nanoparticle
MHC	Major histocompatibility complex
MHO	Disulfide bond crosslinked mannoprotein-human serum albumin-ovalbumin nanoparticle
MIC	Minimum inhibitory concentration
MR	Mannose receptor
NF-κB	Nuclear factor kappa-light-chain-enhancer of activated B cells
NP	Nanoparticle
OIT	Oral immunotherapy
OVA	Ovalbumin
PDI	Polydispersity indexes
PD-L1	Programmed death ligand 1
PLGA	Poly(lactic-co-glycolic acid)
RA	Retinoic acid
SC	Sodium cholate
SCDC	Sodium chenodeoxycholate
SCFAs	Short-chain fatty acids
SCIT	Subcutaneous allergen immunotherapy

SDS-PAGE	Sodium dodecyl sulfate–polyacrylamide gel electrophoresis
SLIT	Sublingual allergen immunotherapy
TCR	T cell receptor
T_{FH}	Follicular T helper
TGF-β	Transforming growth factor-β
T_H1	T helper 1
T_H2	T helper 2
T_{reg}	Regulatory T
VB_1	Vitamin B1
VK_1	Vitamin K1

CHAPTER 1 Introduction

The intestine has 200 m^2 of mucosal area and the largest lymphoid tissue in the body, the intestine is constantly exposed to a variety of antigens and stimuli from dietary components and gut commensal microbiota (Fig. 1.1). The long-term coexistence of host and commensal microbiota has allowed the host to evolve the ability to sense and coordinate microbiota and their metabolic signals to maintain immune homeostasis. Dynamic communication between the host and gut microbiota is important to maintain homeostasis. Gut microbiota is involved in the maturation of host immune tissues and regulation of immune responses through microbial surface antigens and metabolites. When the original homeostasis is disturbed, dysbiosis and allergy may occur. In turn, the altered gut microbiota affects the physiological and pathological processes of the host.

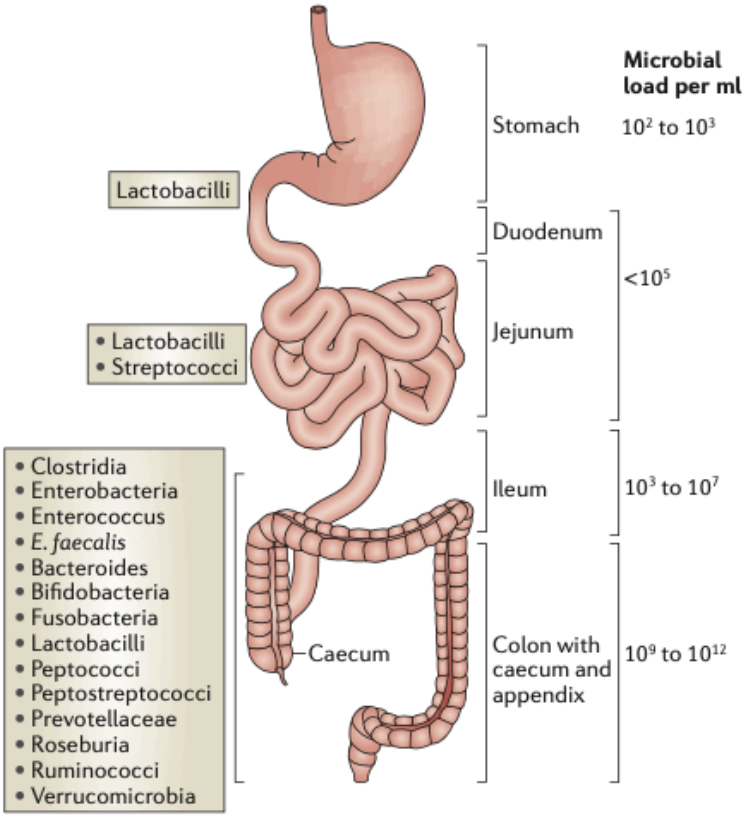

Fig. 1.1 Microbes distribution in the gastrointestinal tract. The intestine is the major source of commensal microbes containing 10^{14} microorganisms of more than 500 different species. The numbers of bacteria generally increase going down the gastrointestinal tract, ranging from 10^2-10^3 per ml in the stomach to ~10^5 per ml in the upper small intestine and up to 10^{12} per ml in the colon.[1]

1.1 Intestinal homeostasis

It is estimated that the intestine contains more than 500 species of microbes and their number reaches 10^{14} (Fig. 1.1).[1] Although some microbes cause disease, many of them provide the host with important metabolites, such as vitamin B family, vitamin K1 (VK_1)[2] and short-chain fatty acids (SCFAs),[3] provide with protection from pathogenic microbes[4, 5] and are also involved in the development and maturation of the intestinal immune system.[6] In a healthy state, the immune system maintains tolerance to beneficial commensal microbes. To do this, it relies on a wide variety of cells and networks that establish for communication, involving transmission of antigens from the intestinal lumen to antigen-presenting cells (APCs), antigen presentation and regulation of T cell response.

Several intestinal epithelial cells are involved in antigen transmission from lumen to lamina propria (Fig 1.2). Microfold cells (M cells) are highly specialized epithelial cells for transferring antigens.[7] M cells and goblet cells carry antigens across the barrier by transcytosis and delivered to CD 103^+ dendritic cells (DCs). Some intestinal epithelial cells that express receptors for immunoglobulin A (IgA) carry IgA-antigen complexes into the lamina propria. Finally, CX_3C-chemokine receptor 1^+ (CX_3CR1^+) cells can extend a process between epithelial cells and capture antigens directly from the lumen.[8, 9] CX_3CR1^+ cells also can transfer antigens to CD 103^+ DCs.[10]

CD 103^+ DCs after receiving antigens migrate to draining lymph nodes, produce transforming growth factor-β (TGF-β) and retinoic acid (RA), and interact with naïve

T to promote regulatory T cell (T_{reg}) differentiation.[10] T_{reg} cells can promote IgA-producing B-cell through a T cell-dependent pathway. CX_3CR1^+ cells produce interleukin-10 (IL-10), an anti-inflammatory cytokine, to maintain T_{reg} cell proliferation after capturing antigens (Fig 1.2).[11]

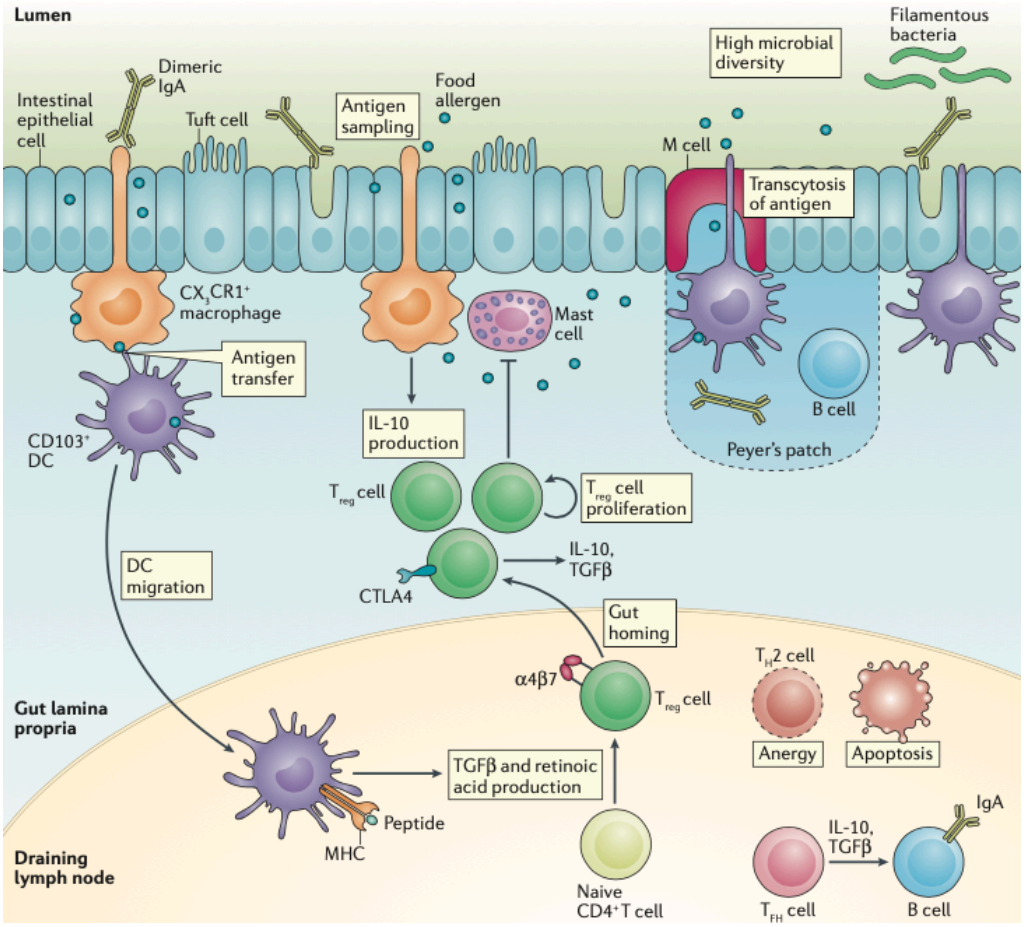

Fig. 1.2 Immune homeostasis in the intestine. Antigen delivery from lumen to APCs. (a) CX_3CR1^+ cells extend process to the gut lumen and take up antigen; (b) Antibody-antigen complexes can be transport by fragment crystallizable region receptors (FcRs); (c) DCs take up antigens via M cell-mediated transcytosis; (d) DCs extend transcellular processes through M cell pores and take up antigens. $CD103^+$ DCs migrate to lymph nodes and stimulate naïve T cells to become T_{reg} cells through expression of TGF-β and RA. T_{reg} cells home to the lamina propria and proliferate in the IL-10 environment. Follicular T helper (T_{FH}) cells provide TGF-β and IL-10 to develop IgA secreting plasma cells.[12]

1.2 Gut microbiota and health

Human commensal bacteria colonize in the gastrointestinal tract, the oral cavity, the respiratory tract, the urogenital tract, and on the skin. Especially, the number of intestinal microorganisms more than 100 trillion and the collection of microbiome is one order magnitude larger than the human genome.[13] Observational findings suggest that the gut microbiota contribute to human health, including contribute to the development of immune system, ferment foods that we cannot digest, provide nutrients, maintain integrity of the intestinal barrier, protect against enteric pathogens and regulate neurological signaling.[14]

1.2.1 Dysbiosis induced by antibiotics

Homeostasis of the gut microbiota is modulated by several factors that continues throughout the life of host. Composition of diet, exercise and living habit can cause important changes of the gut microbiota. In addition, antibiotics also affect composition of gut microbiota.[15] When the balance of the gut microbiota is disrupted and altered homeostasis, it is called dysbiosis. Dysbiosis is often associated with inflammatory bowel disease, but also linked to extraintestinal immune-mediated diseases, including diabetes, autoimmune diseases, and allergies (Fig. 1.3).[16-18]

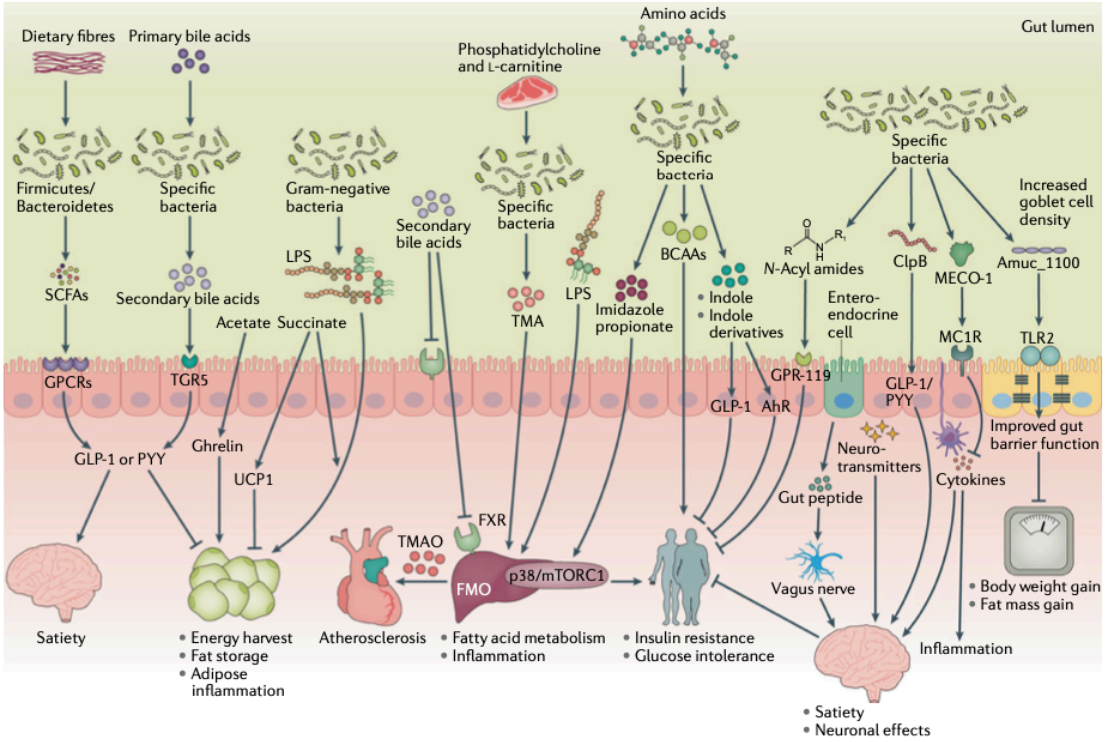

Fig. 1.3 Microbiome-modulated metabolites and disease. Altered levels of microbiome-modulated metabolites have been associated with immune-mediated and immune-associated disease risk. Metabolite-mediated effects on disease processes may be localized to the gastrointestinal tract, such as in IBD or food allergy, or systemically influence remote tissues like the brain, heart and the liver.[19, 20] Copyright © 2020, Springer Nature Limited.

From 1950s, penicillin could be produced on a large scale, and in the next two decades, most of the antibiotic classes we used as medicines today were discovered and introduced to the market. Antibiotics are screened for any negative effects before their approval for clinical use, and are usually considered safe and well tolerated. However, extensive side effects range from mild to severe are induced by some antibiotics, and it is depending on that type of antibiotics, target spectrum of microbiota and individual patients.[21] Side effects include fever, nausea, allergic reaction and diarrhea. Diarrhea is a common side effect of antibiotics, that is caused by dysbiosis.

Usually, antibiotics are administrated orally or intravenously. Part of orally administered antibiotics are absorbed in the small intestine, travel to blood vessels, and are transported to the site where the target pathogenic bacteria are present and kill them.

However, some antibiotics that are not absorbed will reach to the large intestine. Intravenously administered antibiotics also has a part reach to the large intestine by bile excretion. In these ways, when the antibiotics reach to the large intestine, it suppresses the growth of a part of the gut microbiota existing in the large intestine and causes dysbiosis. Furthermore, these changes are not reversed for several months after stopping administration.[22] Clindamycin and cefoperazone (CEF) are known to be the risk factor to induce infection of pathogenic bacteria *Clostridium difficile*.[23] In order to administrate antibiotics without destroying gut microbiota, new strategies are required.

1.2.2 Current approaches to protect gut microbiota from antibiotics

From 2016, Kaleko et al. reported a series of β-lactamases containing pellets to protect gut microbiota from β-lactam antibiotics-mediated dysbiosos.[24-26] β-lactamase is an enzyme that degrades β-lactam family antibiotics. In this method of administration, β-lactamase was orally administered before and after intravenous administration of the antibiotic by incorporation into Eudragit-coated sucrose pellets and delivered to the large intestine. Thereby, even if some antibiotics reach the large intestine, β-lactamase present in the large intestine can degrades the antibiotics, so that the gut flora can be protected. This method can protect the gut microbiota with a small amount of β-lactamases because of high specificity to β-lactam family antibiotics. Now, this product are in phase 2 clinical trials.[27] However, it was pointed out that this method require frequently administration because β-lactamases is administered orally, a part of them degraded by digestive enzymes.

In 2018, Gunzburg et al. reported on the protection of gut microbiota from antibiotics using activated charcoal (AC) (Fig. 1.4).[28, 29] AC has the property of adsorbing hydrophobic substances, and has been used as a adsorbent for overdose of alcohol and some hydrophobic drugs, like cyanide. In their researches, AC which has specific coating was orally administered before and after oral administration of

antibiotics. AC is delivered to large intestine as adsorbent and protects the gut microbiota by capturing antibiotics in the large intestine. Finally, AC and antibiotics are excreted in feces. This product is in phase 2 clinical trial.[30] However, the adsorption by AC is nonspecific, which will absorb essential biological molecules such as vitamins.

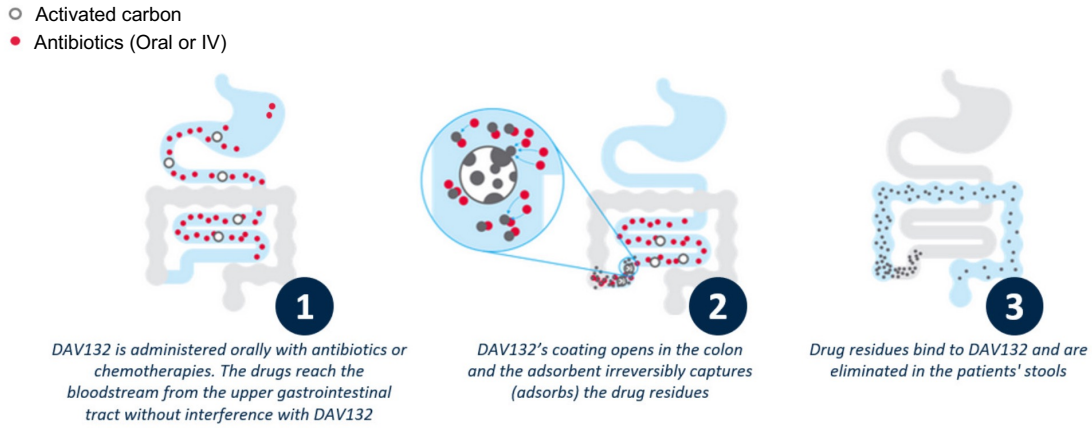

Fig. 1.4 AC is encapsulated in a specific drug delivery system patented by Da Volterra that permits its targeted delivery in the lower gastrointestinal tract.[31]

1.3 Allergy and antigen-specific immunotherapy

Worldwide, the rise in prevalence of allergic diseases has continued in developed countries for more than 50 years (Fig. 1.5), in which the types of allergic diseases can range from localized allergies like dermatitis, food allergy, allergic rhinitis and allergic asthma, to systemic anaphylaxis.

Asthma affected an estimated 262 million people in 2019 and caused 455 thousand deaths.[32] Within them, about 60 % people are allergic asthma.[33] Allergic rhinitis is estimated to affect quarter of the population in western countries.[34] Allergic rhinitis is triggered by antigen such as pollen, dust and mite. Including direct and indirect economic costs, approximately $4.2 million was costed in the United States in 2010.[35] Quality of life was impaired by these disorders to a certain extent.

Environment factors, such as air pollution, animals, bacteria and diet, and genetics affect to allergies.[36, 37] Moreover, microbial exposure during the pregnancy period and

early stage of life influence allergy development by balancing the activities of T helper 1 (T_H1) and T helper 2 (T_H2) cells.[37, 38]

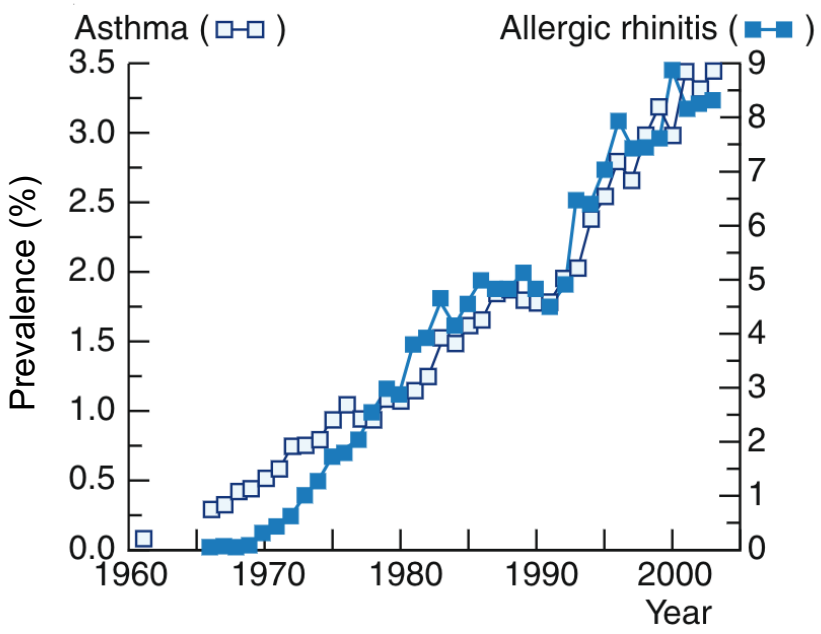

Fig. 1.5 Increasing trends in the prevalence of asthma and allergic rhinitis.[39] Copyright © 2013 The Author(s). Published by Elsevier Inc.

1.3.1 Mechanism of allergy

When antigen crosses the barrier and is presented to naïve T cells by APCs, it promotes T cell differentiation into T_H2 cells, which stimulate B cell proliferation and undergo class switching to IgE by secreting interleukin-4 (IL-4), interleukin-5 (IL-5) and interleukin-13 (IL-13). Secreted IgE circulates in the blood and binds to IgE-specific Fc receptors (FcεRI) on the surface of mast cells and basophils. A second exposure to the antigen leads to the cross-linking of the IgE, triggering the release of inflammatory mediators, including histamine, proteases, leukotrienes. These inflammatory mediators can lead to vasodilation, increased capillary permeability, mucus hypersecretion, smooth muscle contraction, and infiltration of eosinophils, basophils and mast cells in the tissues.

Mast cells and basophils express high levels of the FcεRI which binds to IgE with high affinity. The intracellular part of FcεRI contain immunoreceptor tyrosine-based activation motifs (ITAMs), which are phosphorylated after cross-linking of IgE and FcεRI through antigens. FcεRI signaling regulates degranulation, synthesis of inflammation cytokines and leukotrienes and prostaglandins (Fig. 1.6).

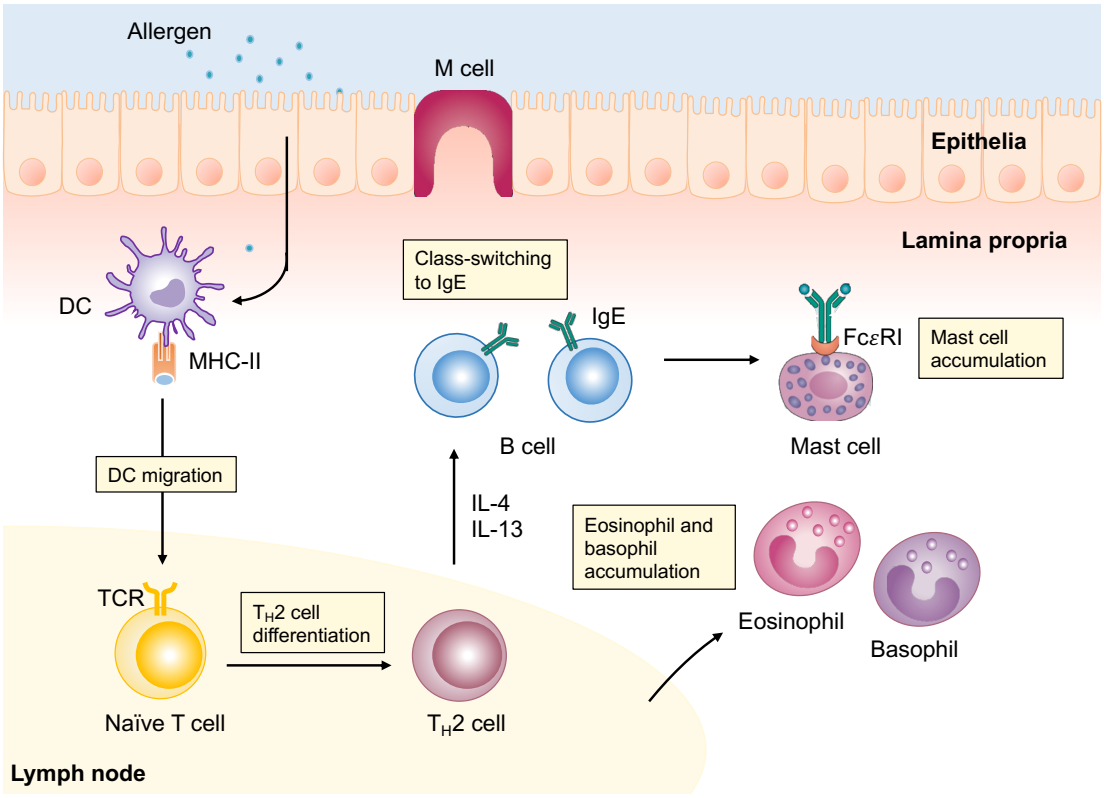

Fig. 1.6 T_H2 cell-mediated allergic response. During the initial sensitization, antigen exposure at the mucosal surface results in activation of epithelial cells, which then activate DCs. DCs take up and present antigens to naive T cells to induce T_H2 cells. Subsequent antigen re-exposure leads to T_H2 cell-mediated immune response promotes accumulation of eosinophils and basophils, production of IgE and degranulation of mast cell and basophil.

1.3.2 Traditional antigen immunotherapy

For many years, patients were desensitized by exposing them to repeated and gradually increasing doses of naked antigens, which termed allergen immunotherapy (AIT). AIT has the potential to reduce allergic response caused by environmental antigens in a long-term and induce tolerance towards antigens, and it is the only available potentially curative treatment.[40] Two major AIT are subcutaneous allergen immunotherapy (SCIT) and sublingual allergen immunotherapy (SLIT) (Table 1.1). SCIT is a classic AIT which injects antigens or crude extracts to patients.[41] SCIT needs to be administered by a physician because even with a low dose of antigens, some patients still occur anaphylaxis.[42] Recently, SLIT of antigen tablet is more studied.[43] A tablet containing the naked antigen is held under the patient's tongue and slowly released antigen is endocytosed by APCs near the oral mucosa, then producing a therapeutic effect. SLIT is simple and convenient, and the risk of severe side effects is lower than that of SCIT.[44] However, some mild to moderate swelling events usually occurred.[45] SCIT and SLIT usually takes more than 2-3 years, even after the treatment was completed, there were still some patients whose allergy symptoms have not been mitigated.[43] Among the potential routes for AIT, oral immunotherapy (OIT) is particularly interested as greater patient compliance, non-invasive and convenient to treat which compared with SCIT and SLIT (Table 1.1). Most OIT are used in the treatment of food allergies, but there are also studies using OIT for the treatment of pollen allergy.[46, 47] OIT requires larger amount of antigen doses compared with other treatment routes because of digestion in the gastrointestinal tract. OIT more likely to be desensitized due to the largest lymphoid tissues in the intestine.[48, 49] But OIT also could induce mild or moderate side effects during treatment.

Table 1.1 Clinical efficiency of AIT

	SCIT	SLIT	OIT
Convenience	+	++	++
Size of lymphoid tissue	+	+	+++
Treatment time	~ 3 years[43]	~ 3 years[43]	Several months to 2 years[50, 51]
Efficiency	+	++[40]	++
Dosage	+	++[44]	+++
Side effect	++[42]	+[44, 45]	+[48]

AIT shifts the T cell response away from T_H2-dominant immune response, and proportion of T_{reg} increased, where T_{reg} cells produce TGF-β and IL-10, both of which downregulate the T_H2 response and inhibit the activation of mast cells, eosinophils and basophils, reducing the inflammatory response (Fig. 1.7). IFN-γ (produced by T_H1 cells), TGF-β and IL-10 induce heavy-chain class switching from IgE to IgG4.[52] IgG4 competes with IgE for binding antigens, while IgG4 binds to inhibitory FcγRIIB receptors on mast cells and basophils, reducing degranulation. FcγRIIB contains immunoreceptor tyrosine inhibitory motifs (ITIMs), cross-linking of FcγRIIB and IgG4 by antigens leads to inhibition of response[53]. Mast cells and basophils express both FcγRIIB and FcεRI. If an antigen binds both IgG4 and IgE, the inhibitory signal dominates downstream expression. Therefore, the higher concentration of IgG4 we have, the higher probability to inhibit allergic response.

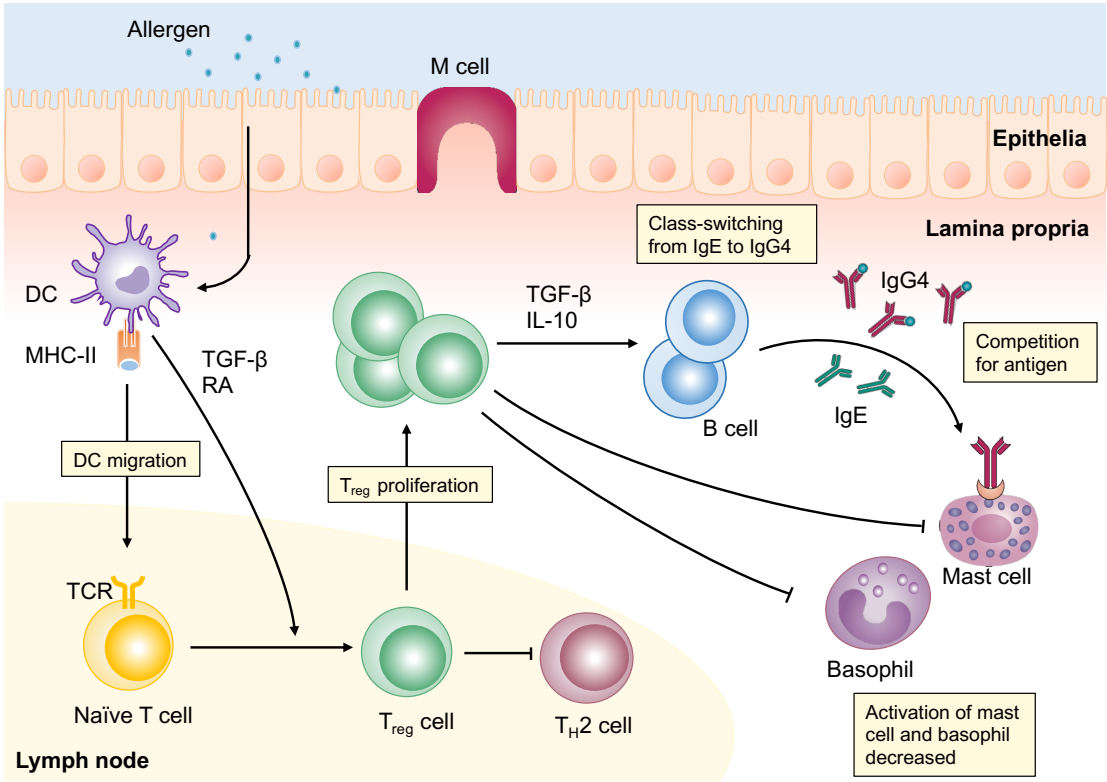

Fig. 1.7 Mechanisms of OIT. Antigen exposure to DCs, which produces TGF-β and RA and migrate to lymph node. Then inducing naïve T cells to differentiate in to T_{reg} cells and inhibit activation of T_H2 cells. TGF-β and IL-10 produced by T_{reg} cells promotes class-switching from IgE to IgG4 which blocking activities of mast cell and basophils.

1.3.3 Nanoparticle-based antigen immunotherapy

A variety of nanoparticle (NP) platforms have been developed for drug delivery. NPs have several advantages, including biodegradation, controllable particle sizes, adjustable ligands modification and drug loading. NPs protect cargos from rapid clearance and target tissue leading to reductions in the systemic therapeutic dose and side effects. A specific application of NPs involving the systemic and local administration to induce immune tolerance for allergy treatment (Fig. 1.8). NPs are used to load antigens and immunosuppressants and deliver them to DCs, which are the critical cells in the first step of immune response for modulation of antigen presentation

and regulation of immune functions. Maldonado et al. used poly(lactic-co-glycolic acid) (PLGA) NPs to co-deliver antigen and rapamycin and successfully induced tolerance to treat allergies.[54] Moreover, NPs can be designed to target receptors on DCs by coating some ligands, which are expected for endocytosis by DCs. Then, DCs promote differentiation of antigen-specific T_{reg} cells to induce immunotolerance for allergy treatment. Thus, NPs are expected to enhance therapeutic efficiency for allergy.

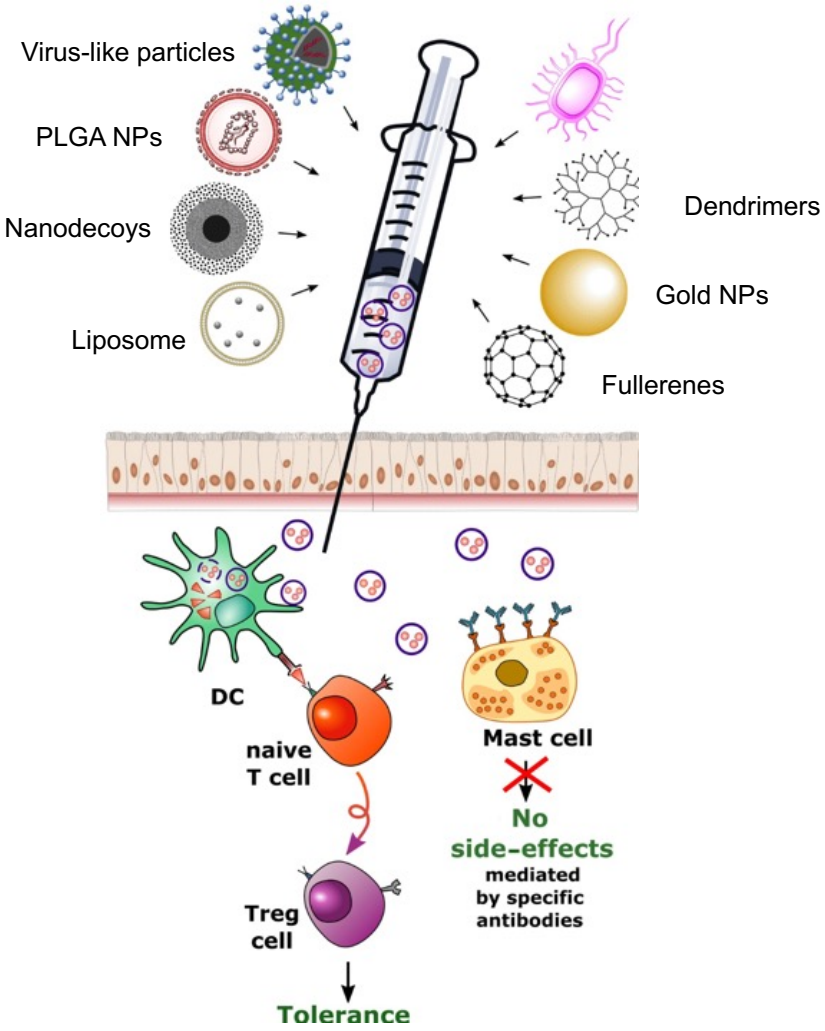

Fig. 1.8 Nanoparticle platforms for AIT. Different kinds of polymer nanoparticles-based nanotherapeutics, i.e., virus-like particles, PLGA NPs, nanodecoys, liposomes and other NPs were applied to treat allergy.[55] © 2017 EAACI and John Wiley and Sons A/S. Published by John Wiley and Sons Ltd.

1.3.4 Mannan-antigen NPs for immunotherapy

Mannoprotein (MAN) is a glycoprotein obtained from yeast. Mannan part of MAN is used as a DC-targeting ligand of mannose receptor (MR) and dendritic cell-specific intercellular adhesion molecule 3-grabbing non-integrin (DC-SIGN) to induce tolerance.[56] Mannan modified NPs such as liposomes and PLGA NPs which encapsulated antigens have been used to treat allergies. Neoglycolipids[57] or cholesterol-mannan[58] were used for mannan-liposomes preparation. The mannan-PLGA NPs were prepared by physical adsorption[59] or chemical conjugation[60]. These mannan modified NPs enhanced DCs targeting efficiency and provided the potential for antigen-specific immunotherapy. However, mannan conjugated polymers and preparation of NPs are usually complicated and difficult to reproduce.

MAN-antigen conjugates are another method for immunotherapy. Oxidized mannan part of MAN possessing aldehyde groups can be conjugated with amine groups on antigens, mannan-antigen conjugation could target DC and induce T_H1-mediated immune response to treat allergy.[61, 62] But the conjugate has following drawback. (1) Oxidization of mannan reduced efficiency for DC targeting because of the opening of mannose ring. (2) The conjugated may decrease immunogenicity probably due to the destruction of .[63] Sirvent et al. recently reported preparation of NP via crosslinking antigenic protein and protein part of MAN with glutaraldehyde to overcome the low DC targeting efficiency caused by oxidation of mannan. The NP was readily taken up by DCs through targeting MR and DC-SIGN, improving the effectiveness for treatment of allergy while also reducing antigenicity.[64, 65] Thus, MAN-antigen NPs have potential for antigen-specific immunotherapy.

1.4 Overview of this thesis

As described above, when the intestinal immune homeostasis is disrupted by antibiotics treatment, results in various diseases, such as *C. difficile* infection (CDI) and allergies. To prevent dysbiosis which induced by CEF, an adsorbent was administrated. To treat allergy, tolerogenic NPs were prepared.

In Chapter 2, an anion exchange resin (AER) was used for adsorbing CEF to protect gut microbiota. The AER adsorbed CEF through electrostatic, hydrophobic and π–π interactions. The AER showed higher affinity with CEF over biological molecules such as bile acids and vitamins. The AER protected *Escherichia coli* from CEF *in vitro*. Furthermore, pre- and post-oral administration of the AER reduced the fecal free CEF concentration, and protected the gut microbiota from CEF-induced dysbiosis.

In Chapter 3, I developed a MAN-coated ovalbumin (OVA) nanoparticle which prepared by thermal aggregation and intermolecular disulfide bonds were formed to cross link OVA and MAN (MDO). I found that MDO could target DCs and induce tolerogenic DCs, meanwhile, antigen presentation efficiency of MDO on DCs was higher than OVA and glutaraldehyde cross linked nanoparticle (MGO). In addition, MDO showed low reactivity with anti-OVA antibodies and did not induce anaphylaxis in allergic mice, which demonstrated high safety of MDO. In mouse allergic asthma model, MDO showed great prevention effect and therapeutic effect through both oral and subcutaneous administration.

In Chapter 4, a new approach for antigen-specific immunotolerance induction was developed. Different from MDO which reported in Chapter 3, I explored a human serum albumin (HSA)-based drug delivery systems that could be universally applied to a variety of antigens. I optimized preparation condition of HSA NP and investigated the effects of OVA loading and MAN modification on the formation of HSA NP. Moreover, the intermolecular disulfide bonds were demonstrated to stabilized HSA NP. I found that HSA-OVA NP (HO) and MAN-HSA-OVA NP (MHO) were more likely to be endocytosed by DCs than OVA, and peptide presentation on major histocompatibility complex (MHC) class II was also enhanced by HO and MHO. MHO

and rapamycin-loaded MHO (MHO-R) successfully induced phenotype of tolerogenic DCs. Importantly, MHO was barely reactive with anti-OVA antibodies which suggested the safety of MHO. These promising properties of MHO will suitable to the antigen-specific immunotherapy for allergy.

Hence, I have found new and direct approaches to maintain intestinal and immunological homeostasis that can hopefully lead to more efficient and convenient treatment of dysbiosis and allergies.

1.5 References

1. A. M. Mowat and W. W. Agace, *Nat Rev Immunol*, 2014, **14**, 667-685.
2. J. G. LeBlanc, C. Milani, G. S. de Giori, F. Sesma, D. van Sinderen and M. Ventura, *Curr Opin Biotechnol*, 2013, **24**, 160-168.
3. J. H. Cummings, E. W. Pomare, W. J. Branch, C. P. Naylor and G. T. Macfarlane, *Gut*, 1987, **28**, 1221-1227.
4. E. Deriu, J. Z. Liu, M. Pezeshki, R. A. Edwards, R. J. Ochoa, H. Contreras, S. J. Libby, F. C. Fang and M. Raffatellu, *Cell Host Microbe*, 2013, **14**, 26-37.
5. T. Ichinohe, I. K. Pang, Y. Kumamoto, D. R. Peaper, J. H. Ho, T. S. Murray and A. Iwasaki, *Proc Natl Acad Sci U S A*, 2011, **108**, 5354-5359.
6. Y. Belkaid and O. J. Harrison, *Immunity*, 2017, **46**, 562-576.
7. N. A. Mabbott, D. S. Donaldson, H. Ohno, I. R. Williams and A. Mahajan, *Mucosal Immunol*, 2013, **6**, 666-677.
8. M. Rescigno, M. Urbano, B. Valzasina, M. Francolini, G. Rotta, R. Bonasio, F. Granucci, J.-P. Kraehenbuhl and P. Ricciardi-Castagnoli, *Nature Immunology*, 2001, **2**, 361-367.
9. J. H. Niess, S. Brand, X. Gu, L. Landsman, S. Jung, B. A. McCormick, J. M. Vyas, M. Boes, H. L. Ploegh, J. G. Fox, D. R. Littman and H. C. Reinecker, *Science*, 2005, **307**, 254-258.
10. E. Mazzini, L. Massimiliano, G. Penna and M. Rescigno, *Immunity*, 2014, **40**, 248-261.
11. U. Hadis, B. Wahl, O. Schulz, M. Hardtke-Wolenski, A. Schippers, N. Wagner, W. Muller, T. Sparwasser, R. Forster and O. Pabst, *Immunity*, 2011, **34**, 237-246.
12. W. Yu, D. M. H. Freeland and K. C. Nadeau, *Nat Rev Immunol*, 2016, **16**, 751-765.
13. S. V. Lynch and O. Pedersen, *N Engl J Med*, 2016, **375**, 2369-2379.
14. I. Rowland, G. Gibson, A. Heinken, K. Scott, J. Swann, I. Thiele and K. Tuohy, *Eur J Nutr*, 2018, **57**, 1-24.

15. N. Hasan and H. Yang, *PeerJ*, 2019, **7**, e7502.
16. K. H. Allin, V. Tremaroli, R. Caesar, B. A. H. Jensen, M. T. F. Damgaard, M. I. Bahl, T. R. Licht, T. H. Hansen, T. Nielsen, T. M. Dantoft, A. Linneberg, T. Jorgensen, H. Vestergaard, K. Kristiansen, P. W. Franks, I.-D. consortium, T. Hansen, F. Backhed and O. Pedersen, *Diabetologia*, 2018, **61**, 810-820.
17. X. Cui, L. Ye, J. Li, L. Jin, W. Wang, S. Li, M. Bao, S. Wu, L. Li, B. Geng, X. Zhou, J. Zhang and J. Cai, *Sci Rep*, 2018, **8**, 635.
18. L. Zhu, S. S. Baker, C. Gill, W. Liu, R. Alkhouri, R. D. Baker and S. R. Gill, *Hepatology*, 2013, **57**, 601-609.
19. E. Blacher, M. Levy, E. Tatirovsky and E. Elinav, *J Immunol*, 2017, **198**, 572-580.
20. Y. Fan and O. Pedersen, *Nat Rev Microbiol*, 2021, **19**, 55-71.
21. B. P. Willing, S. L. Russell and B. B. Finlay, *Nat Rev Microbiol*, 2011, **9**, 233-243.
22. S. Becattini, Y. Taur and E. G. Pamer, *Trends Mol Med*, 2016, **22**, 458-478.
23. T. E. Asempa and D. P. Nicolau, *Clin Interv Aging*, 2017, **12**, 1799-1809.
24. M. Kaleko, J. A. Bristol, S. Hubert, T. Parsley, G. Widmer, S. Tzipori, P. Subramanian, N. Hasan, P. Koski, J. Kokai-Kun, J. Sliman, A. Jones and S. Connelly, *Anaerobe*, 2016, **41**, 58-67.
25. S. Connelly, J. A. Bristol, S. Hubert, P. Subramanian, N. A. Hasan, R. R. Colwell and M. Kaleko, *J Appl Microbiol*, 2017, **123**, 66-79.
26. S. Connelly, B. Fanelli, N. A. Hasan, R. R. Colwell and M. Kaleko, *Front Microbiol*, 2019, **10**, 101.
27. T. Biologics, https://therivabio.com/, (accessed 11, 2022).
28. C. Burdet, S. Sayah-Jeanne, T. T. Nguyen, C. Miossec, N. Saint-Lu, M. Pulse, W. Weiss, A. Andremont, F. Mentré and J. De Gunzburg, *Antimicrobial agents and chemotherapy*, 2017, **61**, e00543-00517.
29. J. de Gunzburg, A. Ghozlane, A. Ducher, E. Le Chatelier, X. Duval, E. Ruppe, L. Armand-Lefevre, F. Sablier-Gallis, C. Burdet, L. Alavoine, E. Chachaty, V. Augustin, M. Varastet, F. Levenez, S. Kennedy, N. Pons, F. Mentre and A.

Andremont, *J Infect Dis*, 2018, **217**, 628-636.

30. D. Volterra, Clinical trials, https://davolterra.com/clinical-trials/, (accessed 11, 2022).
31. D. Volterra, DAV132 in Immuno-Oncology, https://davolterra.com/dav132-immuno-oncology/, (accessed 11, 2022).
32. T. Vos, S. S. Lim, C. Abbafati, K. M. Abbas and e. al., *The Lancet*, 2020, **396**, 1204-1222.
33. J. Pakkasela, P. Ilmarinen, J. Honkamaki, L. E. Tuomisto, H. Andersen, P. Piirila, H. Hisinger-Molkanen, A. Sovijarvi, H. Backman, B. Lundback, E. Ronmark, H. Kankaanranta and L. Lehtimaki, *BMC Pulm Med*, 2020, **20**, 9.
34. V. Bauchau and S. R. Durham, *Eur Respir J*, 2004, **24**, 758-764.
35. M. S. Blaiss, *Allergy Asthma Proc*, 2010, **31**, 375-380.
36. S. L. Prescott, *J Allergy Clin Immunol*, 2013, **131**, 23-30.
37. M. Pascal, M. Perez-Gordo, T. Caballero, M. M. Escribese, M. N. Lopez Longo, O. Luengo, L. Manso, V. Matheu, E. Seoane, M. Zamorano, M. Labrador and C. Mayorga, *Front Immunol*, 2018, **9**, 1584.
38. T. R. Abrahamsson, R. Y. Wu and M. C. Jenmalm, *Pediatr Res*, 2015, **77**, 214-219.
39. T. Haahtela, S. Holgate, R. Pawankar, C. A. Akdis, S. Benjaponpitak, L. Caraballo, J. Demain, J. Portnoy, L. von Hertzen, W. A. O. S. C. o. C. Change and Biodiversity, *World Allergy Organ J*, 2013, **6**, 3.
40. C. James and D. I. Bernstein, *Curr Opin Allergy Clin Immunol*, 2017, **17**, 55-59.
41. L. Noon, *The Lancet*, 1911, **177**, 1572-1573.
42. P. Rodriguez Del Rio, C. Vidal, J. Just, A. I. Tabar, I. Sanchez-Machin, P. Eberle, J. Borja, P. Bubel, O. Pfaar, P. Demoly and M. A. Calderon, *Pediatr Allergy Immunol*, 2017, **28**, 60-70.
43. G. W. Scadding, M. A. Calderon, M. H. Shamji, A. O. Eifan, M. Penagos, F. Dumitru, M. L. Sever, H. T. Bahnson, K. Lawson, K. M. Harris, A. G. Plough, J. L. Panza, T. Qin, N. Lim, N. K. Tchao, A. Togias, S. R. Durham and G. S. T.

Immune Tolerance Network, *JAMA*, 2017, **317**, 615-625.

44. M. A. Calderon, F. E. Simons, H. J. Malling, R. F. Lockey, P. Moingeon and P. Demoly, *Allergy*, 2012, **67**, 302-311.

45. J. Maloney, G. Berman, R. Gagnon, D. I. Bernstein, H. S. Nelson, J. Kleine-Tebbe, A. Kaur, Q. Li and H. Nolte, *J Allergy Clin Immunol Pract*, 2016, **4**, 301-309 e302.

46. S. M. Jones, E. H. Kim, K. C. Nadeau, A. Nowak-Wegrzyn, R. A. Wood, H. A. Sampson, A. M. Scurlock, S. Chinthrajah, J. Wang, R. D. Pesek, S. B. Sindher, M. Kulis, J. Johnson, K. Spain, D. C. Babineau, H. Chin, J. Laurienzo-Panza, R. Yan, D. Larson, T. Qin, D. Whitehouse, M. L. Sever, S. Sanda, M. Plaut, L. M. Wheatley and A. W. Burks, *The Lancet*, 2022, **399**, 359-371.

47. Y. Su, E. Romeu-Bonilla and T. Heiland, *Hum Vaccin Immunother*, 2017, **13**, 2402-2415.

48. A. Anagnostou, *Allergy Asthma Proc*, 2021, **42**, 118-123.

49. P. Varshney, S. M. Jones, A. M. Scurlock, T. T. Perry, A. Kemper, P. Steele, A. Hiegel, J. Kamilaris, S. Carlisle, X. Yue, M. Kulis, L. Pons, B. Vickery and A. W. Burks, *J Allergy Clin Immunol*, 2011, **127**, 654-660.

50. J. M. Skripak, S. D. Nash, H. Rowley, N. H. Brereton, S. Oh, R. G. Hamilton, E. C. Matsui, A. W. Burks and R. A. Wood, *J Allergy Clin Immunol*, 2008, **122**, 1154-1160.

51. A. W. Burks, S. M. Jones, R. A. Wood, D. M. Fleischer, S. H. Sicherer, R. W. Lindblad, D. Stablein, A. K. Henning, B. P. Vickery, A. H. Liu, A. M. Scurlock, W. G. Shreffler, M. Plaut, H. A. Sampson and R. Consortium of Food Allergy, *N Engl J Med*, 2012, **367**, 233-243.

52. M. Akdis and C. A. Akdis, *J Allergy Clin Immunol*, 2014, **133**, 621-631.

53. A. F. Santos, L. K. James, H. T. Bahnson, M. H. Shamji, N. C. Couto-Francisco, S. Islam, S. Houghton, A. T. Clark, A. Stephens, V. Turcanu, S. R. Durham, H. J. Gould and G. Lack, *J Allergy Clin Immunol*, 2015, **135**, 1249-1256.

54. R. A. Maldonado, R. A. LaMothe, J. D. Ferrari, A. H. Zhang, R. J. Rossi, P. N. Kolte, A. P. Griset, C. O'Neil, D. H. Altreuter, E. Browning, L. Johnston, O. C.

Farokhzad, R. Langer, D. W. Scott, U. H. von Andrian and T. K. Kishimoto, *Proc Natl Acad Sci U S A*, 2015, **112**, E156-165.

55. H. Pohlit, I. Bellinghausen, H. Frey and J. Saloga, *Allergy*, 2017, **72**, 1461-1474.
56. S. Sirvent, I. Soria, C. Cirauqui, B. Cases, A. I. Manzano, C. M. Diez-Rivero, P. A. Reche, J. Lopez-Relano, E. Martinez-Naves, F. J. Canada, J. Jimenez-Barbero, J. Subiza, M. Casanovas, E. Fernandez-Caldas, J. L. Subiza and O. Palomares, *J Allergy Clin Immunol*, 2016, **138**, 558-567 e511.
57. M. Ishii, A. Koyama, H. Iseki, H. Narumi, N. Yokoyama and N. Kojima, *Int Immunopharmacol*, 2010, **10**, 1041-1046.
58. Z. Cui, C. H. Hsu and R. J. Mumper, *Drug Dev Ind Pharm*, 2003, **29**, 689-700.
59. Q. Liu, X. Wang, X. Liu, S. Kumar, G. Gochman, Y. Ji, Y. P. Liao, C. H. Chang, W. Situ, J. Lu, J. Jiang, K. C. Mei, H. Meng, T. Xia and A. E. Nel, *ACS Nano*, 2019, **13**, 4778-4794.
60. S. Hamdy, A. Haddadi, A. Shayeganpour, J. Samuel and A. Lavasanifar, *Pharm Res*, 2011, **28**, 2288-2301.
61. V. Apostolopoulos, G. A. Pietersz, B. E. Loveland, M. S. Sandrin and I. F. McKenzie, *Proceedings of the National Academy of Sciences*, 1995, **92**, 10128-10132.
62. E. E. Weinberger, M. Himly, J. Myschik, M. Hauser, F. Altmann, A. Isakovic, S. Scheiblhofer, J. Thalhamer and R. Weiss, *J Control Release*, 2013, **165**, 101-109.
63. S. Lang and X. Huang, *Front Chem*, 2020, **8**, 284.
64. P. J. Tacken, I. J. de Vries, R. Torensma and C. G. Figdor, *Nat Rev Immunol*, 2007, **7**, 790-802.
65. W. W. Unger and Y. van Kooyk, *Curr Opin Immunol*, 2011, **23**, 131-137.

CHAPTER 2

Specific adsorption of a β-lactam antibiotic *in vivo* by an anion-exchange resin for protection of the intestinal microbiota

2.1 Introduction

Antibiotics are essential for treating infectious diseases by killing pathogenic bacteria *in vivo*. However, administration of antibiotics also affects the microbiota in the intestine, which results in dysbiosis of the intestinal microbiota[1, 2] and antibiotic resistance in intestinal bacteria.[3] Dysbiosis is not only the cause of *Clostridioides difficile* infection (CDI)[4] but also is a risk factor for various kinds of chronic diseases including allergies,[5] asthma,[6] cancer,[7] neurological diseases,[8] and nonalcoholic steatohepatitis.[9]

Currently, two approaches have been reported to protect the gut microbiota during antibiotic treatment. The oral administration of a β-lactamase is one strategy.[10-12] The β-lactamase reaches the large intestine where it degrades β-lactam antibiotics to avoid dysbiosis, which can prevent CDI as well as mitigate resistance.[10, 11] The other method is oral administration of adsorbents of antibiotics. Activated charcoal (AC) was the first agent to be reported to adsorb the β-lactam antibiotics cefotaxime and moxifloxacin in the large intestine.[13, 14] AC was used to successfully prevent hamsters from CDI[13] as well as protect the intestinal microbiota in a clinical trial.[15] However, because AC can non-specifically adsorb biomolecules, there is a risk of side effects induced by adsorption of essential nutrients and bile acids.[16, 17] Previously, we reported a specific adsorbent for vancomycin by modifying a peptide ligand on to a water-swellable PEG-based resin. This adsorbent minimized the effect of vancomycin on the microbiota and protected the mice from CDI.[18]

Here I focused on an ion exchange resin (IER) for the adsorption of antibiotics *in vivo*. Typical IERs are copolymers of styrene and divinyl benzene modified with an acidic or basic group, typically sulfonate and tetramethyl ammonium, respectively. Because of their high content of ionic groups, IERs swell in aqueous media and bind to target molecules by electrostatic, hydrophobic, and π-π interactions.[19, 20] Since IERs are insoluble in water, they are not absorbed by the digestive tract and are excreted from the feces after adsorbing the target compounds.[21] Thus, IERs have been used as an oral adsorbent of various ionic biological molecules such as bile acids, potassium ion, and phosphate ion for treatment of diseases.[16, 22, 23] However, IERs have never been utilized as adsorbent for antibiotics. I hypothesized that β-lactam antibiotics with a negatively charged carboxylate have high affinity to anion- exchange resins (AERs) because of both their ionic and hydrophobic characteristics (Fig. 2.1). β-Lactam antibiotics are known to disrupt the balance of the intestinal microbiota and are a risk factor for CDI.[24, 25] Here I examined an AER as an oral adsorbent of cefoperazone (CEF), a β-lactam cephalosporin antibiotic,[26] which is often used in a murine CDI model to deplete protective gut microbes.[27] I found that superior affinity of an AER to CEF over bile acids and vitamins, and successfully demonstrated the adsorption of an AER *in vivo* to protect gut microbiota from CEF-induced dysbiosis.

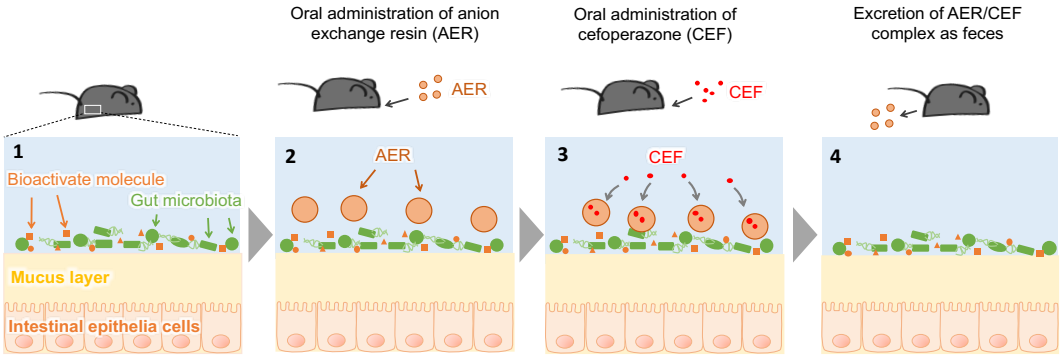

Fig. 2.1 Mechanism of CEF adsorption by the AER in the large intestine. Pre-administration of the AER protects the gut microbiota through selective adsorption of CEF in the large intestine. This strategy avoids dysbiosis induced by CEF treatment.

2.2 Results and discussion

2.2.1 Adsorption of CEF by the AER *in vitro*

Bile acids that exist in intestinal fluid at a concentration in the low mM range[28] are potential competitors for the adsorption of CEF by the AER because of their common properties (anionic, hydrophobic) with CEF (Chart 2.1). First, I compared the adsorption characteristics of CEF and bile acids to the AER in 50 mM Tris-HCl (pH 7.4) (condition 1). The adsorption isotherms are shown in Fig. 2.2a. The binding capacities (Q_m) of CEF and the dissociation constant (K_d) of CEF and sodium cholate (SC) were calculated based on the Langmuir equation and are summarized in Table 2.1. CEF showed a lower Q_m than SC probably because of the larger molecular size of CEF. However, I found that CEF showed much higher affinity to the AER than SC (~200 times). Then I examined the affinity of CEF in the presence of representative bile acids (condition 2: 1 mM SC and 1 mM sodium chenodeoxycholate (SCDC)) that mimic the luminal condition in the small intestine.[29] As shown in Fig. 2.2b, the curves of the adsorption isotherm in the two conditions are almost superimposable and the calculated K_d values are almost the same (Table 2.1). This high specificity of the AER to CEF gives it suitable characteristics to be an *in vivo* adsorbent without capturing bile acids. Interestingly, both SC and CEF have a monocarboxylate anion at pH 7.4, in addition, hydrophobic interactions also cannot explain the higher affinity to CEF because SC is more hydrophobic than CEF according to their log P values.[30, 31] Therefore, the higher affinity of the AER to CEF should be derived from other factors. CEF has π-π conjugation, but not SC. Thus, I conjectured that AER's higher affinity to CEF compared with SC might be derived from π-π interactions.[19, 20]

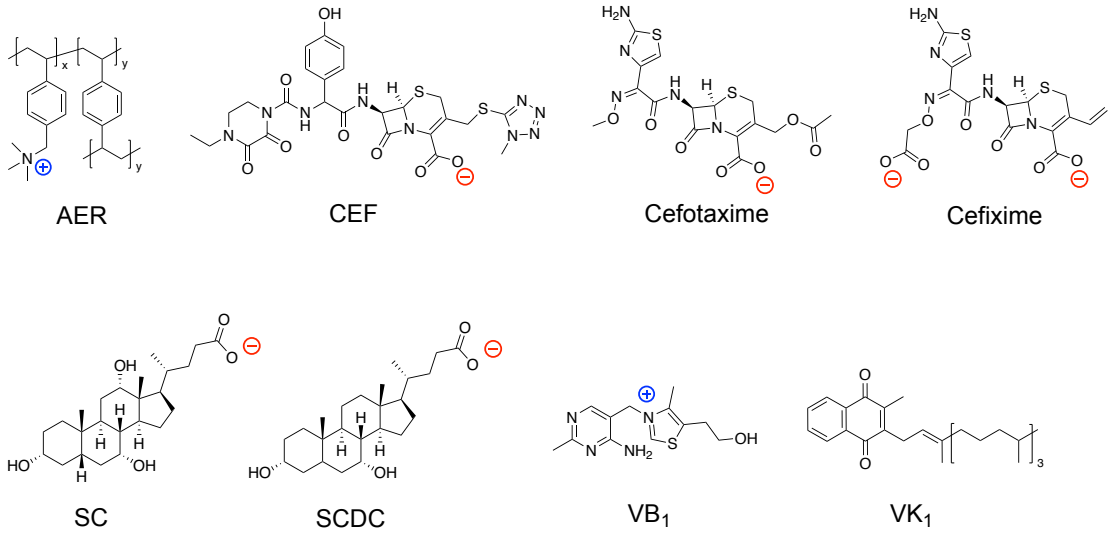

Chart 2.1 Chemical structures of the AER and the target CEF and potential competing molecules used in this study.

An adsorption isotherm in the presence of an additional 120 mM Cl^-, which is the same as the concentration of Cl^- in intestinal fluid, is shown in Fig. 2.2b (condition 3). The affinity of the AER weakened to a quarter of that under condition 2 (Table 2.1). However, the K_d of 45 μM was almost equivalent to that of the vancomycin/resin system that we reported previously.[18] This affinity was high enough to capture vancomycin *in vivo*.

To assess whether the AER could adsorb other β-lactam antibiotics, I determined the adsorption characteristics of cefotaxime and cefixime to the AER in condition 1. These antibiotics have similar structures with CEF, while cefixime has additional carboxylate anion. Adsorption isotherms of these antibiotics are shown in Fig. 2.2c and the calculated parameters are summarized in Table 2.1. Q_m and K_d of these antibiotics were comparable to that of CEF, indicating general high affinity of the AER to the β-lactam antibiotics. It is interesting to note that additional carboxylate anion of cefixime did not so enhance K_d.

Table 2.1 Adsorption parameters for SC and CEF on the AER.

Target	Condition	Q_m (mmol/g)	Q_m (g/g)	K_d (M)
SC	1	3.1	1.3	1.9×10^{-3}
CEF	1	1.1	0.73	7.3×10^{-6}
CEF	2	1.1	0.74	9.8×10^{-6}
CEF	3	1.3	0.85	4.5×10^{-5}
Cefotaxime	1	1.4	0.66	1.2×10^{-5}
Cefixime	1	1.6	0.74	7.3×10^{-6}

Condition 1: 50 mM Tris-HCl (pH 7.4). $[Cl^-]$ = 40 mM.

Condition 2: 50 mM Tris-HCl (pH 7.4) containing 1 mM SC and 1 mM SCDC. $[Cl^-]$ = 40 mM.

Condition 3: 50 mM Tris-HCl (pH 7.4) containing 1 mM SC, 1 mM SCDC, and 80 mM NaCl. $[Cl^-]$ = 120 mM.

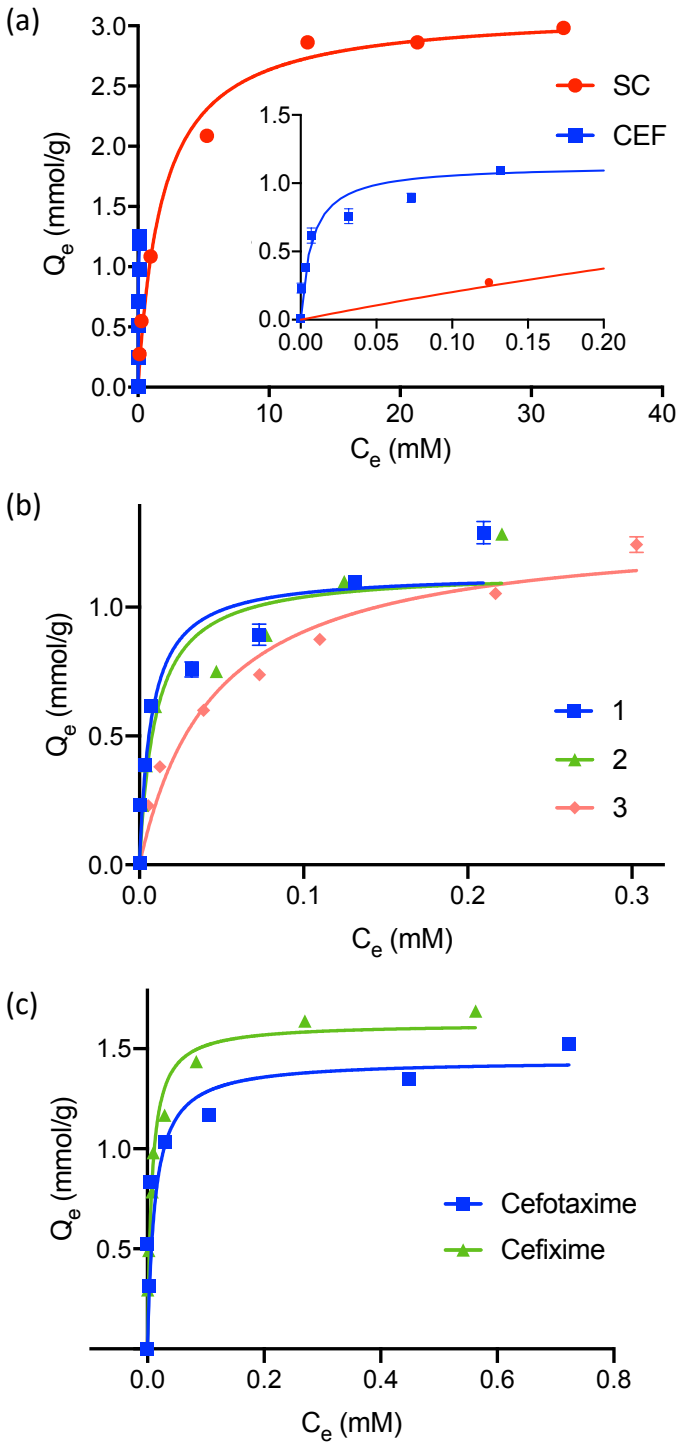

Fig. 2.1 (a) Comparison of the adsorption isotherms of CEF and SC to the AER in condition 1. Graph with a magnified x axis was inserted. (b) Adsorption isotherms of CEF to the AER in the different ionic strength conditions 1 to 3. Adsorption was conducted for 24 h at 37 °C. (c) Adsorption isotherms of cefotaxime and cefixime in condition 1. Data are represented by the mean ± SEM (n = 3).

2.2.2 Contrast the selectivity of the AER and AC

The non-specific capture of micronutrients such as vitamins by adsorbents should be suppressed to avoid the potential side effects associated with the deficiency of these vitamins. Because the vitamin K and B groups are mainly provided by intestinal bacteria,[32] their removal by an AER cannot be supplemented by food intake. Thus, I examined the selectivity of the AER toward CEF, vitamin K1 (VK_1), and vitamin B1 (VB_1). Here I used AC as a control adsorbent. Fig. 2.3 shows a comparison of the adsorption isotherms of the AER and AC toward each compound. The Q_m and K_d values calculated from the curves are summarized in Table 2.2. AC and the AER have similar capacity and affinity to CEF. However, the capacity and affinity of the AER to VB_1 and VK_1 to AER were quite low, although the AC non-specifically adsorbed VB_1 and VK_1 to a similar level as CEF. The specificity of the AER to CEF over VB_1 and VK_1 were calculated from the K_d values to be 10^4 and 10^2, respectively. The high specificity of the AER gives it an advantage over AC to suppress the potential side effects associated with the non-specific adsorption of these vitamins.

Table 2.2. Adsorption parameters for SC and CEF on the AER.

Adsorbent	Target	Q_m (mmol/g)	Q_m (g/g)	K_d (M)
AC	CEF	1.1	7.1×10^{-1}	2.4×10^{-4}
	VB_1	1.7	5.7×10^{-1}	3.7×10^{-7}
	VK_1	1.5	6.8×10^{-1}	4.2×10^{-6}
AER	CEF	1.3	8.4×10^{-1}	1.2×10^{-5}
	VB_1	6.1×10^{-4}	2.1×10^{-4}	3.1×10^{-1}
	VK_1	1.6×10^{-2}	7.2×10^{-3}	2.6×10^{-3}

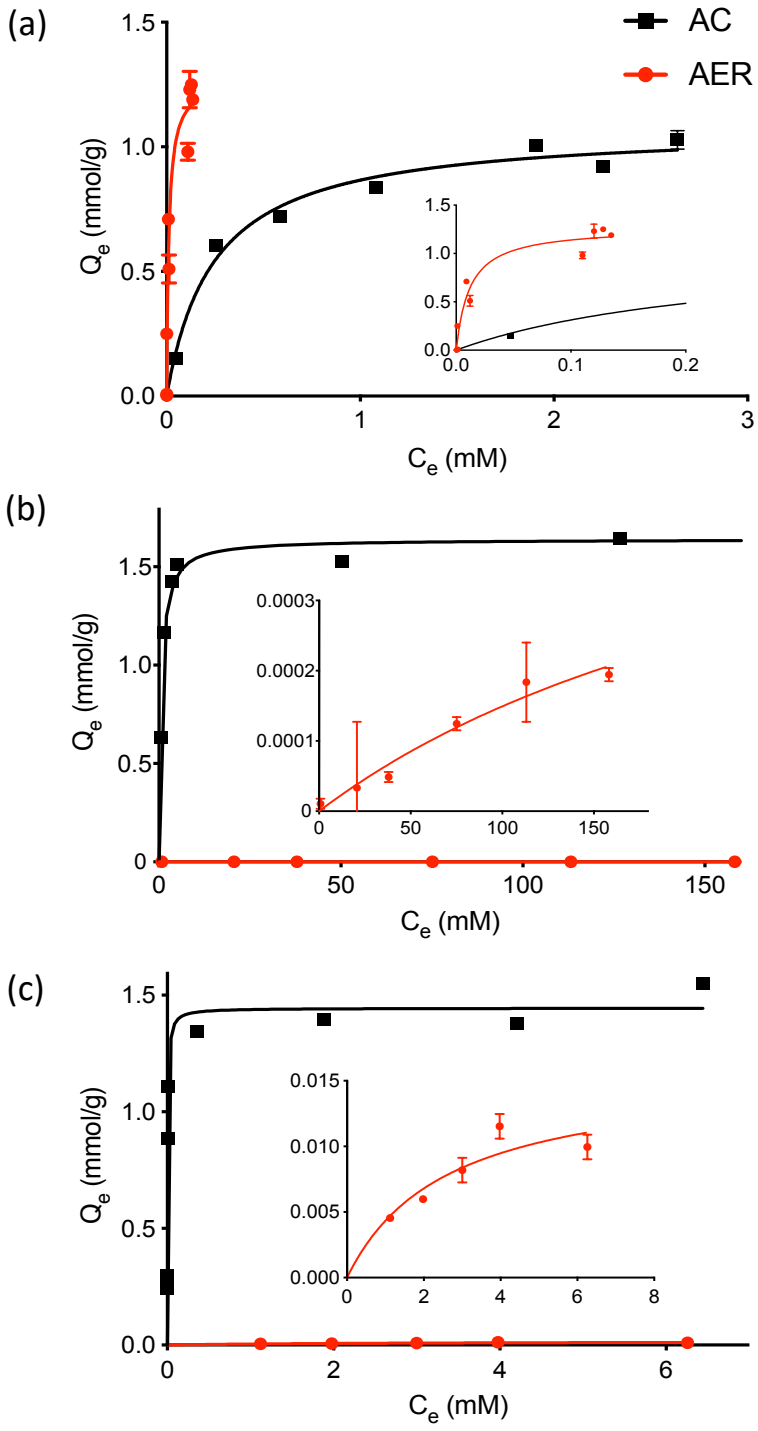

Fig. 2.3 Adsorption isotherms of the AER and AC toward CEF (a), VB_1 (b), and VK_1 (c). In each panel, a magnified graph was inserted. Adsorption was conducted for 2 h at 37 °C in 50 mM Tris-HCl (pH 7.4). Data are presented as the mean ± SEM (n = 3).

2.2.3 Protection of *Escherichia coli* from CEF by the AER

Next, I examined the ability of the AER to protect *E. coli* from CEF based on the minimum inhibitory concentration (MIC) *in vitro*. *E. coli* was treated with CEF in the presence of the AER for 24 h. As shown in Fig. 2.4a, the MIC value of CEF toward *E. coli* in the absence of the AER was 0.16 mg/L, which is consistent with the reported value.[33] The addition of the AER raised the MIC of CEF in a dose-dependent manner, supporting the protective ability of the AER. At 40 mg/mL AER, the MIC became 2.0 × 10^2 mg/L, which is 1,200 times higher than that in the absence of the AER. I confirmed that the AER did not affect the growth of *E. coli* (Fig. 2.4b).

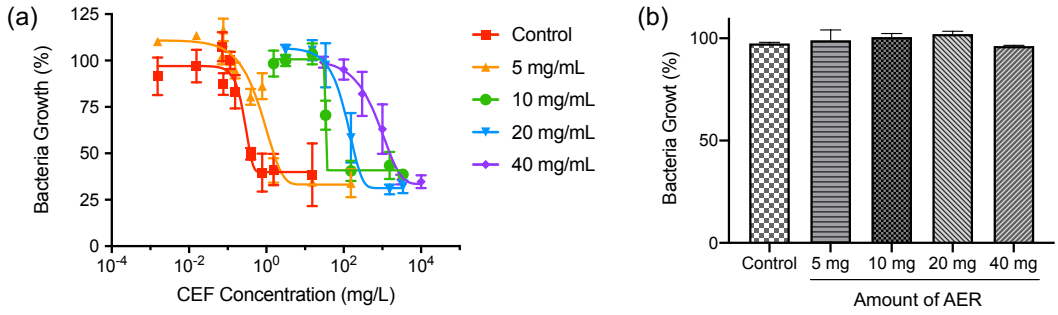

Fig. 2.4 Protection of *E. coli* from CEF by treatment with the AER. (a) *E. coli* (DH5α strain) was cultured in LB broth containing CEF with different amounts of the AER for 24 h at 37 °C. Bacteria growth was evaluated by turbidity at 600 nm. (b) Viability of *E.coli* co-culture with AER. Data are presented as the mean ± SEM (n = 3).

2.2.4 Adsorption of CEF in the intestine by the AER

First, I determined the treatment regimen to adsorb CEF by the AER *in vivo*. The dose of CEF was determined to be 1.5 mg per day, which is enough to induce dysbiosis leading to CDI.[34] It has been reported that AC starts to reach the cecum and the colon within 1 h after oral gavage administration.[35] Thus, I pre-administered the AER 1 h before the application of CEF. I also examined post-administration of the AER 1 h after

the application of CEF in an effort to capture the residual CEF. After CEF administration, the feces were collected over 24 h, and the amount of free CEF in the feces was quantified by HPLC analysis. This treatment was continued for 7 days. Fig. 2.5b shows the amount of free CEF in the feces from the two kinds of treatment regimens on different days. On the first day, about 75% of CEF remained in the feces without application of the AER, while the application of the AER significantly reduced the free CEF in the feces. Pre-administration of the AER reduced CEF to about 10%, while the combination of pre-administration and post-administration further reduced CEF to about 5%, indicating that a second administration of the AER adsorbed leftover CEF from the first administration. On days 3 and 7, a similar adsorption performance of the AER for the two regimens was observed.

At a dose of 30 mg once per day, the adsorption capacity of the AER toward CEF was calculated to be 0.058 μmol/mg in day 1. Compared with the adsorption capacity of 1.3 μmol/mg in simulated intestinal fluid (condition 3 of Table 2.1), the adsorption capacity of the AER *in vivo* was reduced by a factor of 20. This reduction in the adsorption capacity was attributed to the large amounts of biological and feed-derived compounds, which compete with the biding of the AER with CEF.

To confirm the protection of the gut microbiota from CEF by the AER, the colony number of intestinal bacteria included in the feces was evaluated.[36] A suspension of the feces was cultured on an agar plate under anaerobic conditions for 48 h. As shown in Fig. 2.5c, CEF-treated mice showed a significant reduction in colony form units (CFU) from the untreated control group. In contrast, administration of the AER recovered CFU to a similar level as the untreated control group up to day 7. Taken together, these observations indicated that the adsorption of the AER resulted in a reduction of CEF in feces and protection of the microbiota.

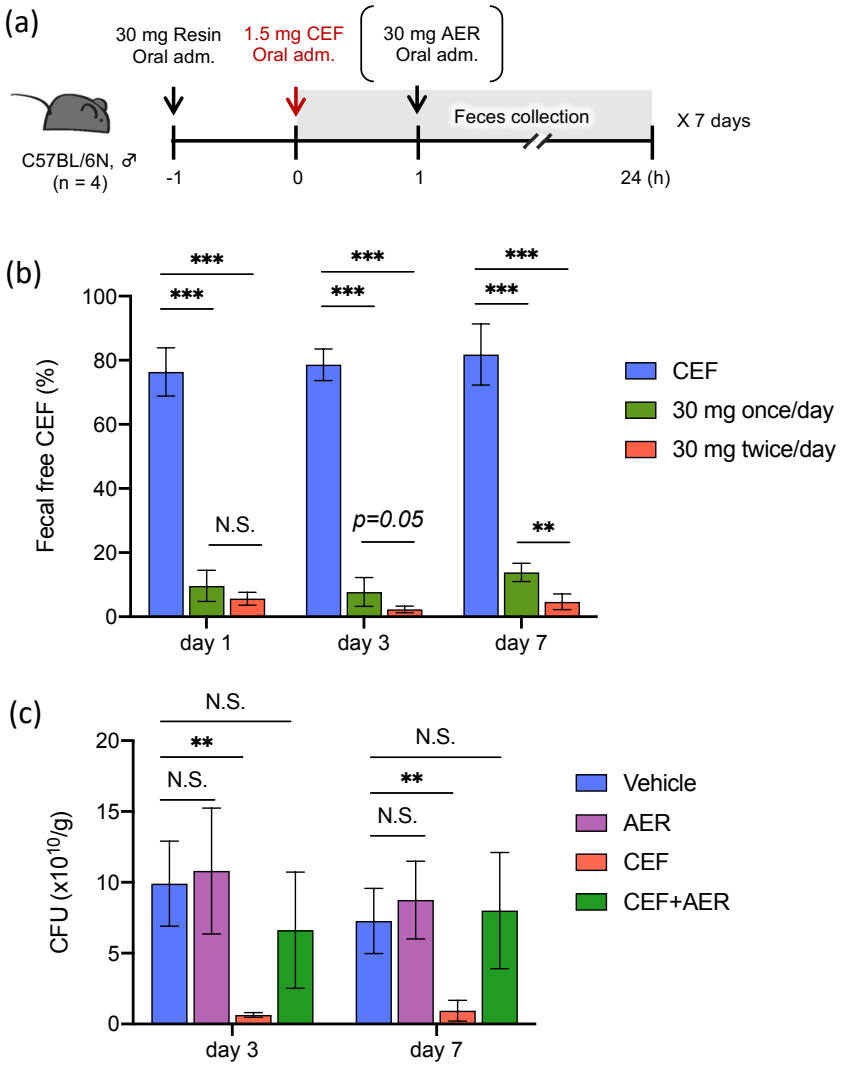

Fig. 2.5 Adsorption of CEF by the AER *in vivo*. (a) Scheme of the daily administration of the AER to adsorb CEF. This dosing scheme was continued for 7 days. Feces were collected within 24 h after CEF administration. (b) The amount of free CEF in the feces after CEF administration. Free CEF in feces was quantified by HPLC at days 1, 3, and 7. (c) CFU of feces on days 3 and 7. The AER was dosed 30 mg twice/day. Data are represented by the mean ± SEM (n = 4). *P<0.05, **P<0.01, ***P < 0.001.

2.2.5 Administration of the AER reduces CEF-induced alternations in the gut microbiota

Based on the above results in Fig. 2.5b, I reasoned that the AER has the ability to suppress the CEF-induced disruption of the gut microbiota by adsorbing intestinal free CEF. To examine whether pre-administration of the AER could prevent CEF-induced alteration of the gut microbiota, I analyzed the gut microbiota composition by 16S rDNA sequencing before and after the CEF treatment with or without the administration of the AER. The unweighted UniFrac distance between day 0 and day 3 was higher in the CEF-treated group than the control group, suggesting that CEF disturbed the gut microbiota (Fig. 2.6a). By contrast, pre-AER administration of the CEF-treated micereduced the UniFrac distance and the distance was not significantly different between the AER+CEF-treated and the control groups (Fig. 2.6a). Specifically, treatment with CEF decreased the abundance of Lachnospiraceae and Ruminococcaceae and increased the abundance of Bacteroidaceae (Fig. 2.6b,c). These alterations were prevented by the administration of the AER (Fig. 2.6c). Furthermore, the protective effects of the AER on the gut microbiota disruption by the CEF were observed even on day 7 (Fig. 2.7b). Several reports have shown that the decrease in commensal *Clostridium* cluster IV and XIVa, including Ruminococcaceae and Lachnospiraceaeare, are related to the colonization of *C. difficile*[37, 38]. Therefore, pre-treatment with the AER before oral CEF intake may prevent the colonization of *C. difficile* through the protection of these bacterial families. Besides, *Clostridium* cluster IV and XIVa bacteria also contribute to the inhibition of intestinal colonization of other bacterial pathogens, such as vancomycin-resistant *Enterococcus* and *Salmonella enterica* serovar Typhimurium[38-40]. Thus, pre-administration of an AER will help to mitigate the disruption of the gut microbiota after antibiotic treatment, resulting in prevention of opportunistic pathogen colonization, and may lead to clinical applications in the future.

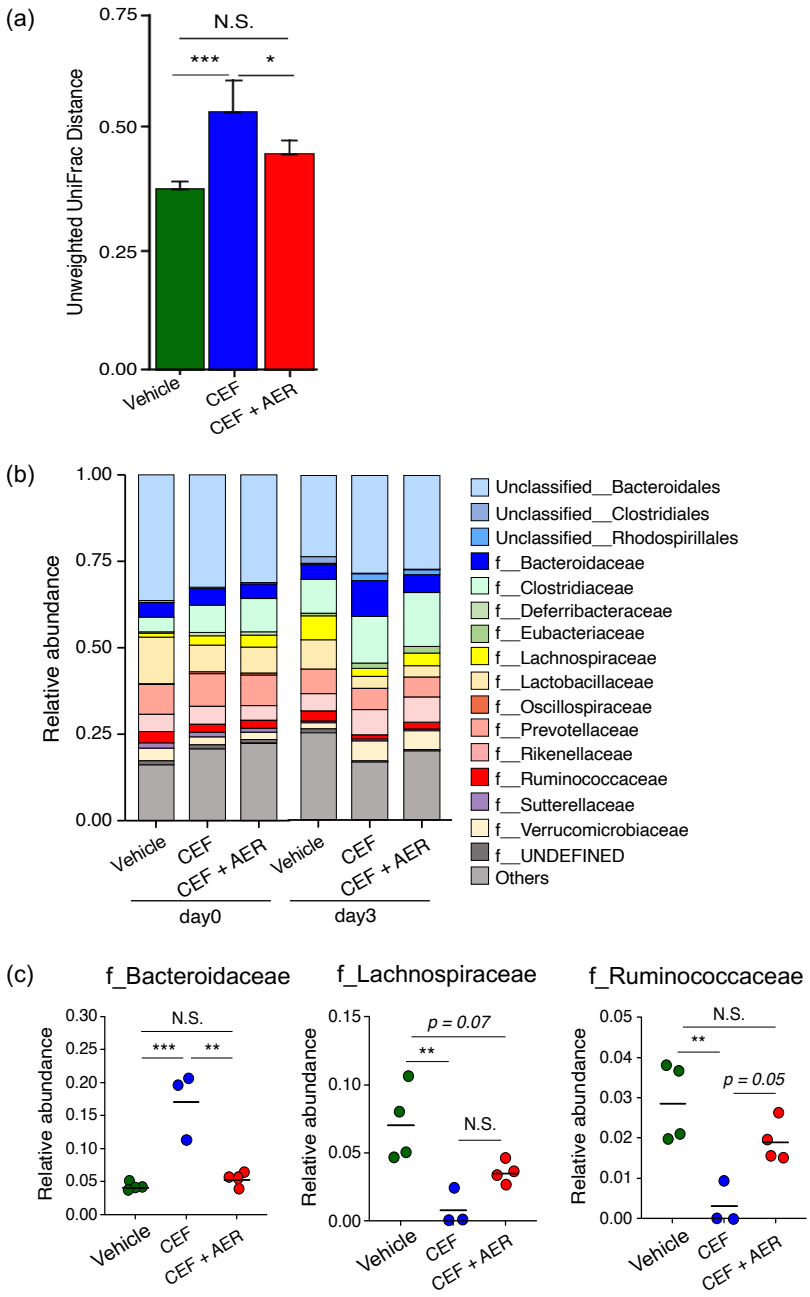

Fig. 2.6 Administration of the AER prevents CEF-induced perturbation in the gut microbiota. (a) Unweighted UniFrac distance between day 0 and day 3 from principal coordinate analysis. Error bars show standard deviation (Vehicle: n = 4, CEF: n = 3, CEF + AER: n = 4). (b) Fecal microbiota composition of vehicle, CEF, or CEF + AER on day 0 and day 3 (Vehicle: n = 4, CEF: n = 3, CEF + AER: n = 4). Each bar shows the mean of the individual mice of each group. (c) The relative abundance of Bacteroidaceae, Lachnospiraceae, and Ruminococcaceae on day 3. Each circle indicates individual mice.

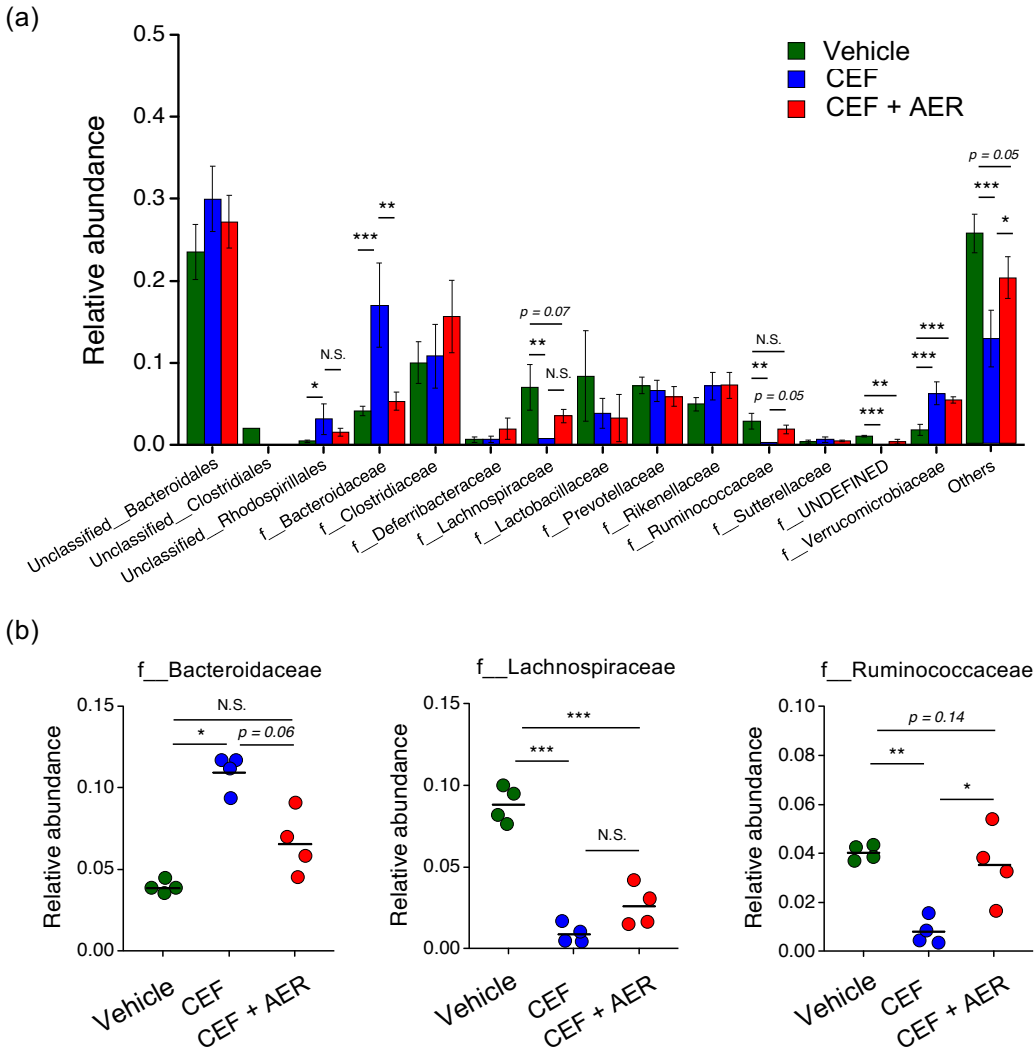

Fig. 2.7 Pre-administration of AER prevents CEF-induced perturbation in gut microbiota. (a) The relative abundance of all detected bacteria of vehicle (green), CEF (blue), or CEF with AER (red)-treated groups on day 3 (Vehicle: n = 4, CEF: n = 3, CEF + AER: n = 4). (b) The relative abundance of Bacteroidaceae, Ruminococcaceae, and Lachnospiraceae in the fecal samples of vehicle (green), CEF (blue), or CEF with AER (red)-treated groups on day 7 (n = 4). Each circle indicates the individual mice of each group.

2.3 Summary

Herein, I proposed an AER as a specific adsorbent of CEF *in vivo*. According to the adsorption isotherm study, the AER maintained its affinity to CEF in the presence of bile acids, showing its high specificity to CEF over bile acids. The non-specific adsorption of the AER to VB_1 and VK_1 was quite small, although AC adsorbed them to the same extent as CEF. The specificity of the AER to CEF will be important not only for adsorption in a contaminated *in vivo* system but also for reducing the risk of side effects associated with the adsorption of micronutrients. Oral application of the AER to mice successfully protected the microbiota from CEF, maintaining the signature of resistance toward *C. difficile* colonization. Thus, I concluded that the AER described herein will be a superior *in vivo* adsorbent of CEF compared with AC because of its high specificity.

2.4 Experimental section

2.4.1 Materials

Activated charcoal (AC) was obtained from Ueda Environmental Solutions Co., Ltd. (Sakai, Japan). Cefoperazone (CEF), sodium cholate (SC), sodium chenodeoxycholate (SCDC) and thiamine hydrochloride hydrate (VB_1) were purchased from Tokyo Chemical Industry Co., Ltd. (Tokyo, Japan). Vitamin K_1 (VK_1), cefixime trihydrate and cefotaxime were purchased from FUJIFILM Wako Pure Chemical Corporation (Osaka, Japan). Luria-Bertani (LB) broth and agar were purchased from BD Biosciences (San Jpse, CA, USA). Dried yeast extract was purchased from Nacalai Tesque, Inc. (Kyoto, Japan). Sheep defibrinated blood was purchased from Kohjin Bio Co., Ltd (Saitama, Japan). Brucella agar with hemin and vitamin K was purchased from Sigma-Aldrich (St. Louis, MO, USA). *Escherichia coli* DH5α was provided by the ATCC (Manassas, VA, USA).

2.4.2 Preparation of the AER

IRA402Cl resin (AER) was obtained from Organo Corporation (Tokyo, Japan). This AER is composed of styrene and divinyl benzene containing the tetramethyl ammonium group as an anion exchange site. The AER is a gel, amber, translucent, spherical beads which with a particle size of 0.70-0.95 mm. Total exchange capacity ≥ 1.25 mol/L of wet resin; water retention capacity 58-62% (Cl^- form). The AER with chloride as the counter ion was pretreated following the manufacturer's protocol. Briefly, the AER was pretreated with 1 M NaOH and HCl solutions to remove monomers and porogenic agents trapped inside the pores during the synthesis process.[41] Then AER was soaked in methanol for at least 24 h. The methanol in a certain amount of resin was thoroughly replaced with deionized water prior to the adsorption experiments.[42]

2.4.3 Adsorption properties of the AER

To determine the adsorption properties of the resin, static adsorption tests were performed. In the adsorption experiment, CEF (0.01–1.5 mg) was dissolved in 1.0 mL of an aqueous solution in a test tube. The solution conditions are summarized in Table 2.1. Then, 2.0 mg of AER was added into the solution. The tube was shaken (200 rpm) in a shaker at 37 °C for 24 h, and then the concentration of CEF in the liquid phase was determined by high performance liquid chromatography (HPLC).

CEF was quantified by an HPLC validated method using an Elite Lachrom L-2455 diode array detector (Hitachi, Japan) and a Sunfire C_{18} column (5 μm, 10 mm×150 mm). An isocratic mobile phase consisting of 10% methanol and 90% milli-Q water was used with a flow rate of 1.5 mL/min, a 20 μL injection volume, and a column oven temperature of 25 °C. Photodiode array detection was used to detect CEF at 220 nm. Adsorption properties of the AER to cefotaxime and cefixime were determined similarly.

2.4.4 Comparison of the selectivity of the AER and AC

SC and VB_1 were dissolved in 2.0 mL of 50 mM Tris-HCl buffer (pH 7.4). VK_1 was first dispersed in 50 μL dimethyl sulfoxide, and then dissolved in 1.95 mL of 50 mM Tris-HCl buffer (pH 7.4). A total of 5.0 mg AER or AC was added into the solution. The tube was shaken (200 rpm) at 37 °C for 2 h. Samples were centrifuged for 10 min at 9,100 ×*g* and the supernatant was passed through a 0.22 μm syringe filter. Then the concentrations of SC, VB_1, and VK_1 in the liquid phase were determined by HPLC.

SC was analyzed using a YMC-Pack ODS-AL column (5 μm, 4.6 mm×250 mm). The mobile phase consisted of 60% acetonitrile and 40% milli-Q water, the flow rate was set at 1.0 mL/min, the column oven temperature was 25 °C, and the injection volume was 20 μL. SC was detected at 205 nm. VB_1 and VK_1 were analyzed using a Sunfire C_{18} column (5 μm, 10 mm×150 mm). The mobile phase for VB_1 consisted of

30% methanol and 70% milli-Q water, the flow rate was set at 1.0 mL/min, the column oven temperature was 25 °C, and injection volume was 20 μL. VB_1 was detected at 256 nm. The mobile phase for VK_1 consisted of 80% methanol and 20% acetonitrile, the flow rate was 1.5 mL/min, the column oven temperature was 25 °C, and the injection volume was 20 μL. VK_1 was detected at 246 nm.

2.4.5 Analysis of adsorption isotherms

To calculate the capacity of the AER and AC, a Langmuir adsorption model was used to derive the Langmuir isotherm. The capacity was expressed according to the equation for a single adsorbate case:

$$Q_e = \frac{Q_m \times C_e}{(K_d + C_e)}$$

where C_e (mM) represents the equilibrium drug concentration in the medium, Q_e (mmol/g) is the amount of drug adsorbed by the AER, Q_m (mmol/g) represents the capacity and K_d (mM) represents the dissociation constant.

2.4.6 Protection of *E.coli* from CEF

The protection activity of AER was evaluated by a microtiter broth dilution MIC assay. Briefly, the initial inoculum of *E. coli* was added to the LB broth and incubated at 37 °C for 24 h in a shaker (200 rpm). The CEF was serially diluted to between AER 5–40 mg/mL was prepared in broth medium and aliquoted into a 2 mL tube. *E. coli* were inoculated at 37 °C for 24 h. Turbidity was measured using a plate reader (λ = 600 nm) after 24 h of incubation to indicate the growth percentage. The protection activity of the AER against the antibiotic activity was compared with the sample without the AER. The MIC value was defined as the lowest concentration of CEF that inhibited the visible growth of bacteria.

2.4.7 Animals and housing

C57BL/6N mice (8 weeks old; male) were purchased from Kyudo Co., Ltd. (Saga, Japan). Mice were fed a diet of CE-2 (Kyudo Co., Ltd., Saga, Japan), with access to bedding and water. Cage changes were performed in a laminar flow hood. Mice were exposed to a cycle of 12 h of light and 12 h of darkness. Animal experiments were performed according to the Guidelines of the Animal Care and Use Committee, Kyushu University (A19-164-0).

2.4.8 CEF capturing determination *in vivo*

C57BL/6N mice (8 weeks; male) were housed in one cage per group. Mice were dosed by gastric gavage with 1.5 mg CEF (group 1, n = 4), 30 mg AER 1 h prior to administration of 1.5 mg CEF (group 2, n = 4), 30 mg AER 1 h prior and 1 h after 1.5 mg CEF (group 3, n = 4) once daily for seven days. Feces were collected after gavaging CEF for 24 h to determine the fecal free CEF concentration. Feces were added to 10 mL of milli-Q water and homogenized by vortexing. After mixing and centrifugation, the supernatants were collected and passed through a 0.22 μm syringe filter. Purified feces samples were analyzed by HPLC.

2.4.9 Protection of the gut microbiota from CEF using the AER

C57BL/6N mice (8 weeks; male) were administered 1.5 mg CEF via gastric gavage for seven days. Mice were divided into three study groups: water only (group 1, n = 4), AER only (group 2, n = 4), CEF 1.5 mg only (group 3, n = 3), and 30 mg AER 1 h prior to administration of 1.5 mg CEF (group 4, n = 4). Fecal specimens were collected in nonsterile tubes, diluted 10-fold in 0.5% yeast extract solution, and emulsified in a vortex mixer. Serial 10-fold dilutions were made in yeast extract, and volumes of 0.1 mL of selected dilutions were plated by a rotator-pipette method onto

the following media: Brucella agar supplemented with VK_1, hemin, and 5% sheep blood. The number of CFU was counted following 48 h of growth on plates at 37 ºC under anaerobic conditions.

2.4.10 16S ribosomal DNA analysis

Mouse fecal samples were collected according to the procedures described in section 2.9 and stored at -80 °C. Fecal DNA was extracted by complying with the E.Z.N.A. Stool DNA Kit Pathogen Detection protocol (OMEGA Bio-Tek, Norcross, GA, USA) and purified using magLead 12gc (Precision System Science Co., Ltd., Matsudo, Japan). The V3-V4 region of the 16S rDNA gene was amplified following DNA extraction using universal primers (Table 2.3). The PCR reaction mixture contained 2.5 µL of 5 ng/µL of DNA extraction, 12.5 µL 2 x CAPA HiFi mix (Illumina, San Diego, CA, USA), and 5 µL of 1 µM of each primer. The cycling conditions were 95 °C (3 min), 25 cycles of 95 °C (30 sec), 55 °C (30 sec), and 72 °C (30 sec) followed by a final elongation step at 72 °C (5 min).

The amplified DNA was purified using AMPure XP beads (Beckman Coulter, Brea, CA, USA) followed by a second PCR reaction where the mixture contained 5 µL purified DNA, 25 µL 2 x CAPA HiFi mix (Illumina, San Diego, CA, USA), 10 µL distilled water, and 5 µL of 1 µM of each primer from the Nextera XT index kit (Illumina, San Diego, CA, USA). The PCR conditions were 95 °C (3 min), 8 cycles of 95 °C (30 sec), 55 °C (30 sec) and 72 °C (30 sec) followed by a final elongation step at 72 °C (5 min). Likewise, tagged DNA was purified with AMPure XP beads and diluted in 10 mM Tris-HCl buffer (pH 8.5) to 12 pM and all samples were pooled. The completed library was sequenced on an Illumina Miseq 600 cycle V3-V4 kit (Illumina, San Diego, CA, USA).

Table 2.3 Primers for 16S rDNA gene amplification

Forward	5’TCGTCGGCAGCGTCAGATGTGTATAAGAGACAGGTGCCAGC MGCCGCGGTAA-3’
Reverse	5’GTCTCGTGGGCTCGGAGATGTGTATAAGAGACAGGGACTAC HVGGGTWTCTAAT-3’

M: A or C; H: A, T or C; V: A, G or C

2.4.11 Statistical analysis

Statistical analyses were performed using R studio (Version 1.4.1103). Bartlett’s test was used to determine the significance of variance between three groups. If differences were significant ($p < 0.05$), Scheffe’s test was used for comparisons of discontinuous variables between the three groups. The Turkey HSD test was used for comparisons among the three groups with similar variance. The diversity of the gut microbiota was analyzed by QIIME and R using R vegan and multcomp packages. * $p < 0.05$, ** $p < 0.01$, *** $p < 0.001$.

2.5 References

1. C. Jernberg, S. Lofmark, C. Edlund and J. K. Jansson, *ISME J*, 2007, **1**, 56-66.
2. M. F. De La Cochetiere, T. Durand, P. Lepage, A. Bourreille, J. P. Galmiche and J. Dore, *J Clin Microbiol*, 2005, **43**, 5588-5592.
3. L. Zhang, Y. Huang, Y. Zhou, T. Buckley and H. H. Wang, *Antimicrob Agents Chemother*, 2013, **57**, 3659-3666.
4. M. F. De La Cochetiere, T. Durand, V. Lalande, J. C. Petit, G. Potel and L. Beaugerie, *Microb Ecol*, 2008, **56**, 395-402.
5. M. C. Noverr, R. M. Noggle, G. B. Toews and G. B. Huffnagle, *Infect Immun*, 2004, **72**, 4996-5003.
6. K. Wickens, N. Pearce, J. Crane and R. Beasley, *Clinical and experimental allergy: journal of the British Society for Allergy and Clinical Immunology*, 1999, **29**, 766-771.
7. L. Zitvogel, L. Galluzzi, S. Viaud, M. Vétizou, R. Daillère, M. Merad and G. Kroemer, *Science Translational Medicine*, 2015, **7**, 271ps271-271ps271.
8. M. T. Bailey, S. E. Dowd, J. D. Galley, A. R. Hufnagle, R. G. Allen and M. Lyte, *Brain Behav Immun*, 2011, **25**, 397-407.
9. W. C. Wu, W. Zhao and S. Li, *World J Gastroenterol*, 2008, **14**, 313-317.
10. M. Kaleko, J. A. Bristol, S. Hubert, T. Parsley, G. Widmer, S. Tzipori, P. Subramanian, N. Hasan, P. Koski, J. Kokai-Kun, J. Sliman, A. Jones and S. Connelly, *Anaerobe*, 2016, **41**, 58-67.
11. S. Connelly, J. A. Bristol, S. Hubert, P. Subramanian, N. A. Hasan, R. R. Colwell and M. Kaleko, *J Appl Microbiol*, 2017, **123**, 66-79.
12. G. W. Welling, A. Holtrop, C. Slootmaker-van der Meulen, G. J. Meijer-Severs, E. van Santen, R. H. Tonk, H. G. de Vries-Hospers and D. van der Waaij, *J Antimicrob Chemother*, 1992, **30**, 234-236.
13. C. Burdet, S. Sayah-Jeanne, T. T. Nguyen, C. Miossec, N. Saint-Lu, M. Pulse, W. Weiss, A. Andremont, F. Mentré and J. De Gunzburg, *Antimicrobial agents and chemotherapy*, 2017, **61**, e00543-00517.

14. N. Grall, L. Massias, T. T. Nguyen, S. Sayah-Jeanne, N. Ducrot, E. Chachaty, J. de Gunzburg and A. Andremont, *Antimicrob Agents Chemother*, 2013, **57**, 5423-5425.
15. J. de Gunzburg, A. Ghozlane, A. Ducher, E. Le Chatelier, X. Duval, E. Ruppe, L. Armand-Lefevre, F. Sablier-Gallis, C. Burdet, L. Alavoine, E. Chachaty, V. Augustin, M. Varastet, F. Levenez, S. Kennedy, N. Pons, F. Mentre and A. Andremont, *J Infect Dis*, 2018, **217**, 628-636.
16. Y. Araki, T. Tsujikawa, A. Andoh, M. Sasaki, Y. Fujiyama and T. Bamba, *Dig Liver Dis*, 2000, **32**, 691-698.
17. M. Abbas, S. Kaddour and M. Trari, *Journal of Industrial and Engineering Chemistry*, 2014, **20**, 745-751.
18. K. Yuzuriha, K. Yakabe, H. Nagai, S. Li, T. Zendo, K. Zai, A. Kishimura, K. Hase, Y. G. Kim, T. Mori and Y. Katayama, *Biosci Microbiota Food Health*, 2020, **39**, 128-136.
19. J. Kammerer, J. Boschet, D. R. Kammerer and R. Carle, *LWT - Food Science and Technology*, 2011, **44**, 1079-1087.
20. M. Ghafari, Y. Cui, A. Alali and J. D. Atkinson, *J Hazard Mater*, 2019, **361**, 162-168.
21. Y. Honda and M. Nakano, *CHEMICAL & PHARMACEUTICAL BULLETIN*, 2000, **48**, 978-981.
22. H. M. Burt, E. C. Cameron, H. Erber and J. D. Price, *Journal of pharmaceutical sciences*, 1987, **76**, 379-383.
23. L. Scherr, D. A. Ogden, A. W. Mead, N. Spritz and A. L. Rubin, *New England Journal of Medicine*, 1961, **264**, 115-119.
24. C. M. Theriot, C. C. Koumpouras, P. E. Carlson, I. I. Bergin, D. M. Aronoff and V. B. Young, *Gut Microbes*, 2011, **2**, 326-334.
25. M. L. Jenior, J. L. Leslie, V. B. Young and P. D. Schloss, *mSphere*, 2018, **3**.
26. A. M. Schubert, H. Sinani and P. D. Schloss, *mBio*, 2015, **6**, e00974.
27. C. M. Theriot, C. C. Koumpouras, P. E. Carlson, Bergin, II, D. M. Aronoff and V. B. Young, *Gut Microbes*, 2011, **2**, 326-334.

28. L. Kalantzi, K. Goumas, V. Kalioras, B. Abrahamsson, J. B. Dressman and C. Reppas, *Pharm Res*, 2006, **23**, 165-176.
29. J. M. Ridlon, D. J. Kang and P. B. Hylemon, *J Lipid Res*, 2006, **47**, 241-259.
30. National Center for Biotechnology Information. PubChem Compound Summary for CID 221493, Cholic acid, https://pubchem.ncbi.nlm.nih.gov/compound/Cholic-acid, (accessed Accessed May 28, 2021).
31. National Center for Biotechnology Information. PubChem Compound Summary for CID 44187, Cefoperazone, https://pubchem.ncbi.nlm.nih.gov/compound/Cefoperazone, (accessed Accessed May 28, 2021).
32. M. Hill, *European journal of cancer prevention: the official journal of the European Cancer Prevention Organisation (ECP)*, 1997, **6**, S43-45.
33. C. C. Lai, C. C. Chen, Y. C. Lu, T. P. Lin, Y. C. Chuang and H. J. Tang, *Infect Drug Resist*, 2018, **11**, 1441-1445.
34. T. J. De Wolfe, A. E. Kates, L. Barko, B. J. Darien and N. Safdar, *Antimicrob Agents Chemother*, 2019, **63**.
35. P. Padmanabhan, J. Grosse, A. B. M. A. Asad, G. K. Radda and X. Golay, *EJNMMI Research*, 2013, **3**, 60.
36. L. J. Mata, C. Carrillo and E. Villatoro, *Appl Microbiol*, 1969, **17**, 596-602.
37. V. C. Antharam, E. C. Li, A. Ishmael, A. Sharma, V. Mai, K. H. Rand and G. P. Wang, *J Clin Microbiol*, 2013, **51**, 2884-2892.
38. A. E. Reeves, M. J. Koenigsknecht, I. L. Bergin and V. B. Young, *Infect Immun*, 2012, **80**, 3786-3794.
39. S. Caballero, S. Kim, R. A. Carter, I. M. Leiner, B. Susac, L. Miller, G. J. Kim, L. Ling and E. G. Pamer, *Cell Host Microbe*, 2017, **21**, 592-602 e594.
40. Y. G. Kim, K. Sakamoto, S. U. Seo, J. M. Pickard, M. G. Gillilland, 3rd, N. A. Pudlo, M. Hoostal, X. Li, T. D. Wang, T. Feehley, A. T. Stefka, T. M. Schmidt, E. C. Martens, S. Fukuda, N. Inohara, C. R. Nagler and G. Núñez, *Science*, 2017, **356**, 315-319.

41. R.-S. Juang and L.-D. Shiau, *Industrial & Engineering Chemistry Research*, 1998, **37**, 555-560.

42. R.-S. Juang and J.-Y. Shiau, *Journal of Hazardous Materials*, 1999, **70**, 171-183.

CHAPTER 3

Mannan-coated antigen nanoparticles prepared by heat-induced self-assembly for oral allergen immunotherapy

3.1 Introduction

Allergic diseases are caused by aberrant immune response to environmental molecules and affect approximately 20% of global populations.[1] The only curative treatment for allergic diseases is allergen immunotherapy (AIT). AIT increases antigen-specific immune tolerance via repeated administration of antigens for several years.[2] AIT achieves tolerance by reduction of T helper 2 (T_H2) cell and induction of regulatory T (T_{reg}) cells through antigen presentation by dendritic cells (DCs).[3] Present AIT utilizes sublingual and subcutaneous administration of antigens. Oral administration utilizes intestinal immune system which is the largest lymphoid tissue in the body is usually used for the treatment of food allergies. but it is considered an alternative route for the treatment of allergic rhinitis and allergic asthma, due to better patient compliance, non-invasive route.[4, 5] Although different routes of AIT showed therapeutic effects for many allergic patients, there are still a small number of people did not get relief.[6, 7] Thus, AIT still lacks therapeutic efficacy, safety and patient adherence in some clinical trials.[8-10] Therefore, effective and safe approaches for the allergic diseases treatment are required.

Dendritic cells (DCs) are key regulator of allergy and tolerance, which present antigens on the major histocompatibility complex (MHC) class II to regulate $CD4^+$ T cell-mediated immune response. DCs recognize antigens using various pattern recognition receptors such as C-type lectin receptors (CLRs) which including dendritic cell-specific intracellular adhesion molecule 3-grabbing non-integrin (DC-SIGN) and mannose receptor (MR).[11, 12] CLRs not only mediate endocytosis but also cell signaling,

like enhancing expression of programmed death ligand 1 (PD-L1) and increasing secretion of interleukin-10 (IL-10) both of which facilitate differentiation of regulatory T (T_{reg}) cells.[13, 14] Therefore, targeting CLRs may induce antigen-specific tolerance. Mannoprotein (MAN) obtained from *Saccharomyces cerevisiae* is a glycoprotein whose mannan part is an effective ligand of MR and DC-SIGN to induce tolerance.[15] So, MAN-antigen nanoparticles (NPs) have been used for antigen-specific tolerance induction to treat allergy.

Mannan modified NPs such as liposomes and poly(lactic-co-glycolic acid) (PLGA) NPs which encapsulated antigens have been used to treat allergies.[16, 17] However, mannan conjugated polymers and preparation of NPs are usually complicated and difficult to reproduce. Conjugation of mannan and antigens are another simple methods. Oxidative or reductive mannan generated aldehyde groups on mannan and could conjugate with amine groups on antigens, but opened mannose ring maybe reduced efficiency for DC targeting and conjugated antigen may decrease immunogenicity.[18, 19] Sirvent et al. recently reported preparation of NP via crosslinking between antigenic protein and mannan protein (MAN) with glutaraldehyde. The NP was easy to be taken up by DCs through targeting mannose receptor and DC-SIGN, improving the effectiveness of treatment of allergy while also reducing antigenicity.[20, 21] However, random crosslinking may lead to non-uniform size distribution of NPs.[22] In addition, glutaraldehyde-treated viral vaccines reduced antibodies production *in vivo*, suggesting that the immunogenicity of glutaraldehyde-crosslinked viral proteins was reduced.[23, 24] To overcome these problems, I wanted to develop a MAN-antigen nanoparticle which is easy to prepare and can be easily disassembled inside cells.

Here I proposed a preparation method of NP from MAN and allergen protein. MAN will work as amphiphilic molecule with hydrophilic mannan and hydrophobic protein when heat denatured. Thus, heating the mixture of MAN and allergen protein will form NP with core of denatured allergen protein and protein part of MAN which is surrounded by hydrophilic mannan. The obtained particle can be crosslinked via disulfide bonds inside the thiol group of cysteine residues (Fig. 3.1a).[25] Higher order structure of the B-cell epitope of OVA was disrupted[26] as well as MAN coating on the

surface of NP which may decrease the reactivity of OVA with immunoglobulin E (IgE) and reduce the risk of anaphylaxis during treatment. In this study, I showed that MAN-disulfide bond crosslinked OVA (MDO) was a DC targeting NP. I evaluated tolerogenic DC and T_{reg} induction by MDO *in vitro* and preventive and therapeutic effect of MDO through oral and subcutaneous administration in mouse allergic asthma model.

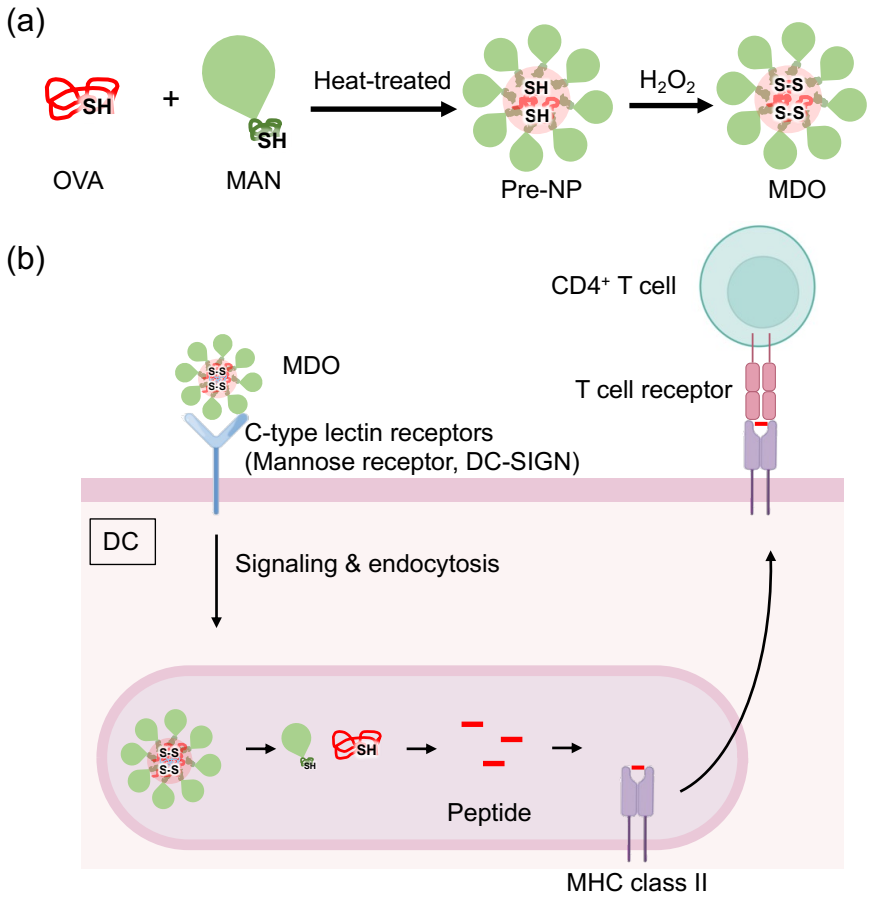

Fig.3.1 (a) Preparation of MDO and (b) intracellular process of antigen targeted to C-type lectin receptors of DC. MDO targeted DCs via C-type lectin receptors and is internalized through endocytosis. MDO in the lysosomes are dissociated by cleave disulfide bonds. The resulting peptides are loaded on MHC class II molecules and presented to $CD4^+$ T cells to induce regulatory T cells.

3.2 Results and discussion

3.2.1 Preparation of MDO

MDO was prepared by mixing varying concentration of MAN with constant concentration of OVA (5 mg/mL) and heated at 85°C for 60 min. The obtained nanoparticles (NPs) were treated with H_2O_2 for disulfide bond formation followed by removal of excess MAN and OVA by ultrafiltration. As shown in Fig. 3.2a, with increasing MAN content, the size and size distribution of MDO became larger. The content of OVA in NPs was almost quantitative in all NPs while the MAN content in NP seems to be saturated at 15 mg/mL (Table 3.1), indicating that filling of the surface of NPs with mannan chain at MDO-15. Residual free thiol group which was quantified by Ellman's assay was plotted with heating time (Fig. 3.2b). Reactive thiol group of OVA and MAN was very low in the beginning but increased with time, showing the exposure of free thiol groups on the surface of OVA and MAN aggregates. However, after treatment with H_2O_2, free thiol was reduced significantly, indicating the formation of disulfide bonds in MDOs. Disulfide formation was further confirmed by sodium dodecyl sulfate–polyacrylamide gel electrophoresis (SDS-PAGE). As shown in Fig. 3.2c, MDOs without H_2O_2 treatment showed remaining free OVA band, while H_2O_2 treatment resulted in disappearance of free OVA in non-reduced condition, showing the necessity of H_2O_2 treatment. Fig. 3.2d shows the SDS-PAGE after reducing disulfide bonds of MDOs. MDOs were completely dissociated into single OVA molecule. Collecting the results of Fig. 3.2c and d, most of the intermolecular disulfide bonds was formed by heat treatment and H_2O_2 treatment enhanced the disulfide bond formation. In contrast, reduction responsive dissociation of particles obtained by crosslinking of OVA and MAN by glutaraldehyde (MGO) was not observed (Fig. 3.2e).

The presentation of mannan on the surface of MDOs was estimated by the *Con*A agglutination assay. *Con*A is a tetrameric lectin possessing four binding sites for α-mannose. As shown in Fig. 3.2f, OD value of MDO-0 did not change upon addition of *ConA*. In contrast, MDOs containing MAN showed increase in the OD value due to the

agglutination and the OD values became higher with increasing MAN content, implying more mannan on the MDO surface.

Table 3.1 Characteristics of prepared NPs

No.	Feed		Size (nm)	PDI	ζ-potential (mV)	Incorporated		Man/OVA ratio (mol/mol)
	OVA (mg/mL)	MAN (mg/mL)				OVA (mg/mL)	MAN (mg/mL)	
MDO-0	5	0	57.3 ± 2.9	0.23 ± 0.01	-17.1 ± 1.7	4.7	0	-
MDO-5	5	5	63.0 ± 0.4	0.22 ± 0.02	-16.9 ± 1.9	4.6	1.7	0.37
MDO-10		10	72.3 ± 1.2	0.27 ± 0.02	-17.5 ± 2.0	4.7	2.9	0.62
MDO-15		15	110.7 ± 1.0	0.32 ± 0.03	-22.2 ± 2.9	4.8	4.1	0.85
MDO-20		20	190.4 ± 1.6	0.53 ± 0.03	-19.3 ± 2.3	4.8	4.3	0.90
MGO	10	10	33.2 ± 0.6	0.59 ± 0.05	-16.6 ± 2.8	4.8	7.1	0.73

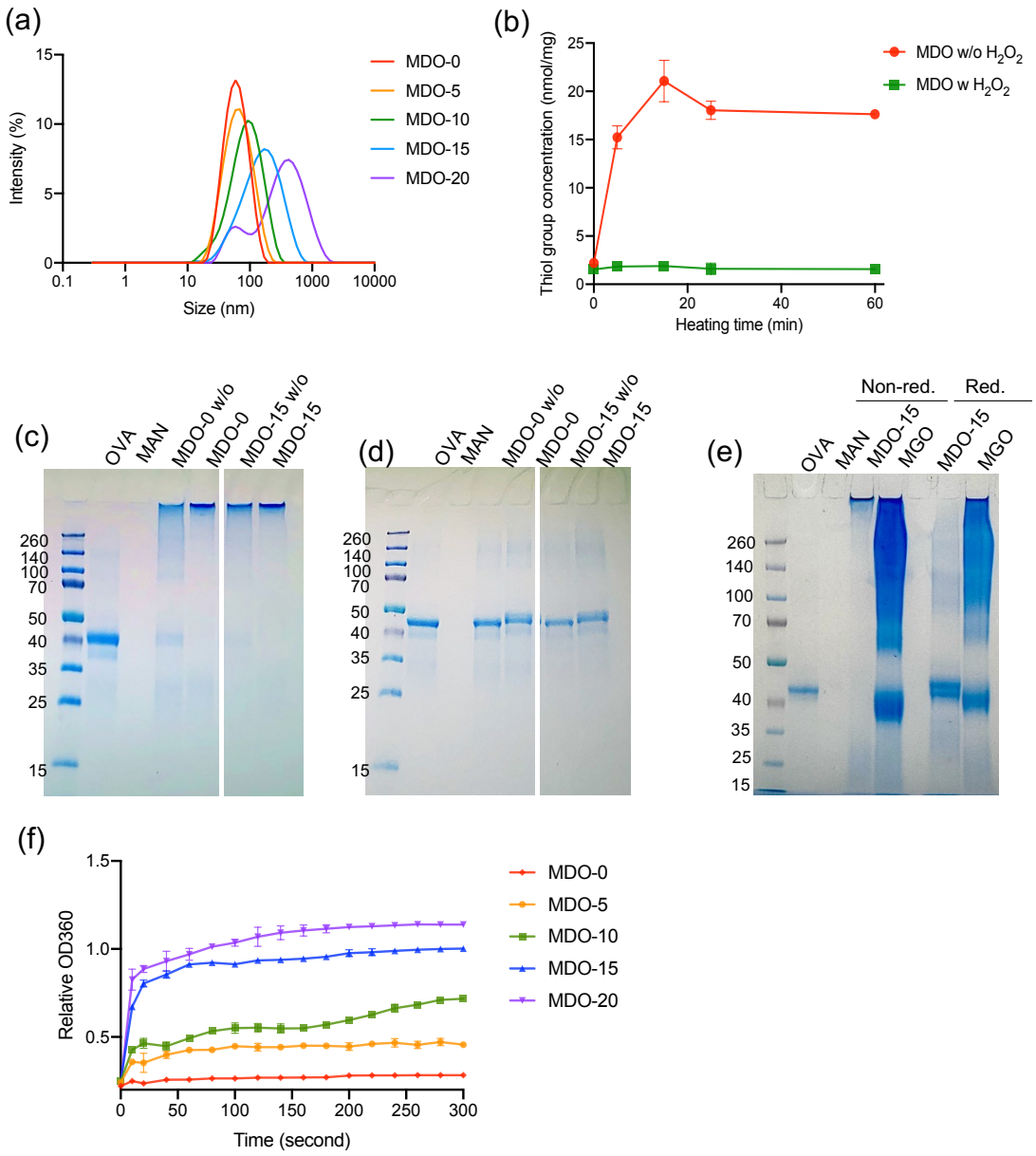

Fig. 3.2 (a) Effect of MAN modification on size distribution of MDO. (b) Free thiol groups in MDO without H_2O_2 treatment and MDO with H_2O_2 treatment. Data are expressed as the mean ± SEM (n = 3). SDS-PAGE of MDOs in (c) non-reduced condition, (d) reduced condition. (e) SDS-PAGE of MDO and MGO. Each well is loaded with a sample equivalent to 2.5 μg OVA. (f) Confirmation of mannan coating on the surface of MDO by *Con*A induced agglutination. Data are expressed as the mean ± SEM (n = 3).

3.2.2 MDO promoted OVA uptake, IL-10 production in BMDCs and induced T_{reg} cells *in vitro*

To evaluate the targeting ability of MDO to BMDC, I used fluorescence labelled MDO. Fig. 3.3a showed cellular uptake evaluated by flow cytometry. Mean fluorescence intensity (MFI) of BMDCs was increased with time and MDO-15 was more efficiently taken up by BMDCs than OVA and MDO-0. Fluorescence microscopy images after 30 min of incubation were shown in Fig. 3.3b. Bright fluorescence in cytosol were observed especially in MDO and MGO. These results demonstrated that formation of nanoparticles improved the uptake efficiency and modification of MAN further improved the uptake depending on receptors-mediated endocytosis. MDO also significantly promoted anti-inflammatory cytokine IL-10 production in BMDCs, which may help the differentiation of naïve T cell to T_{reg} cell (Fig. A1).

Next, I evaluated T cell activation by T cell recognition of the peptide/MHC complex presented by BMDC. BMDCs were first pulsed with MDO for 3 h, followed by co-culture with OT-II $CD4^+$ T cells for 24 h. Secreted IL-2 which is the measure of T cell activation were quantified by ELISA. BMDCs pulsed with MDO showed significantly high IL-2 level compared with those with OVA and MGO, indicating more peptides presentation in the MDO-pulsed BMDCs (Fig. 3.3c). Superior peptide presentation of MDO will be due to the efficient cellular uptake as well as the complete dissociation of MDO observed in Fig. 3.2e. The amount of peptide presentation on BMDCs may also affect the efficiency of T_{reg} induction and therefore I analyzed the generation of T_{reg} cells from naïve T cells. BMDCs treated with MDO and MGO induced higher percentage of T_{reg} cells than OVA, which was matched with peptide presentation level in Fig. 3.3c. This result indicated that MDO may regulate allergic response through T_{reg} cells (Fig. A2).

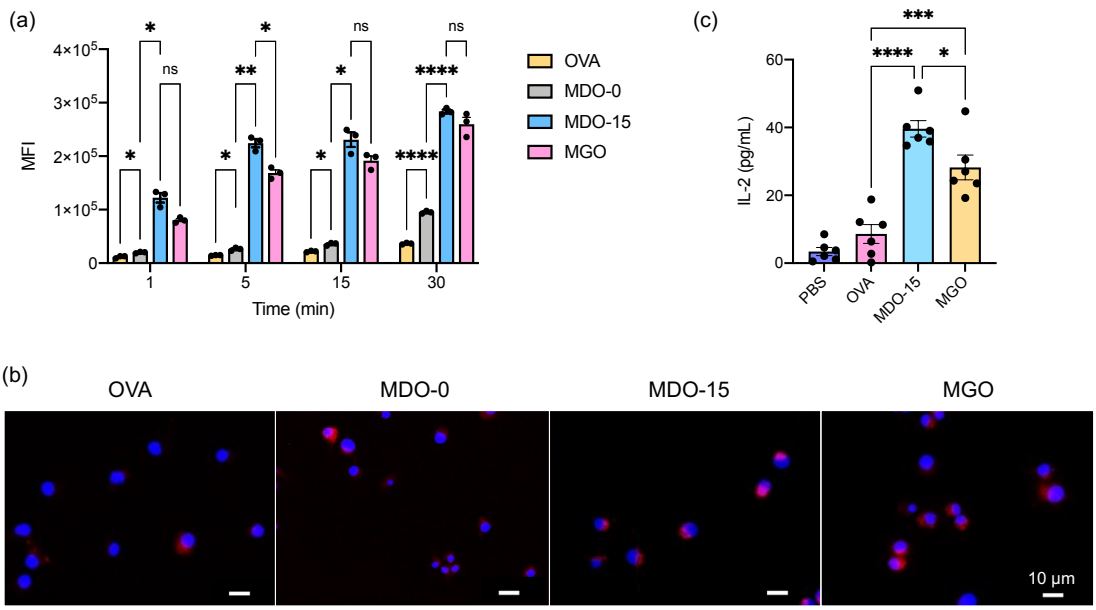

Fig. 3.3 Cellular uptake of NPs and antigen presenting by BMDCs. (a) Rhodamine labelled-OVA was used to prepare NPs. BMDCs were treated with OVA, MDO-0, MDO-15 and MGO at 37 °C. Flow cytometry analysis of MFI of BMDCs after each incubation time. (b) Fluorescence microscope images of BMDCs after 30 min incubation. Blue and red colors represent nucleus and rhodamine, respectively. (c) MHC class II-restricted antigen presentation and $CD4^+$ T cell stimulation. BMDCs were pulsed by PBS, OVA, MDO-15 or MGO for 3 h. After washing, co-cultured with OT-II $CD4^+$ T cells for 24 h. IL-2 secretion to culture supernatant was determined by ELISA. Data are expressed as the mean ± SEM (n = 3). *P < 0.05, **P < 0.01,***P < 0.001, ****P < 0.0001.

3.2.3 MDO reduced the risk of anaphylaxis

The safety of MDO during allergy treatment was evaluated by systemic anaphylaxis reaction. After intraperitoneal administration of various samples to OVA-immunized mice, reduction of rectal temperature due to the severe anaphylaxis reaction was monitored. OVA-administered group exhibited a decrease in rectal temperature to 3.5 °C below the basal temperature by 40 min (Fig. 3.4a). In contrast, mice administered with MDO-0, MDO-15 and MGO did not show the change of rectal temperature,

suggesting that MDO and MGO will not cause severe systemic anaphylaxis.

Potential risk of anaphylaxis of MDO-15 was evaluated by the binding of anti-OVA antibodies toward MDO-15 by ELISA. The anti-OVA antibodies collected from mice serum immunized with OVA was used here. Although MGO exhibited lower reactivity compared to naked OVA, it still remained a significant reactivities with anti-OVA antibodies, showing that crosslinking by glutaraldehyde remains binding sites toward anti-OVA antibodies. In contrast, MDO-0 and MDO-15 showed very low reactivity with anti-OVA antibodies (Fig. 3.4b), indicating that denaturation of OVA disrupted the structure of antibodies binding sites which was enough to inhibit the recognition of antibodies.[26] Thus, MDOs is safer formulation than MGO.

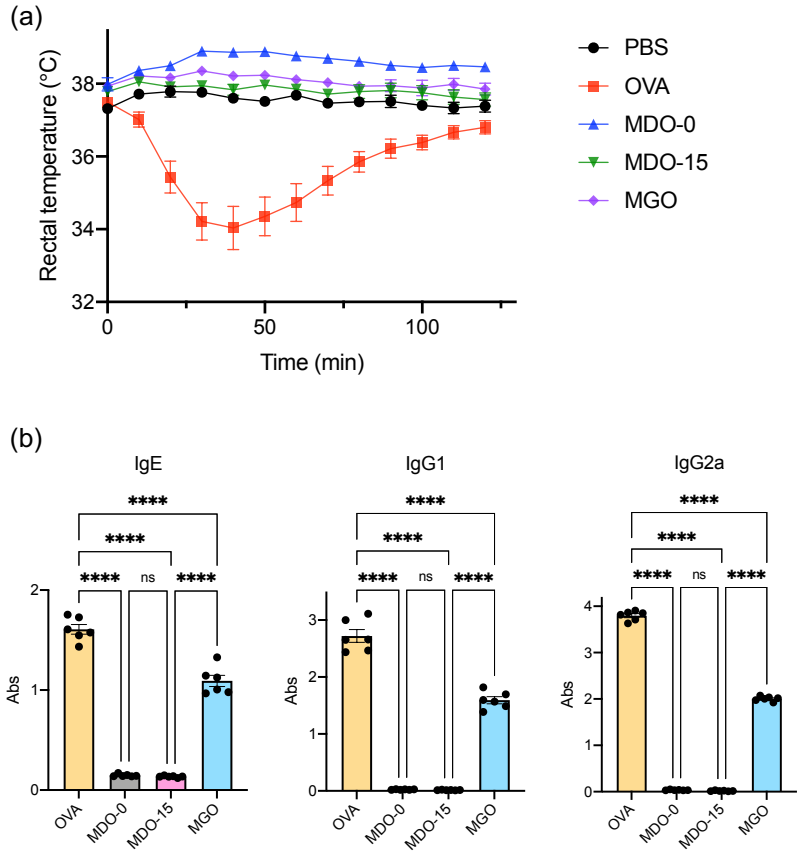

Fig. 3.4 MDO reduced systemic anaphylaxis by interfering anti-OVA antibodies recognition. (a) The change of rectal temperature in OVA-allergic mice (n = 6) sensitized with PBS, OVA, MDO-0, MDO-15 and MGO. (b) Reactivity of OVA, MDO-0, MDO-15 and MGO toward anti-OVA antibodies. Anti-OVA antibodies were collected from serum of OVA sensitized BLAB/c mice. Data are expressed as the mean ± SEM (n = 6). ****P < 0.0001, "ns" indicates no significant difference.

3.2.4 Prevention of allergic asthma by oral administration

Prevention and treatment performance of MDO toward allergic asthma was evaluated. Two administration routes, oral and subcutaneous was selected. For these experiments, MDO-15 was used as MDO because of its saturated MAN content with monomodal size distribution. First, prevention of allergic asthma by oral administration of MDO was evaluated by BALB/c mice model. Following the protocol shown in Fig. 3.5a, mice were treated with MDO orally for ten times, and then sensitized by OVA with alum through i.p. injection twice. Next, the mice were challenged four times by OVA through intranasal administration and after 24 hours, allergic symptoms were investigated. MDO triggered allergy prevention profile in the serum antibodies response (Fig. 3.5b). Naked OVA reduced serum anti-OVA IgE level, while MDO and MGO showed much stronger reduction in the IgE level. MDO increased T_H1-driven anti-OVA IgG2a level and reduced T_H2-driven IgG1 levels comparing with naked OVA and MGO. IgG2a inhibits IgE-mediated degranulation of mast cells and basophils.[27] As shown in Fig. 3.5c, suppression of neutrophile and eosinophile accumulation in bronchoalveolar lavage (BAL) fluid by MDO was similar level with naked OVA and MGO. This result matched with the reduction of T_H2 cytokines in BAL fluid (Fig. 3.5d). Levels of IL-6 and IL-5, which lead to recruitment of neutrophils and eosinophils, respectively[28], and IL-4 and IL-13 was related to IgE production. The histology of the lung tissues demonstrated that MDO suppressed infiltration of mononuclear cells more strongly than naked OVA and MGO (Fig. 3.5e). Collectively, it was concluded that MDO showed the superior prevention effect of allergic asthma response to naked OVA and MGO.

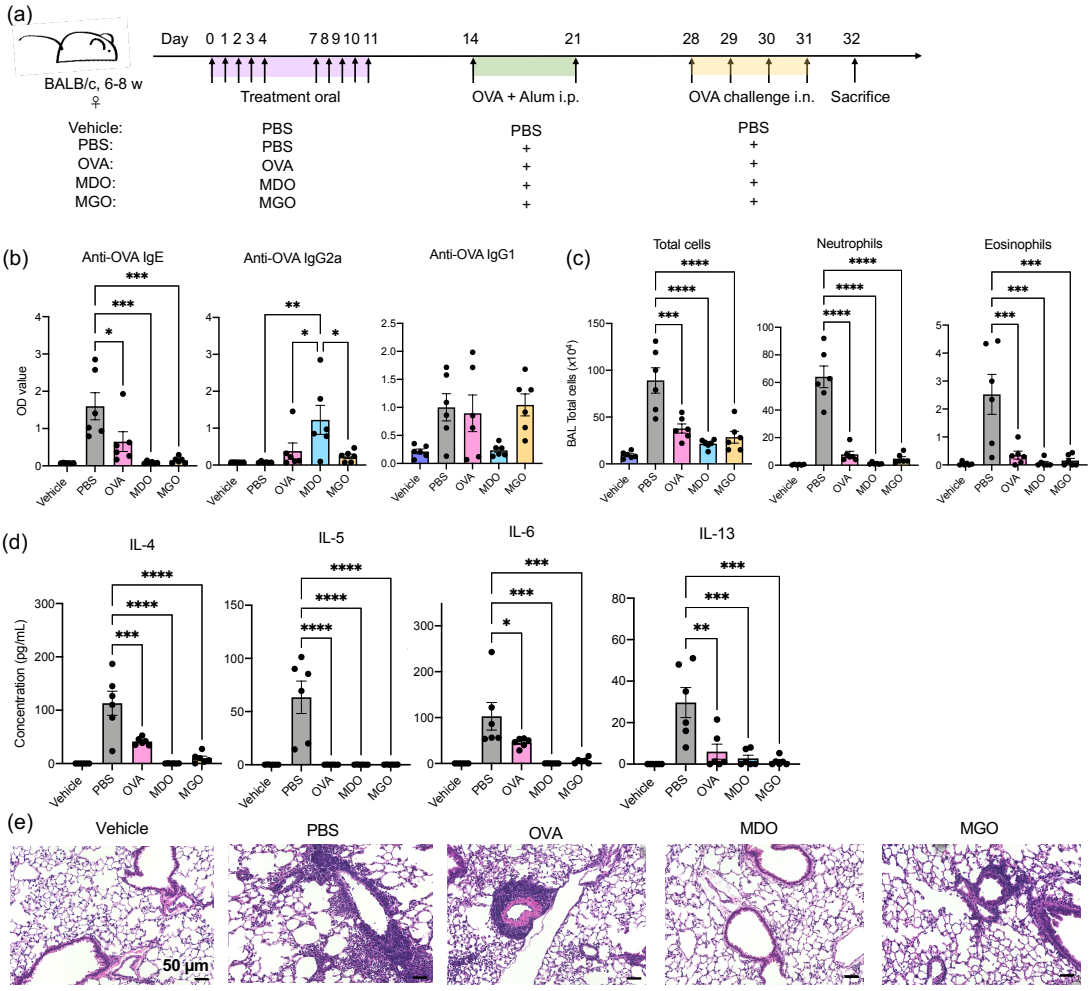

Fig. 3.5 Prevention of allergic asthma by oral administration. (a) Scheme of oral preventive administration. Mice were treated with PBS, OVA, MDO or MGO, equivalent as 500 μg of OVA, on days 0-4 and days 7-11, once per day. Mice were sensitized by 10 μg of OVA and 1 mg of alum through i.p. injection on days 14 and 21, finally challenged by 25 μg of OVA through intranasal route on days 28-31. One day after OVA challenge, mice were sacrificed. (b) Serum anti-OVA antibodies titer were measured by ELISA. OD, optical density. (c) Total cell, neutrophil and eosinophil counts in BAL fluid. Cytospin of each sample was prepared, stained by Diff-Qick and counted. (d) T_H2 cytokines (IL-4, IL-5, IL-6, IL-13) concentration in BAL fluid were measured by Cytometric Bead Array Kit. (e) Histological sections of lung tissue. Slides were stained by H&E. The scale bar represent 50 μm. Data are expressed as the mean ± SEM ($n = 6$). *$P < 0.05$, **$P < 0.01$,***$P < 0.001$, ****$P < 0.0001$.

3.2.5 Treatment of allergic asthma by oral administration

The allergy treatment by MDO were evaluated for the OVA-sensitized mice following the protocol shown in Fig. 3.6a. The superior effect of MDO than naked OVA and MGO was more clearly observed here than prevention. IgE reduction by MDO was stronger than naked OVA and MGO (Fig. 3.6b). MDO significantly reduced accumulation of neutrophils and eosinophils in the BAL fluid (Fig. 3.6c). MDO and MGO reduced IL-4 and IL-6 levels in BAL fluid (Fig. 3.6d). Although there is no statistical significance, MDO tended to reduce IL-5 and IL-13 more than MGO. Histological evaluation of migration of mononuclear cells showed that MDO reduced more than MGO and naked OVA (Fig. 3.6e). These results revealed that although the treatment of already-established allergic immune response is more difficult than prevention, MDO showed superior therapeutic effect.

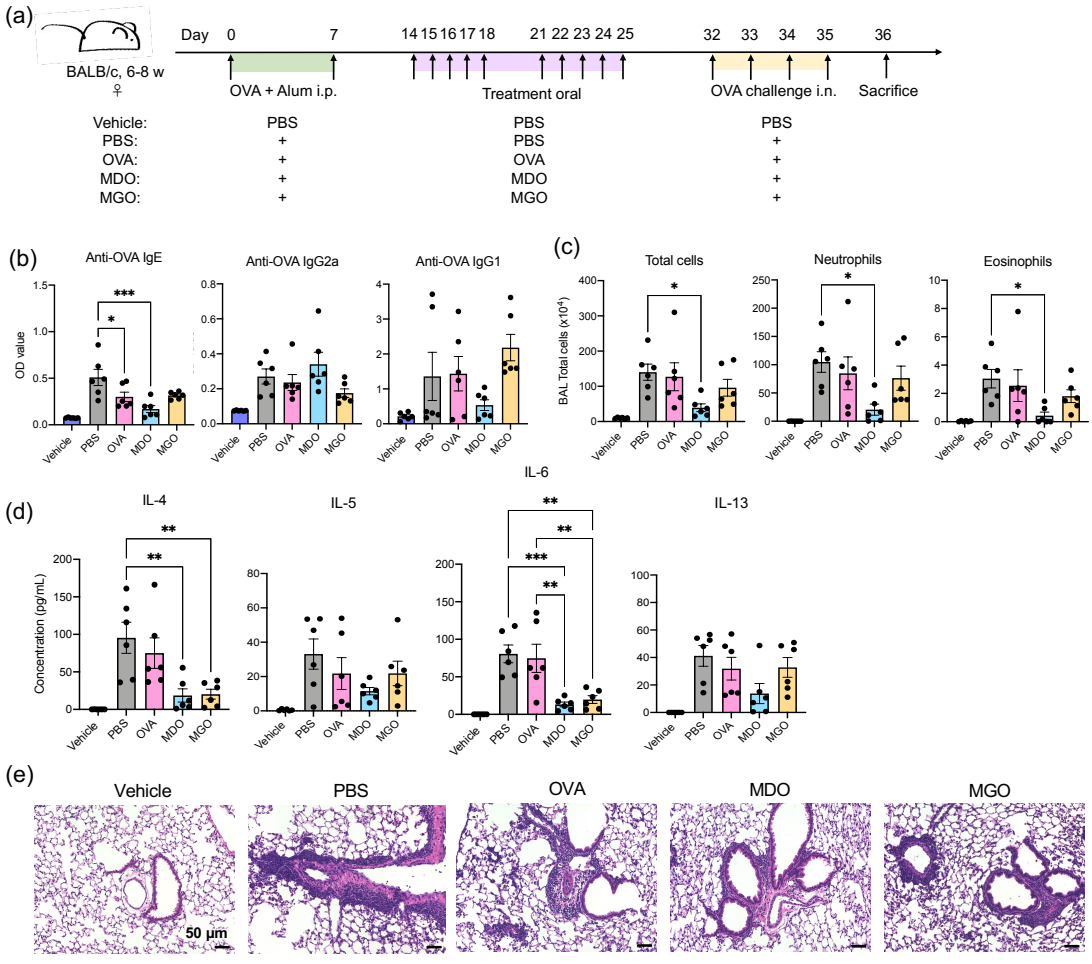

Fig. 3.6 Treatment of allergic asthma by oral administration. (a) Scheme of oral treatment. Mice were sensitized by OVA and alum on days 0 and 7, then received oral administration of PBS, OVA, MDO or MGO, equivalent as 500 μg of OVA, on days 14-18 and days 21-25. Finally challenged by OVA through intranasal route on days 32-35. One day after OVA challenge, mice were sacrificed. (b) Serum anti-OVA antibodies titer were measured by ELISA. OD, optical density. (c) Differential cell counts in BAL fluid. (d) T_H2 cytokines concentration in BAL fluid were measured by Cytometric Bead Array Kit. (e) Histological sections of lung tissue. The scale bar represent 50 μm. Data are expressed as the mean ± SEM (n = 6). *P < 0.05, **P < 0.01,***P < 0.001, ****P < 0.0001.

3.2.6 Prevention and treatment of allergic asthma by subcutaneous administration

Next, effect of subcutaneous administration route was investigated. For prevention of allergy, mice were treated with MDO subcutaneously for 6 times, and the subsequent steps were the same as for oral protocol (Fig. 3.7a). The obtained results were basically same with oral administration but in the granulocyte accumulation (Fig. 3.7c) and cytokine level in BAL fluid (Fig. 3.7d), superior effect of MDO to MGO was clearer than oral administration. For the allergy treatment, MDO was administrated six times orally (Fig. 3.8a). The results were basically same with oral treatment and subcutaneous treatment (Fig. 3.8 b-e). These results demonstrated that prevention and treatment effect of MDO by subcutaneous administration is superior to naked OVA and MGO.

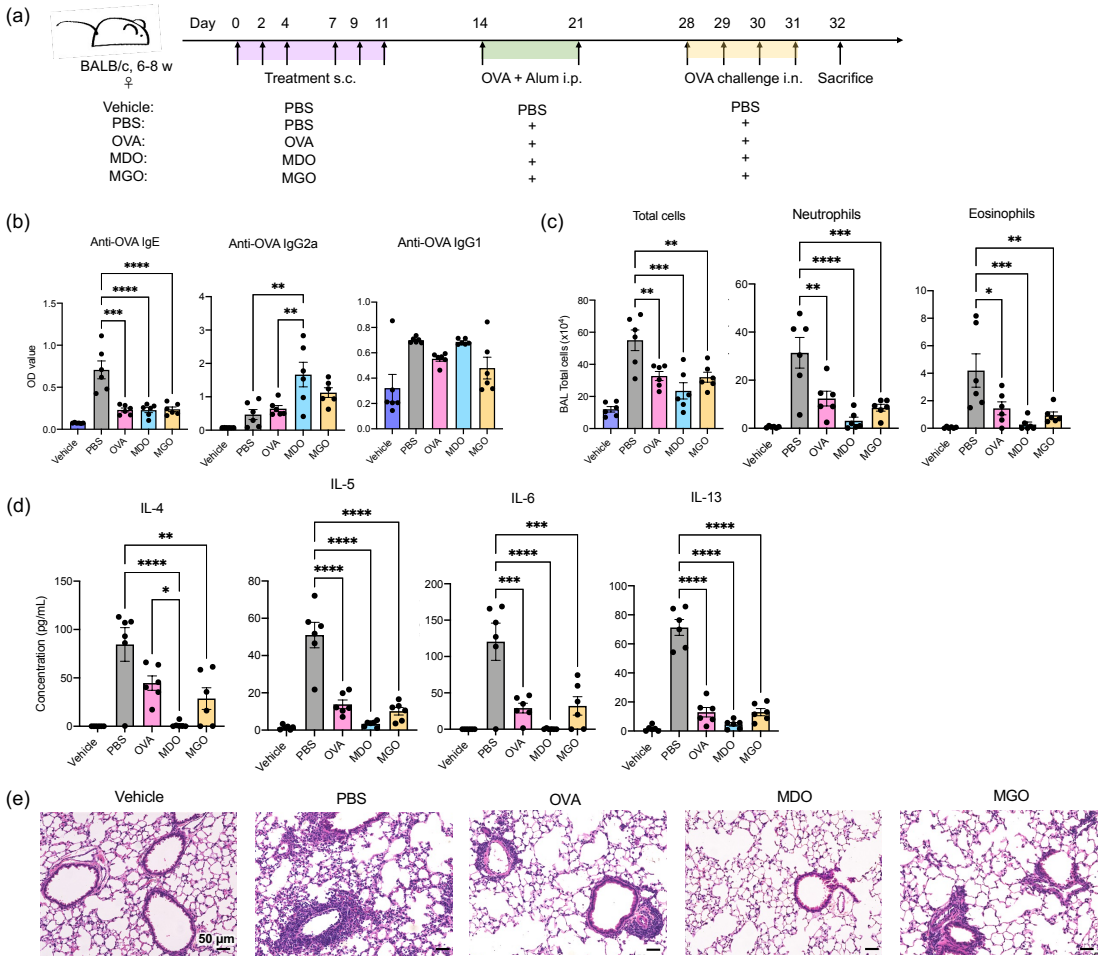

Fig. 3.7 Prevention of allergic asthma by subcutaneous administration. (a) Scheme of oral treatment. Mice were treated with PBS, OVA, MDO or MGO, equivalent as 20 μg of OVA, on days 0, 2, 4, 7, 9 and 11. The subsequent steps were same as oral administration (Fig. 5a). (b) Serum anti-OVA antibodies titer were measured by ELISA. OD, optical density. (c) Differential cell counts in BAL fluid. (d) T_H2 cytokines concentration in BAL fluid were measured by Cytometric Bead Array Kit. (e) Histological sections of lung tissue. The scale bar represent 50 μm. Data are expressed as the mean ± SEM ($n = 6$). *$P < 0.05$, **$P < 0.01$,***$P < 0.001$, ****$P < 0.0001$.

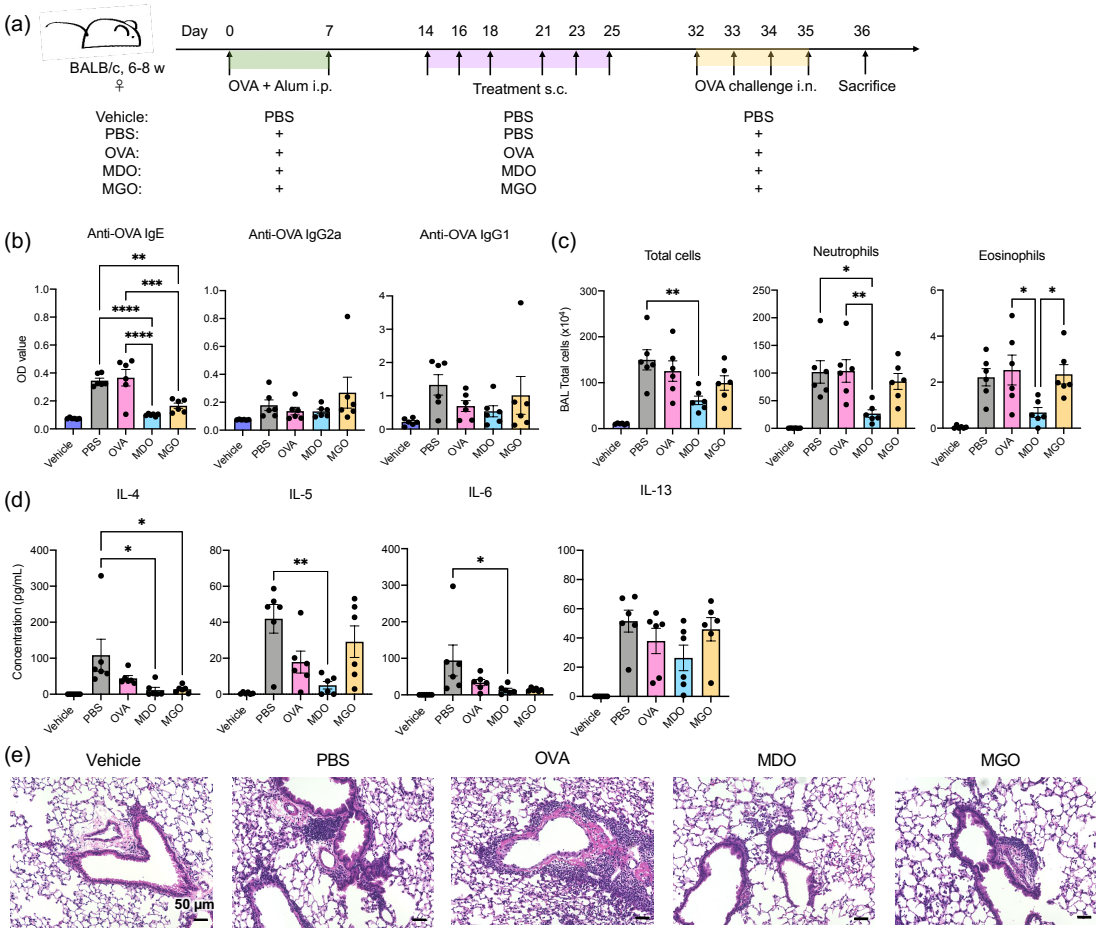

Fig. 3.8 Treatment of allergic asthma by subcutaneous administration. (a) Scheme of oral treatment. Mice were treated with PBS, OVA, MDO or MGO, equivalent as 20 μg of OVA, on days 14, 16, 18, 21, 23 and 25. The subsequent steps were same as oral administration (Fig. 6a). (b) Serum anti-OVA antibodies titer were measured by ELISA. OD, optical density. (c) Differential cell counts in BAL fluid. (d) T_H2 cytokines concentration in BAL fluid were measured by Cytometric Bead Array Kit. (e) Histological sections of lung tissue. The scale bar represent 50 μm. Data are expressed as the mean ± SEM ($n = 6$). *$P < 0.05$, **$P < 0.01$,***$P < 0.001$, ****$P < 0.0001$.

3.3 Summary

In this study, I developed an approach for the preparation of MAN-coated OVA NP that can target DCs without affecting OVA dissociation. Thermal aggregation of OVA and protein part of MAN formed core of NP and MAN presented on the surface of NP. Intermolecular disulfide bonds were formed by oxidation to crosslink OVA and MAN, but we demonstrated that MDO was degradable in DCs and DCs could present antigen to T cells. Due to the coating of MAN, MDO was possible to target DCs and induce tolerogenic DC. MDO did not induce systemic anaphylaxis in allergic mice because of low reactivity with anti-OVA antibodies. Furthermore, MDO showed preventive effect and therapeutic effect to allergic asthma through both oral and subcutaneous routes. Hence, I provided an effective and safe preventive and therapeutic strategy for allergy treatment.

3.4 Experimental section

3.4.1 Materials

Ovalbumin (OVA, grade V), mannan protein (MAN), concanavalin A (*Con*A), L-cysteine, tris(hydroxymethyl)aminomethane (Tris) and lipopolysaccharide (LPS, O111:B4) were purchased from Sigma-Aldrich (St. Louis, MO, USA). Hydrogen peroxide (H_2O_2, 30 wt % in water), dithiothreitol (DTT), sulfuric acid (98%, H_2SO_4), calcium chloride ($CaCl_2$), magnesium chloride hexahydrate ($MgCl_2$), sodium dodecyl sulfate (SDS), glycine, sodium chloride (NaCl) and Mildform 10N (10 % Formalin neutral buffer solution) were purchased from FUJIFILM Wako Pure Chemical Corporation (Osaka, Japan). 2,2′-dinitro-5,5′-dithiodi-benzoic acid (DTNB) was purchased from Dojindo Laboratories (Kumamoto, Japan). 5(6)-Carboxytetramethylrhodamine N-succinimidyl ester (HNS- rhodamine) and imject™ Alum were purchased from Thermo Fisher Scientific (Carlsbad, CA, USA). NuPAGE sample reducing agent (10x), NuPAGE LDS sample buffer (4x), ELISA-ELISPOT diluent (5x), TMB (3,3′,5,5′-tetramethylbenzidine) solution (1x), HRP-conjugated streptavidin (horseradish peroxidase) were purchased from Invitrogen (Carlsbad, CA, USA). QuickBlue staining solution was purchased from BioDynamics Laboratory Inc. (Tokyo, Japan). Protein assay CBB solution, 4% paraformaldehyde solution (PFA), disodium hydrogen phosphate and sodium dihydrogen phosphate were purchased from Nacalai Tesque Inc. (Kyoto, Japan). D-glucose was purchased from Tokyo Chemical Industry Co., Ltd. (Tokyo, Japan). Biotin anti-mouse IgE Antibody, biotin anti-mouse IgG1 Antibody, biotin anti-mouse IgG2a Antibody were purchased from BioLegend (San Diego, CA, USA).

3.4.2 Preparation of MAN-coated OVA nanoparticles

OVA and MAN were dissolved in 10 mM phosphate buffer (PB) with 50 mM

NaCl (pH 7.4) and kept overnight at 4 ℃, respectively. 5 mg/mL of OVA and various concentration of MAN were mixed to obtain the working solution, respectively. 1 mL of the working solution was heated at 85 ℃ for 60 min. The NPs formation was stopped by cooling down in an ice bath, here, I obtained MAN-OVA NPs without disulfide bonds. H_2O_2 was added to the NP solution to 0.3 wt % and reacted overnight at 4 ℃, in order to form intermolecular disulfide bonds.[25] Free OVA, MAN and H_2O_2 were removed by ultrafiltration (100 kDa Amicon, Merck Millipore, Temecula, CA, USA), then disulfide-crosslinked MAN-OVA NPs (MDO) were recovered for further evaluation. MDO in 1 wt % of glucose solution were lyophilized for a long time storage.

For positive control, 20 mg/mL of OVA was mixed with 20 mg/mL of MAN in equal volume, then conjugated by glutaraldehyde (final concentration 25 mM) to obtain MAN-OVA conjugation (MGO).

3.4.3 Characterizations

The particle size, distribution and zeta potential were determined by dynamic light scattering spectrophotometer (DLS, Zetasizer Pro ZSU3200, Malvern, UK) at 25 ℃.

3.4.4 OVA and MAN quantification

Protein assay CBB solution based on Bradford method was used to measure OVA concentration.[29] OVA standard was preformed 2-fold serial dilution and linear regression was used to fit the standard curve. Samples were mixed with CBB solution, and incubated at room temperature for 10 min. Absorbance were measured at 595 nm on a plate reader (Infinite200PRO M Plex, Tecan, Switzerland).

Phenol-sulfuric acid assay was used to measure MAN concentration.[30] MAN was gradient diluted and used to make standard curve. 5% (w/v) phenol was mixed with samples, followed by adding H_2SO_4 and mixing well. Mixtures were incubated for 40 min at room temperature and absorbance were measured at 490 nm.

3.4.5 Sulfhydryl (SH) group quantification

Exposed SH group of OVA, MAN, MDO (Without H_2O_2 treatment) and MDO were quantified by Ellman's regent.[31] Mixed sample solutions and DTNB solution were incubated at room temperature for 15 min, then measured absorbance at 412 nm. Plot the values obtained for L-cysteine to generate a standard curve.

3.4.6 Confirmation of the intermolecular disulfide bond

Denaturing SDS-PAGE was used to investigate formation mechanism of MDO (without H_2O_2) and MDO (with H_2O_2). 2.5 μL of samples were mixed with 2.5 μL of 4× LDS sample buffer. In reducing condition, 1 μL of 10× reducing agent and 4 μL of water were added, in non-reducing condition, 5 μL of water was added. Total 10 μL of mixtures were heated at 95 ℃ for 3 min. After running electrophoresis, staining and washing, the gel was scanned on a scanner.

3.4.7 *Con*A agglutination assay

*Con*A agglutination assay was performed as previous report.[32] Briefly, *Con*A was dissolved into phosphate buffered saline (PBS, 10 mM, pH 7.4) with 5 mM of $CaCl_2$ and 5mM of $MgCl_2$ to obtain 1 mg/mL *Con*A solution. 40 μL of samples were mixed with 200 μL of *Con*A solution. The turbidity were measured at 360 nm for 300 s.

3.4.8 Mice

C57BL/6J mice (7-8 weeks old, male) and BALB/c mice (6-8 weeks old, female) were purchased from Kyudo Co., Ltd. (Saga, Japan). Mice were fed with CE-2 (Kyudo Co., Ltd., Saga, Japan), with access to bedding and water. Cage changes were

performed in a laminar flow hood. Mice had a cycle of 12 h of light and 12 h of darkness. OT-II Tg/wt, Ly5.1/Ly5.1 mice were obtained from Prof. Yoshihiro Baba. Animal experiments were performed according to the Guidelines for animal care and use committee, Kyushu University (A21-431, A21-425).

3.4.9 Differentiation and isolation of bone marrow dendritic cells (BMDCs) from bone marrow

Bone marrow cells were obtained from the tibias and the femurs of C57BL/6J mice. Bone marrow cells were grown in advanced RPMI 1640 medium (Thermo Fisher Scientific, CA, USA) containing 10 % fetal bovine serum (FBS, Thermo Fisher Scientific, CA, USA), 50 μM 2-mercaptoethanol, 2 mM GlutaMAX™ Supplement (Thermo Fisher Scientific, CA, USA), 100 U/mL penicillin, 100 μg/mL streptomycin, 10 mM HEPES buffer solution (Nacalai Tesque Inc., Kyoto, Japan), 20 ng/mL recombinant mouse granulocyte–macrophage colony-stimulating factor (GM-CSF), 10 ng/mL recombinant mouse Interleukin-4 (IL-4) and 5 ng/mL recombinant mouse FMS-like tyrosine kinase 3 ligand (FLT-3L) for 6 days. Then LPS was added to medium in day 7. After stimulation with LPS for 24 hours, BMDCs were first negatively selected from bone marrow cells with biotin anti-mouse F4/80 and streptavidin nanobeads, then positively selected with anti-mouse CD11c nanobeads.

3.4.10 Cellular uptake

OVA-rhodamine was used to make fluorescent labelled NPs. BMDCs (2×10^5 cells/well) were seeded in a 12-well plate and cultured with rhodamine labeled OVA, MDO-0, MDO-15 and MGO in different times. Dead cells were stained with SYTOX™ Green (Thermo Fisher Scientific, MA, USA). Mean fluorescence intensity (MFI) of rhodamine in BMDCs were determined by flow cytometry (CyroFLEX-S, Beckman Coulter Inc., IN, USA). For observation in florescence microscope, BMDC (5×10^4

cells/well) were seeded in a 96-well glass plate. After incubation with rhodamine labeled samples, fixed with 4% PFA, then stained with 10 % Hoechst. BMDCs were observed for the uptake of NPs-rhodamine by florescence microscope (BZ-X800, KEYENCE, Osaka, Japan)

3.4.11 MHC class II-restricted OVA presentation

BMDCs were seeded in 96-well plates (5×10^4 cells/well) and pulsed with PBS, OVA, MDO-15 and MGO for 3 h, respectively. Next, BMDCs and OT-II $CD4^+$ T cells (2.5×10^5 cells/well) were co-cultured for 24 h. OT-II $CD4^+$ T cells were isolated from the spleen of OT-II mice with Mouse CD4 T Cell Isolation Kit (Biolegend, San Diego, CA, USA). IL-2 concentration in the culture medium was measured by IL-2 Mouse ELISA Kit (Thermo Fisher Scientific, CA, USA).

3.4.12 OVA-specific antibodies reactivity with NPs

BALB/c mice were sensitized by intraperitoneal (i.p.) injecting 10 μg of OVA and 1 mg of alum in 200 μL of PBS thrice, 7 days apart. Mice were sacrificed 7 days after last sensitization and peripheral blood was collected by retro-orbital bleeding. Serum were collected for later measurement.

Indirect-ELISA protocol was used. 100 μL of OVA, MDO-0, MDO-15 and MGO (as 100 μg/mL of OVA) were coated on 96-well plate for 24 h at 4 ℃. The plate was blocked with ELISA-ELISPOT diluent, then added serial diluted serum to the plate, incubated at 4 ℃ overnight. Biotin anti-mouse IgE antibody, biotin anti-mouse IgG1 antibody and biotin anti-mouse IgG2a antibody were added, respectively. After incubation, streptavidin-HRP was added and TMB solution was used as substrate. Finally, the reaction was stopped and optical density (OD) of each well were measured at 450 nm.

3.4.13 Passive systemic anaphylaxis

BALB/c mice were sensitized by i.p. injecting 10 μg of OVA and 1 mg of alum in 200 μL of PBS at days 0 and days 14. Mice were challenged by 200 μg OVA, MDO-0, MDO-15 and MGO (containing 200 μg of OVA) by i.p. injection at days 28. After challenge, rectal temperature were measured by thermometer (Physitemp PTM1, Muramachi Kikai Co., Ltd., Tokyo, Japan) every 10 min.

3.4.14 Induction of tolerance by administration of NPs in mouse allergic asthma model

6-8 week old BALB/c mice were used to establish allergic asthma model. For preventive administration protocol, mice were received (a) oral administration of PBS, OVA, MDO and MGO (containing 0.5 mg of OVA) on day 0-4, and 7-11, or (b) subcutaneous (s.c.) administration of PBS, OVA, MDO and MGO (containing 20 μg of OVA) on day 0, 2, 4, 7, 9 and 11. Mice were sensitized by i.p. injection of 10 μg of OVA and 1 mg of alum on day 14 and 21. Finally, mice were received 25 μg of OVA challenge by intranasal administration on day 28-31. Mice were sacrificed on day 32, BAL fluid, peripheral blood, lung tissues were collected.

For therapuetic administration protocol, mice were first sensitized by i.p. injection of 10 μg of OVA and 1 mg of alum on day 0 and 7. Next, mice were received (a) oral administration of PBS, OVA, MDO and MGO (containing 0.5 mg of OVA) on day 14-18, and 21-25, or (b) subcutaneous (s.c.) administration of PBS, OVA, MDO and MGO (containing 20 μg of OVA) on day 14, 16, 18, 21, 23 and 25. Finally, mice were received 25 μg of OVA challenge by intranasal administration on day 32-35. Mice were sacrificed on day 36, BAL fluid, peripheral blood, lung tissues were collected.

3.4.15 Analysis of BAL fluid cell composition

The mouse lung was lavaged through tracheal cannula with 1 mL cold PBS. After centrifugation, cells were resuspended in 500 µl PBS and counted. Cytospins were prepared by using Cytospin 4 (Thermo Fisher Scientific, Carlsbad, CA, USA) and stained with Diff-Quik (Sysmex, Kobe, Japan). The cell differentials were evaluated by standard morphology.

3.4.16 Quantification of cytokines in BAL fluid

IL-4, IL-5, IL-6 and IL-13 in BAL fluid were detected by using BD Cytometric Bead Array (BD Life Sciences-Biosciences, NJ, USA). Then measured in flow cytometer (CyroFLEX-S, Beckman Coulter Inc., IN, USA).

3.4.17 Quantification of OVA-specific antibodies in serum

Blood was collected as described before. Serum was diluted in ELISA-ELISPOT diluent and OVA-specific IgE, IgG1 and IgG2a were evaluated by indirect-ELISA protocol as described before.

3.4.18 Histological analysis of lung tissue

Lungs were perfused by injection of PBS into the right ventricle of the heart. Then isolated lungs from mice and inflated lungs with 10 % formalin solution through trachea. Inflated lungs were fixed in 10 % formalin, embedded in paraffin and stained by hematoxylin and eosin (H&E) staining. Stained sections were used to evaluate the airway inflammation in lungs.

3.4.19 Statistical analysis

Statistical analyses were performed using GraphPad Prism 9 (GraphPad Software, La Jolla, CA, USA). One-way ANOVA was used to determine the significance of means from all groups. Then the Tukey's multiple comparisons was used to compare every mean to every other mean. *$P < 0.05$, **$P < 0.01$,***$P < 0.001$, ****$P < 0.0001$.

3.5 References

1. R. Pawankar, G. Canonica, S. Holgate, R. Lockey and M. Blaiss, *Milwaukee, WI: World Allergy Organization*, 2011, **3**, 156-157.
2. S. M. Jones, E. H. Kim, K. C. Nadeau, A. Nowak-Wegrzyn, R. A. Wood, H. A. Sampson, A. M. Scurlock, S. Chinthrajah, J. Wang, R. D. Pesek, S. B. Sindher, M. Kulis, J. Johnson, K. Spain, D. C. Babineau, H. Chin, J. Laurienzo-Panza, R. Yan, D. Larson, T. Qin, D. Whitehouse, M. L. Sever, S. Sanda, M. Plaut, L. M. Wheatley and A. W. Burks, *The Lancet*, 2022, **399**, 359-371.
3. M. H. Shamji and S. R. Durham, *J Allergy Clin Immunol*, 2017, **140**, 1485-1498.
4. P. G. o. C. Investigators, B. P. Vickery, A. Vereda, T. B. Casale, K. Beyer, G. du Toit, J. O. Hourihane, S. M. Jones, W. G. Shreffler, A. Marcantonio, R. Zawadzki, L. Sher, W. W. Carr, S. Fineman, L. Greos, R. Rachid, M. D. Ibanez, S. Tilles, A. H. Assa'ad, C. Nilsson, N. Rupp, M. J. Welch, G. Sussman, S. Chinthrajah, K. Blumchen, E. Sher, J. M. Spergel, F. E. Leickly, S. Zielen, J. Wang, G. M. Sanders, R. A. Wood, A. Cheema, C. Bindslev-Jensen, S. Leonard, R. Kachru, D. T. Johnston, F. C. Hampel, Jr., E. H. Kim, A. Anagnostou, J. A. Pongracic, M. Ben-Shoshan, H. P. Sharma, A. Stillerman, H. H. Windom, W. H. Yang, A. Muraro, J. M. Zubeldia, V. Sharma, M. J. Dorsey, H. J. Chong, J. Ohayon, J. A. Bird, T. F. Carr, D. Siri, M. Fernandez-Rivas, D. K. Jeong, D. M. Fleischer, J. A. Lieberman, A. E. J. Dubois, M. Tsoumani, C. E. Ciaccio, J. M. Portnoy, L. E. Mansfield, S. B. Fritz, B. J. Lanser, J. Matz, H. N. G. Oude Elberink, P. Varshney, S. G. Dilly, D. C. Adelman and A. W. Burks, *N Engl J Med*, 2018, **379**, 1991-2001.
5. Y. Su, E. Romeu-Bonilla and T. Heiland, *Hum Vaccin Immunother*, 2017, **13**, 2402-2415.
6. G. W. Scadding, M. A. Calderon, M. H. Shamji, A. O. Eifan, M. Penagos, F. Dumitru, M. L. Sever, H. T. Bahnson, K. Lawson, K. M. Harris, A. G. Plough, J. L. Panza, T. Qin, N. Lim, N. K. Tchao, A. Togias, S. R. Durham and G. S. T. Immune Tolerance Network, *JAMA*, 2017, **317**, 615-625.

7. A. W. Burks, S. M. Jones, R. A. Wood, D. M. Fleischer, S. H. Sicherer, R. W. Lindblad, D. Stablein, A. K. Henning, B. P. Vickery, A. H. Liu, A. M. Scurlock, W. G. Shreffler, M. Plaut, H. A. Sampson and R. Consortium of Food Allergy, *N Engl J Med*, 2012, **367**, 233-243.
8. H. Wang, X. Lin, C. Hao, C. Zhang, B. Sun, J. Zheng, P. Chen, J. Sheng, A. Wu and N. Zhong, *Allergy*, 2006, **61**, 191-197.
9. G. Passalacqua, A. Rogkakou, M. Mincarini and G. W. Canonica, *Asthma Res Pract*, 2015, **1**, 6.
10. F. Asamoah, A. Kakourou, S. Dhami, S. Lau, I. Agache, A. Muraro, G. Roberts, C. Akdis, M. Bonini, O. Cavkaytar, B. Flood, K. Izuhara, M. Jutel, O. Kalayci, O. Pfaar and A. Sheikh, *Clin Transl Allergy*, 2017, **7**, 25.
11. M. Emara, P. J. Royer, J. Mahdavi, F. Shakib and A. M. Ghaemmaghami, *J Biol Chem*, 2012, **287**, 5756-5763.
12. P. J. Royer, M. Emara, C. Yang, A. Al-Ghouleh, P. Tighe, N. Jones, H. F. Sewell, F. Shakib, L. Martinez-Pomares and A. M. Ghaemmaghami, *J Immunol*, 2010, **185**, 1522-1531.
13. F. Salazar, L. Hall, O. H. Negm, D. Awuah, P. J. Tighe, F. Shakib and A. M. Ghaemmaghami, *J Allergy Clin Immunol*, 2016, **137**, 1841-1851 e1842.
14. P. B. Wright, E. McDonald, A. Bravo-Blas, H. M. Baer, A. Heawood, C. C. Bain, A. M. Mowat, S. L. Clay, E. V. Robertson, F. Morton, J. S. Nijjar, U. Z. Ijaz, S. W. F. Milling and D. R. Gaya, *Sci Rep*, 2021, **11**, 19616.
15. S. Sirvent, I. Soria, C. Cirauqui, B. Cases, A. I. Manzano, C. M. Diez-Rivero, P. A. Reche, J. Lopez-Relano, E. Martinez-Naves, F. J. Canada, J. Jimenez-Barbero, J. Subiza, M. Casanovas, E. Fernandez-Caldas, J. L. Subiza and O. Palomares, *J Allergy Clin Immunol*, 2016, **138**, 558-567 e511.
16. M. Ishii, A. Koyama, H. Iseki, H. Narumi, N. Yokoyama and N. Kojima, *Int Immunopharmacol*, 2010, **10**, 1041-1046.
17. Q. Liu, X. Wang, X. Liu, S. Kumar, G. Gochman, Y. Ji, Y. P. Liao, C. H. Chang, W. Situ, J. Lu, J. Jiang, K. C. Mei, H. Meng, T. Xia and A. E. Nel, *ACS Nano*, 2019, **13**, 4778-4794.

18. V. Apostolopoulos, G. A. Pietersz, B. E. Loveland, M. S. Sandrin and I. F. McKenzie, *Proceedings of the National Academy of Sciences*, 1995, **92**, 10128-10132.
19. E. E. Weinberger, M. Himly, J. Myschik, M. Hauser, F. Altmann, A. Isakovic, S. Scheiblhofer, J. Thalhamer and R. Weiss, *J Control Release*, 2013, **165**, 101-109.
20. P. J. Tacken, I. J. de Vries, R. Torensma and C. G. Figdor, *Nat Rev Immunol*, 2007, **7**, 790-802.
21. W. W. Unger and Y. van Kooyk, *Curr Opin Immunol*, 2011, **23**, 131-137.
22. H. D. Singh, G. Wang, H. Uludag and L. D. Unsworth, *Acta Biomater*, 2010, **6**, 4277-4284.
23. B. E. Cham, K. Vickery, R. Tohidi-Esfahani and Y. Cossart, *J Virol Methods*, 2006, **137**, 160-163.
24. I. Delrue, P. L. Delputte and H. J. Nauwynck, *Vet Res*, 2009, **40**, 62.
25. Y. Wen, H. Dong, K. Wang, Y. Li and Y. Li, *ACS Appl Mater Interfaces*, 2018, **10**, 11457-11466.
26. J. Golias, M. Schwarzer, M. Wallner, M. Kverka, H. Kozakova, D. Srutkova, K. Klimesova, P. Sotkovsky, L. Palova-Jelinkova, F. Ferreira and L. Tuckova, *PLoS One*, 2012, **7**, e37156.
27. C. Uermosi, R. R. Beerli, M. Bauer, V. Manolova, K. Dietmeier, R. B. Buser, T. M. Kundig, P. Saudan and M. F. Bachmann, *J Allergy Clin Immunol*, 2010, **126**, 375-383.
28. C. Radermecker, R. Louis, F. Bureau and T. Marichal, *Curr Opin Immunol*, 2018, **54**, 28-34.
29. M. M. Bradford, *Analytical Biochemistry*, 1976, **72**, 248-254.
30. M. DuBois, K. A. Gilles, J. K. Hamilton, P. A. Rebers and F. Smith, *Analytical Chemistry*, 1956, **28**, 350-356.
31. G. L. Ellman, *Archives of Biochemistry and Biophysics*, 1959, **82**, 70-77.
32. Z. Cui and R. J. Mumper, *J Control Release*, 2002, **81**, 173-184.

CHAPTER 4

Preparation of mannan-coated antigen nanoparticles using human serum albumin as a non-antigenic proteinous matrix

4.1 Introduction

Allergen immunotherapy (AIT) aims to induce antigen-specific immune tolerance via inducing regulatory T cells through antigen presentation by dendritic cells (DCs).[1] Nanoparticles (NPs) such as emulsions and liposomes have used into pre-clinical allergy treatment in recent years. In contrast to conventional AIT using naked antigens, encapsulation of antigens within NPs made them resistant to degradation and prevented recognition of antigens by immunoglobulin E (IgE).[2, 3] Modification of ligands on the surface of NPs provides targeting ability toward DCs.[4, 5] Furthermore, NPs enables co-delivery of immunosuppressive drugs with antigen for efficient induction of tolerogenic DCs.[6, 7] However, preparation of such multi-functional NPs is usually complicated and difficult to reproduce.

Previously, I reported simple preparation method of NP, in which mannan-coated protein aggregate was spontaneously formed by heat denaturation. Mannan was used to target DCs through C-type lectin receptors (mannose receptor (MR) and dendritic cell-specific intercellular adhesion molecule 3-grabbing non-integrin (DC-SIGN)) as well as to induce tolerogenic phenotype of DC.[5, 8, 9] Upon heating, antigenic protein and protein part of mannoprotein (MAN) are denatured to form core then the hydrophilic mannan chain is spontaneously exposed on the surface of NPs as a corona.[10] Then, disulfide bonds were formed by oxidation of cysteine residues inside the core to crosslink antigenic protein and MAN, which stabilized the structure of the NPs (Fig. 4.1a).[11] I succeeded in treating allergy model mice by using these NPs via oral and subcutaneous administration. In spite of the promising feature of our NPs, the

preparation method of NPs includes weakness. It requires relatively high concentration of antigenic protein enough to grow the aggregate size of a few hundred nanometers. Antigenic proteins are generally precious, and some proteins are colloidally unstable to prepare high concentrations.

To overcome the limitation of our preparation method of NPs, I proposed here utilization of proteinous matrix to incorporate precious antigen proteins in the core of NPs (Fig. 4.1a). I chose human serum albumin (HSA) as a proteinous matrix because it is non-antigenic for human and relatively inexpensive. In addition, aggregates of denatured HSA will allow to incorporate small molecular drugs as well as antigenic proteins via various interactions.[12] A free thiol group in Cys34 of HSA can help to stabilize the aggregates via disulfide bond.[13] In this study, I established the preparation of such NPs and evaluated the safety and T cell-activation efficiency of the NPs as the formulation of allergy immunotherapy.

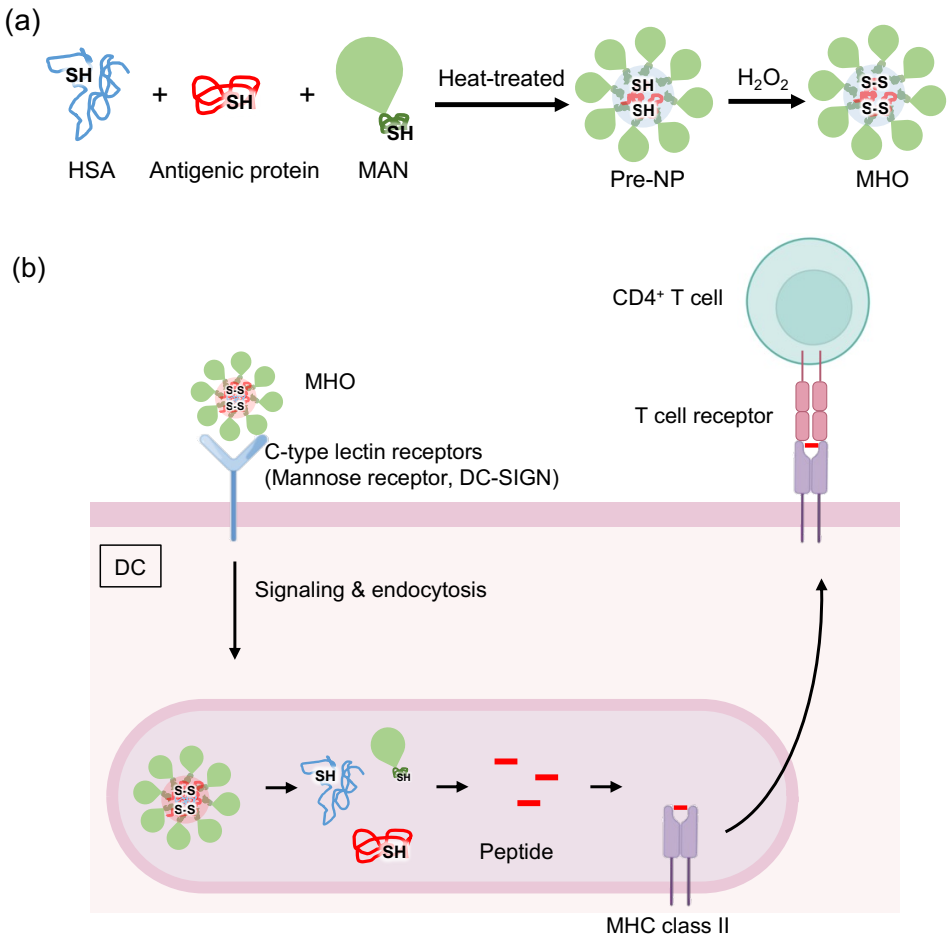

Fig. 4.1 (a) Preparation of MHO and (b) intracellular process of antigens targeted to C-type lectin receptors of DC. MHO binds to C-type lectin receptors and is internalized through endocytosis. MHO in the lysosomes is dissociated by reductase to cleave disulfide bonds[14]. The resulting peptides are loaded on MHC class II molecules and presented to $CD4^+$ T cells to induce regulatory T cells.

4.2 Results and discussion

4.2.1 Optimization of preparation conditions of NPs

First, the optimum condition for preparation of NPs from matrix HSA was screened. Due to the negative charge of HSA at neutral pH, aggregate of HSA is stably dispersed.[13, 15] HSA solution was heated at a specific temperature (65-85 ℃) up to 60 min. Then H_2O_2 was added for crosslinking of disulfide bonds. Size distribution and polydispersity indexes (PDI) of HSA NPs are summarized in Fig.4.2 and Table 4.1. The size of HSA NPs increased with heating temperature probably due to the progress of denaturation with temperature (Fig. 4.2). HSA is known to be denatured between 65 to 80℃.[16] I chose 85 ℃ for preparation because the complete denaturation is expected to enhance the aggregation. Addition of sodium chloride increase the size of aggregates probably due to the suppression of electrostatic repulsion (Fig. 4.2).[17] Since the excess sodium chloride destabilized NPs, 50 mM NaCl was selected as a suitable condition.

Table 4.1 Size and PDI of HSA NPs

Temp. (℃)	Time (min)	Solution	Concentration (mg/mL)	Size (nm)	PDI
65	5	10 mM PB + 50 mM NaCl	5	12.6 ± 0.1	0.25 ± 0.01
	10			14.7 ± 0.1	0.21 ± 0.01
	30			20.8 ± 0.2	0.21 ± 0.01
	60			23.9 ± 0.1	0.19 ± 0.01
75	5			24.2 ± 0.2	0.18 ± 0.01
	10			27.5 ± 0.1	0.15 ± 0.01
	30			32.8 ± 0.5	0.15 ± 0.01
	60			36.2 ± 0.5	0.15 ± 0.01
85	5			30.6 ± 0.3	0.16 ± 0.01
	10			34.3 ± 0.1	0.16 ± 0.01
	30			43.8 ± 0.3	0.15 ± 0.01
	60			52.8 ± 0.9	0.20 ± 0.01
85	5	10 mM PB	5	15.1 ± 0.1	0.14 ± 0.01
	10			16.8 ± 0.1	0.13 ± 0.01
	30			17.8 ± 0.1	0.10 ± 0.01
	60			18.8 ± 0.2	0.13 ± 0.01
	5	10 mM PB + 50 mM NaCl		31.1 ± 0.2	0.15 ± 0.01
	10			35.2 ± 0.2	0.15 ± 0.01
	30			45.2 ± 0.3	0.17 ± 0.01
	60			53.9 ± 1.0	0.19 ± 0.01
	5	10 mM PB + 150 mM NaCl		46.1 ± 0.3	0.16 ± 0.01
	10			69.9 ± 0.8	0.24 ± 0.02
	30			229.5 ± 3.8	0.47 ± 0.02
	60			603.3 ± 7.9	1.00 ± 0.04

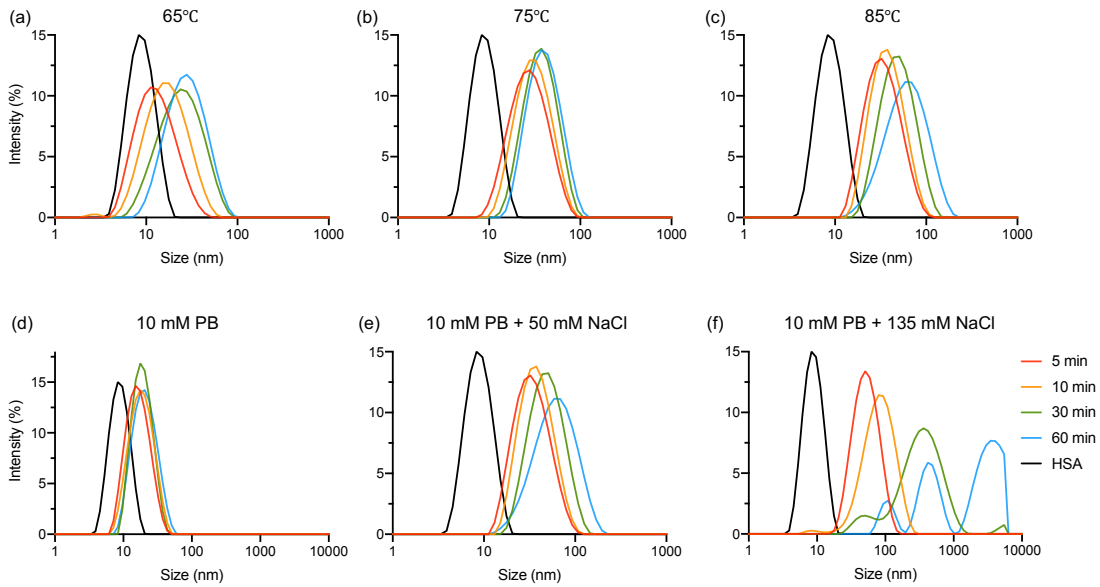

Fig. 4.2 Size distribution of HSA NPs. HSA NPs prepared at (a) 65℃, (b) 75℃ and (c) 85℃ for 5, 10, 30 and 60 min. HSA was 5 mg/mL and buffer was 10 mM PB + 50 mM NaCl. HSA NPs prepared in (d) 10 mM PB, (e) 10 mM PB + 50 mM NaCl and (f) 10 mM PB + 135 mM NaCl at 85℃ for 5, 10, 30 and 60 min. HSA was 5 mg/mL.

Subsequently, I examined the effect of mixing ratio of HSA with OVA for the aggregate formation. The mixing ratio was varied with constant total concentration (5.0 mg/mL). The size distributions of the prepared NPs (HO series) were unimodal with 50 nm size irrespective of the mixing ratio (Fig. 4.3a and Table 4.2). Almost quantitative conversion of two proteins to NPs were confirmed by the absence of the proteins in the filtrate of NP dispersions (Fig. 4.3d). These results indicates the compatibility of the two proteins will be due to the overlapping of denaturation temperature range of OVA with HSA; OVA is denatured between 70-80℃.[16, 18] After treatment by H_2O_2, remaining free thiol group was decreased (Table 4.2), indicating the formation of disulfide bonds in HO series NPs. SDS-PAGE of NPs also provided evidence for disulfide bonds formation (Fig. 4.3c). The bands of HO series NPs appeared near the loading wells without DTT treatment. In contrast, the DTT treatment dissociated NPs into component proteins, HSA and OVA. This revealed the presence of intramolecular disulfide bonds in the NPs.

Then, the effect of MAN addition to the preparation condition of HSA/OVA NPs was evaluated in which HSA/OVA ratio was fixed at 4:1. The obtained NPs (MHO series) showed increase in the particle size and PDI with the increase of MAN concentration (Fig. 4.3b and Table 4.2). The content of MAN in MHO which was quantified by phenol sulfuric acid method increased with the increase of MAN concentration (Table 4.2), indicating that incorporation of MAN into NPs was concentration dependent. Due to the hydrophilic nature of mannan part of MAN, mannan will coat the surface of NPs. I checked the storage stability of dispersion of MHO-10 in buffer (10 mM PB + 50 mM NaCl, pH 7.4) at 4 ℃. No size change was observed at least 28 days for storage (Fig. 4.3f).

The presentation of mannan on the MHO surface was demonstrated by

agglutination of MHO with *Con*A, a tetrameric lectin which possessing four binding sites for α-mannose. As shown in Fig. 4.3e, there was no change in the turbidity of HO after addition of *Con*A. In contrast, MHO showed increase of turbidity with *Con*A and the MHO with higher MAN content showed higher turbidity, which may result from the higher density of mannan on the surface of MHO-10 than MHO-5. Therefore, MHO-10 was used for subsequent studies.

Next, I tried to incorporate the immunosuppressant rapamycin in MHO-10. The loading was performed by simply mixing rapamycin (10 μg/mL = 10.9 μM) in the preparation system of MHO-10. I confirmed almost quantitative incorporation of rapamycin by HPLC analysis of remaining rapamycin in the filtrate of NP dispersion.

Table 4.2 Comparison of characteristics of different NP

	HSA (mg/mL)	OVA (mg/mL)	OVA ratio (%)	MAN (mg/mL)	Size (nm)	PDI	ζ-potential (mV)	Incorporation of MAN (%)	Thiol content (nmol/mg)	
									before	after
HO-0	5.0	-	-	-	52.8 ± 0.9	0.20 ± 0.01		-	3.6	2.3
HO-5	4.75	0.25	5		48.9 ± 1.1	0.18 ± 0.02	-16.9 ± 0.2		3.9	2.5
HO-10	4.5	0.5	10	-	49.2 ± 0.8	0.19 ± 0.01	-16.6 ± 0.1	-	4.1	2.4
HO-20	4.0	1.0	20		46.8 ± 1.3	0.19 ± 0.01	-16.6 ± 0.3		3.9	2.5
HO-50	2.5	2.5	50		52.1 ± 0.5	0.18 ± 0.01	-14.2 ± 0.1		8.8	2.1
MHO-0				-	52.3 ± 0.3	0.20 ± 0.01	-19.8 ± 0.2	-	-	-
MHO-5	4.0	1.0	20	5.0	79.4 ± 1.2	0.27 ± 0.02	-17.5 ± 0.1	46	-	-
MHO-7.5				7.5	99.8 ± 1.8	0.26 ± 0.01	-22.6 ± 0.2	61	-	-
MHO-10				10	123.1 ± 2.2	0.31 ± 0.01	-17.7 ± 0.2	78	4.2	2.8
MHCryj	4.5	0.5*	10*	10	110.3 ± 3.9	0.39 ± 0.02	-17.5 ± 0.5	72	-	-

* Cry j was used for preparation instead of OVA.

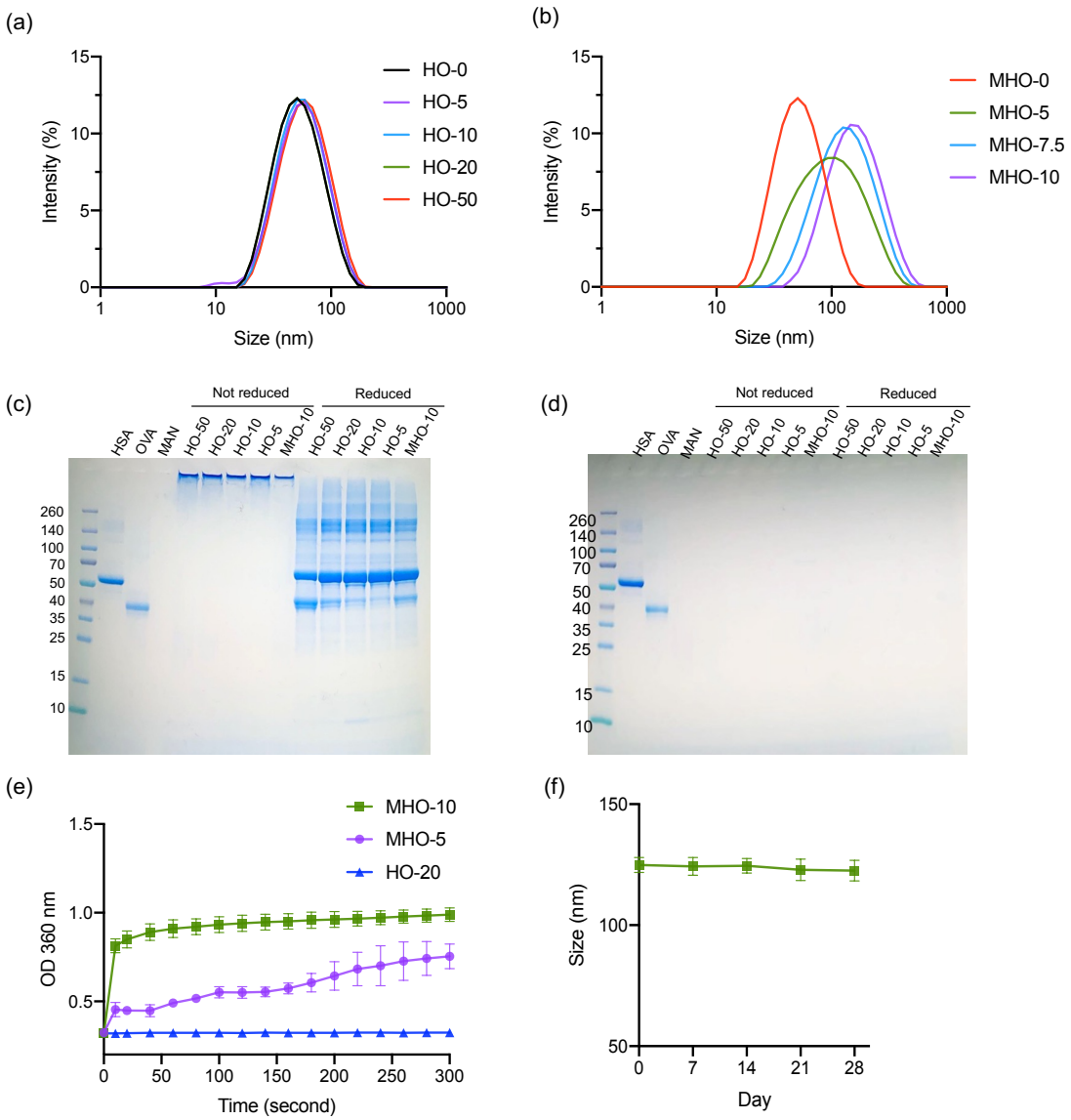

Fig. 4.3 (a) Effect of OVA loading and (b) MAN modification on size distribution of NPs. SDS-PAGE to confirm intermolecular disulfide bond. SDS-PAGE of (c) NPs and (d) filtrations. Each well is loaded with a sample equivalent to 2.5 μg OVA. MAN was not detectable by CBB staining. (e) Confirmation of mannan coating on the surface of NPs by *Con*A induced agglutination. (f) Stability of MHO-10 in buffer (10 mM PB + 50 mM NaCl, pH 7.4) at 4 °C. Data are expressed as the mean ± SEM (n = 3).

4.2.2 Application to Cry j for NP preparation

To verify the ability of MAN-coated HSA NP to integrate other antigen, I replaced OVA with Japanese cedar pollen antigen (a mixture of Cry j 1 and Cry j 2) which was used for AIT of Japanese cedar pollen. 4.5 mg/mL of HSA, 0.5 mg/mL of Cry j and 10 mg/mL of MAN were used to prepared MHCryj with the method described above. Although the size distribution of MHCryj is somewhat larger than MHO-10, it provided unimodal size distribution (Fig. 4.4a, Table 4.2). PAGE analysis of MHCryj showed that bands of Cry j and HSA were observed under reduced condition (Fig. 4.4b) and no bands were observed in the filtrate of MHCryj, indicating that almost quantitative incorporation of Cry j in MHCryj via disulfide bonds.

However, when I tried to incorporate human anti-CD20 IgG (~ 150 kDa) into the NP with the same condition with MHCryj (0.5 mg/mL of IgG), precipitate appeared in the solution (data not shown). Because denaturation temperature of IgG is lower (55-65℃) [19] than that of HSA, IgG made insoluble aggregate before denaturation of HSA. In contrast, Cry j has similar denaturation temperature (55-75 ℃) with HSA,[20] so the denatured Cry j was incorporated in HSA before precipitation. I speculated that there are two requirements for the successful incorporation of cargo proteins into HSA matrix. (1) Cargo proteins should have similar denaturation temperature as HSA. (2) Cargo proteins are better to keep solubility during heat denaturation to avoid phase separation with denatured HSA and MAN.

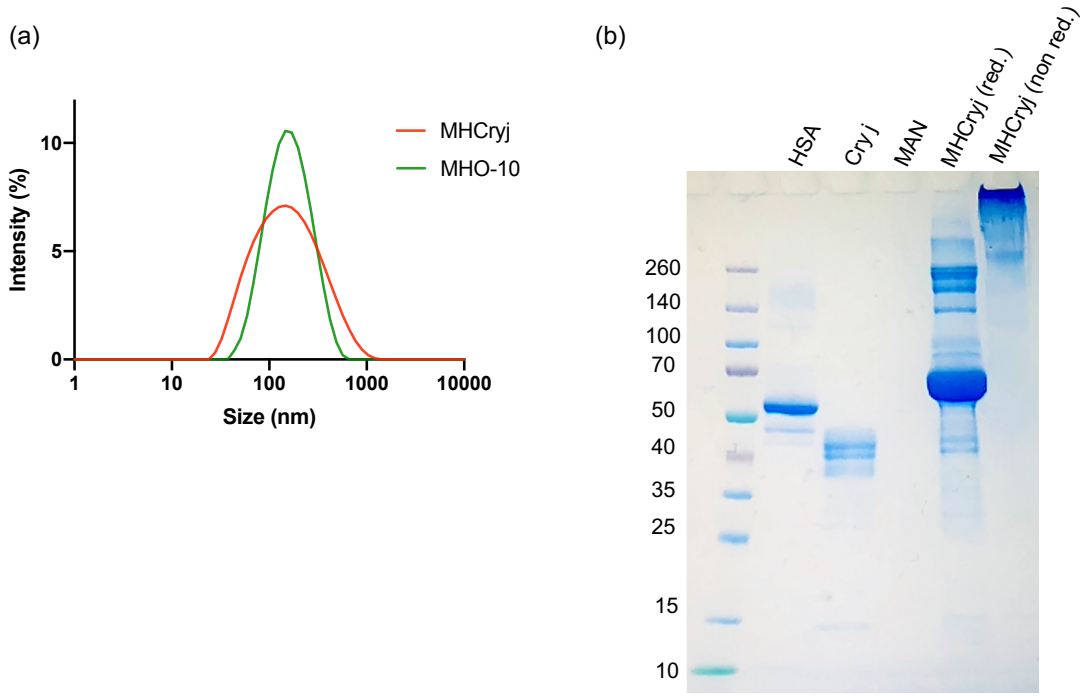

Fig. 4.4 (a) Size distribution of MHCryj and MHO-10. (b) SDS-PAGE of MHCryj. Cry j 1 is composed of three proteins (50 kDa, 30 kDa and 17 kDa), and Cry j 2 is composed of single protein (38 kDa).

4.2.3 Induction of tolerogenic DC and antigen-specific T cell activation

The targeting ability of MHO to BMDCs was estimated by flow cytometry. Here rhodamine-labelled OVA was used to prepare MHO. As shown in Fig. 4.5a, the fluorescence intensity of BMDCs was increased with time and BMDCs incubated with MHO-10 had stronger fluorescence than OVA and HO-20 at each time point. Observation of BMDCs by fluorescence microscopy at 4 hours of incubation showed bright fluorescence in cytosol especially in MHO-10 (Fig. 4.5b). These results indicated that formation of NPs improved the uptake efficiency by BMDCs, while the modification of MAN further improved the uptake level via targeting C-type lectin receptors on BMDCs. Therefore, MHO is expected to improve the delivery efficiency of antigen and drug to DCs *in vivo*.

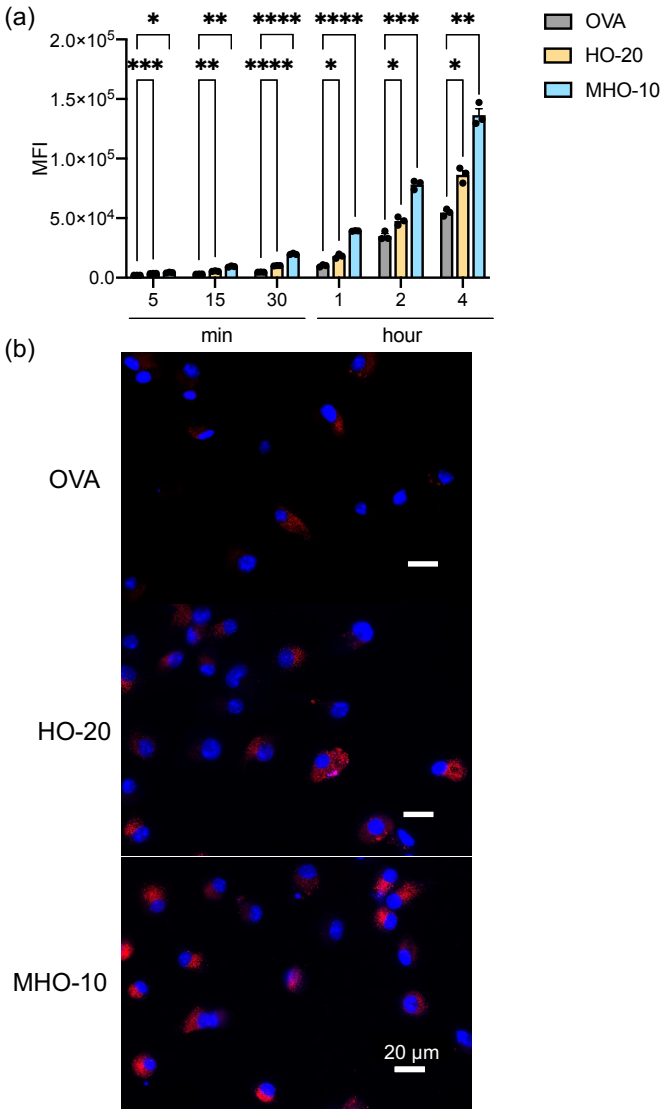

Fig. 4.5 Cellular uptake of NPs by BMDCs. Rhodamine labelled-OVA was used to prepare NPs. BMDCs were treated with OVA, HO-20 and MHO-10 at 37 °C. (a) Flow cytometry analysis of MFI of BMDCs after each incubation time. (b) Fluorescence microscope images of BMDCs after 4 h incubation. Blue and red colors represent nucleus and rhodamine, respectively. Data are expressed as the mean ± SEM (n = 3). *P < 0.05, **P < 0.01,***P < 0.001, ****P < 0.0001.

To evaluate whether the NPs have the effect of inducing tolerogenic DCs, I determined the phenotype changes of BMDCs after the incubation with NPs. As shown in Fig. 4.6, BMDCs stimulated with LPS expressed higher level of MHC class II (I-A^b), co-stimulatory factors CD80 and CD86, indicating the maturation of BMDCs. Treatment of BMDCs with OVA and HO-20 did not change the expression of these

three proteins significantly. In contrast, MHO-10 and especially MHO-10-R reduced the expression of the three proteins, which are the sign of tolerogenic phenotype of DC. Since both MAN[4] and rapamycin[21] induce the activation of nuclear factor-κB (NF-κB) via different pathways, MAN and rapamycin may synergistically work to induce tolerogenic DCs.

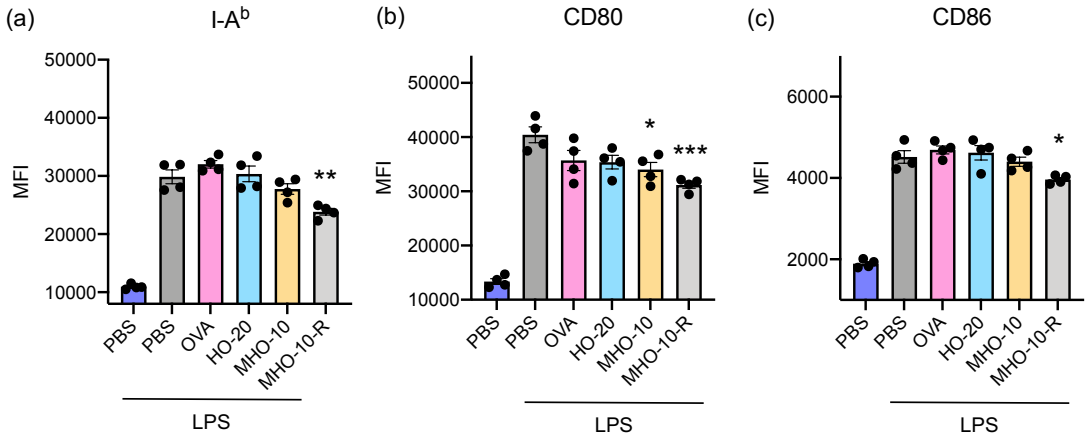

Fig. 4.6 Effect of MHO and MHO(Rapa) on the expression of BMDC surface molecules. BMDCs were incubated with 100 ng/mL LPS or PBS for 24 h, then treated with PBS, OVA or NPs for 24 h. Mean fluorescence intensity of (a) I-A^b, (b) CD80 and (c) CD86 on BMDCs. Significant difference between LPS(+)-PBS and the groups were compared. Data are expressed as the mean ± SEM (n = 4). *P < 0.05, **P < 0.01,***P < 0.001.

In the induction of antigen-specific tolerance, the antigen proteins should be degraded into peptides in DCs then the peptides were presented on the MHC class II and recognized by the T cell receptor (TCR) on T cells. Here I used OT-II CD4$^+$ T cells which has specific TCR for an OVA peptide/I-A^b complex to confirm antigen presentation and recognition. BMDCs were first pulsed with OVA, HO or MHO for 3 h, respectively, followed by the addition of OT-II CD4$^+$ T cells and incubation for 24 h. As shown in Fig. 4.7, level of IL-2 secreted from stimulated T cells was similar in the OVA and HO-treated groups, suggesting that disulfide crosslinking in HO was cleaved in lysosome to produce peptide fragments which are presented on BMDCs. In

the MHO-treated group, IL-2 concentration was significantly increased due to the efficient presentation of OVA peptides in BMDCs which was probably because of higher uptake efficiency of MHO by BMDCs, which was confirmed in Fig. 4.5. Collectively, MHO is an efficient carrier of antigens to BMDCs to enable the presentation of peptide with tolerogenic phenotype of BMDCs.

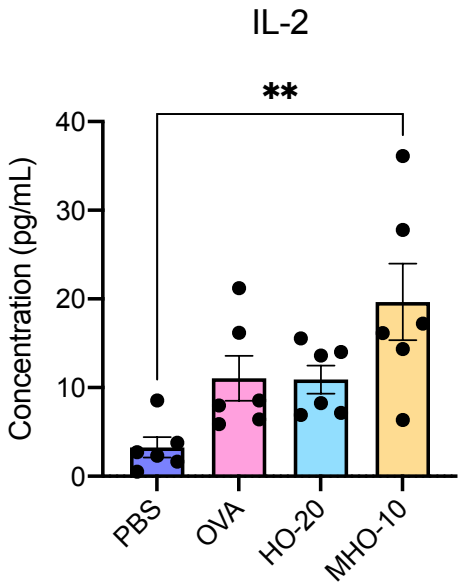

Fig. 4.7 Effect of MHO on MHC class II-restricted antigen presentation and OT-II T cell stimulation. Data are expressed as the mean ± SEM ($n = 6$). $^{**}P < 0.05$.

4.2.4 NPs eliminate OVA reactivity with anti-OVA antibodies

For *in vivo* application of NPs, I need to consider the safety of MHO. Therefore, I investigated the reactivity of HO and MHO with anti-OVA antibodies by ELISA. The anti-OVA antibodies were obtained from serum of mice in which OVA-specific allergy was induced. As shown in Fig. 4.8, HO-20 and MHO-10 showed much lower reactivity with anti-OVA antibodies than naked OVA and difference between these two NPs were not significant. This indicated that denaturation of OVA buried the surface IgE epitope inside the NP, reducing the antigenicity of OVA.[20] Further mannan coating might also mask the antigenicity of OVA.[22] Therefore, OVA may be used for allergy treatment without safety risk.

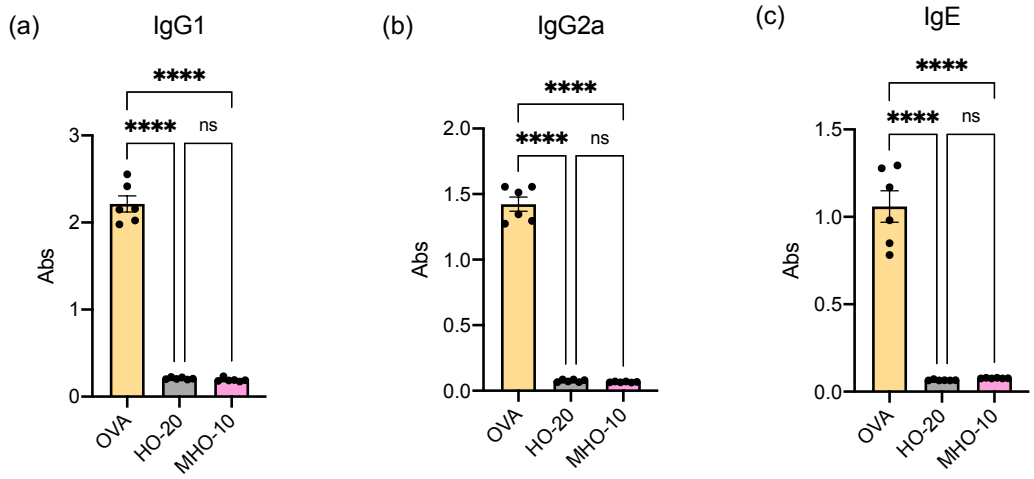

Fig. 4.8 Reactivity of OVA, HO and MHO toward anti-OVA antibodies evaluated by ELISA. Anti-OVA antibodies were collected from serum of immunized BLAB/c mice. Data are expressed as the mean ± SEM (n = 4). ****P < 0.0001, "ns" indicates no significant difference.

4.3 Summary

In this study, I proposed the utilization of HSA as a matrix to prepare antigen-HSA NPs coated with MAN. I found that matching of denaturation temperature between allergen proteins and HSA will be the requirement for the successful incorporation of allergen proteins into the core of NPs. Mannan coating enhanced uptake by BMDC and induced tolerogenic phenotype to activate T cells. Co-incorporation of rapamycin into the protein core enhanced the tolerogenic phenotype. The safety of the NP was demonstrated by the low reactivity with anti-OVA antibodies. The preparation method of MAN-coated antigen-HSA NPs proposed here will be applicable to various antigen proteins for efficient and safe AIT.

4.4 Experimental section

4.4.1 Materials

Human serum albumin (HSA), ovalbumin (OVA, grade V), mannan protein (MAN), rapamycin, concanavalin A (*Con*A), L-Cysteine and lipopolysaccharide (LPS, O111:B4) were purchased from Sigma-Aldrich (St. Louis, MO, USA). Japanese cedar pollen antigen (Cry j 1 and Cry j 2) was purchased from BioDynamics Laboratory Inc. (Tokyo, Japan). Hydrogen peroxide (H_2O_2, 30 wt % in water), sulfuric acid (98%, H_2SO_4), calcium chloride ($CaCl_2$), magnesium chloride hexahydrate ($MgCl_2$) and sodium chloride (NaCl) were purchased from FUJIFILM Wako Pure Chemical Corporation (Osaka, Japan). 2,2′-dinitro-5,5′-dithiodi-benzoic acid (DTNB) was purchased from Dojindo Laboratories (Kumamoto, Japan). 5(6)-Carboxytetramethylrhodamine N-succinimidyl ester was purchased from Thermo Fisher Scientific (Carlsbad, CA, USA). NuPAGE sample reducing agent (10×), NuPAGE LDS sample buffer (4×), ELISA-ELISPOT diluent (5×), TMB (3,3′,5,5′-tetramethylbenzidine) solution (1×), HRP-conjugated streptavidin (horseradish peroxidase) were purchased from Invitrogen (Carlsbad, CA, USA). QuickBlue staining solution was purchased from BioDynamics Laboratory Inc. (Tokyo, Japan). 4% paraformaldehyde solution (PFA), disodium hydrogen phosphate and sodium dihydrogen phosphate were purchased from Nacalai Tesque Inc. (Kyoto, Japan). Biotin anti-mouse IgE Antibody, biotin anti-mouse IgG1 Antibody, biotin anti-mouse IgG2a Antibody were purchased from BioLegend (San Diego, CA, USA).

4.4.2 Preparation of NPs

First, HSA NPs were prepared in various buffer (10 mM phosphate buffer containing 0, 50 and 135 mM NaCl (pH 7.4)), heating temperature (65, 75 and 85 ℃) and heating time (5, 10, 30 and 60 min). HSA was dissolved in buffer and was kept

overnight at 4 ℃. HSA dispersions were filtered with 0.22 μm membrane to remove aggregation. 1 mL of HSA solutions were heated in a water bath, then immediately cooled in an ice bath. Finally, added H_2O_2 to the NPs solution to a final concentration of 0.3 wt % and kept overnight at 4 ℃, in order to form disulfide bonds inside the NPs.[11] Free HSA and H_2O_2 were removed by ultrafiltration (100 kDa Amicon, Merck Millipore, Temecula, CA, USA), filtrate and NPs were used for further evaluation.

Similarly, the effect of HSA to OVA ratio (2.5:2.5, 4:1, 4.5:0.5 and 4.75:0.25 mg/mL) on the HSA-OVA NP (HO) and the effect of MAN concentration (0, 5, 7.5 and 10 mg/mL) were investigated. For rapamycin encapsulation, 10 μL of 1 mg/mL rapamycin was added to 1 mL of MAN, HSA and OVA mixing solution. In this part, the buffer to dissolve HSA, OVA and MAN was 10 mM PB + 50 mM NaCl (pH 7.4). Mixtures were heated at 85 ℃ for 60 min. H_2O_2 was added to the NPs solutions and kept overnight at 4 ℃. All the NPs were collected by ultrafiltration with 100 kDa filter, filtrate and NPs were used for further evaluation.

4.4.3 Size distribution and zeta potential

The size distribution and zeta potential of NPs were determined by dynamic light scattering spectrophotometer (DLS, Zetasizer Pro ZSU3200, Malvern, UK) at 25 ℃.

4.4.4 Quantification of the thiol group in NPs

Exposed thiol group was quantified using Ellman's regent.[23] Briefly, 5 μL of DTNB solution, 250 μL of 0.1 M PB containing 0.1 mM EDTA (pH 8.0) and 25 μL of samples were mixed and incubated at room temperature for 15 min, then measured absorbance at 412 nm on a plate reader (Infinite200PRO M Plex, Tecan, Switzerland).

4.4.5 MAN coating efficiency

200 μL of 5% (w/v) phenol was mixed with 200 μL of samples, then added 1mL of H_2SO_4. Mixtures were incubated for 40 min at room temperature and absorbance were measured at 490 nm.[24]

4.4.6 Rapamycin loading efficiency

Rapamycin was quantified by high performance liquid chromatography (HPLC) validated method using Elite Lachrom L-2455 diode array detector (Hitachi, Japan) on a Inertsil C_8 column (5μm, 4.6mm×150mm). The mobile phase changed within 20 min from 70% of methanol and 30% of milli-Q water to 90% of methanol and 10% of milli-Q water. Flow rate was 1.0 mL/min, injection volume was 20 μL, and the column oven temperature was set at 25℃. Photodiode array detection was used to detect rapamycin at the wavelength of 277 nm.

4.4.7 *Con*A agglutination assay

*Con*A agglutination assay was performed according to previously description.[25] Briefly, *Con*A was dissolved in phosphate buffered saline (PBS) containing 5 mM of $CaCl_2$ and 5mM of $MgCl_2$. 40 μL of samples were added to 200 μL of 1 mg/mL *Con*A solution. The turbidity were measured at 360 nm.

4.4.8 OVA loading efficiency determination and intermolecular disulfide bond conformation by SDS-PAGE

Denaturing SDS-PAGE was used to investigate formation of HO and MHO under reducing or non-reducing conditions. 2.5 μL of samples were mixed with 2.5 μL of 4×

LDS sample buffer. In reducing condition, 1 μL of 10× reducing agent and 4 μL of water were added, in non-reducing condition, 5 μL of water was added. Total 10 μL of mixtures were heated at 95 ℃ for 3 min. Samples were loaded into each lane and run electrophoresis. Proteins were detected by QuickBlue staining.

4.4.9 Investigation of universal applicability

To investigate the ability of HSA NP for delivery other antigenic proteins, I substituted OVA to Japanese cedar pollen antigen which is mixture of Cry j 1 & Cry j 2. Briefly, HSA and Cry j were dissolved in 10 mM PB + 50 mM NaCl buffer in ratio of 4.5:0.5 mg/mL, MAN was added to solution with final concentration of 10 mg/mL. Then heated at 85 ℃ for 60 min, cooled down on ice, and formed disulfide bonds by H_2O_2 administration. MAN-HSA-Cry j NP (MHCryj) was obtained after ultrafiltration.

4.4.10 Mice

C57BL/6J mice (7-8 weeks old, male) and BALB/c mice (7-8 weeks old, female) were purchased from Kyudo Co., Ltd. (Saga, Japan). Mice were fed with CE-2 (Kyudo Co., Ltd., Saga, Japan), with access to bedding and water. Cage changes were performed in a laminar flow hood. Mice had a cycle of 12 h of light and 12 h of darkness. OT-II Tg/wt, Ly5.1/Ly5.1 mice were obtained from Prof. Yoshihiro Baba. Animal experiments were performed according to the Guidelines for animal care and use committee, Kyushu University (A21-431, A21-425).

4.4.11 Isolation of bone marrow dendritic cells

Bone marrow cells were harvest from C57BL/6J mice. Bone marrow cells were cultured in advanced RPMI 1640 medium (Thermo Fisher Scientific, CA, USA)

containing 10% fetal bovine serum (FBS, Thermo Fisher Scientific, CA, USA), 50 μM 2-mercaptoethanol, 2 mM GlutaMAX™ Supplement (Thermo Fisher Scientific, CA, USA), 100 U/mL penicillin, 100 μg/mL streptomycin, 10 mM HEPES buffer solution (Nacalai Tesque Inc., Kyoto, Japan), 20 ng/mL recombinant mouse granulocyte–macrophage colony-stimulating factor (GM-CSF), 10 ng/mL recombinant mouse Interleukin-4 (IL-4) and 5 ng/mL recombinant mouse FMS-like tyrosine kinase 3 ligand (FLT-3L) for 6 days. Bone marrow dendritic cells (BMDCs) were obtained on day 6 after negative selection with biotin anti-mouse F4/80 and streptavidin nanobeads and positive selection with anti-mouse CD11c nanobeads (Biolegend, San Diego, CA, USA).

4.4.12 Cellular uptake of NPs

OVA was conjugated with NHS-rhodamine through amine group according to the manufacturer's instructions. OVA-rhodamine was used to prepare HO-20 and MHO-10.

To evaluate cellular uptake efficiency by flow cytometry, BMDCs were seeded in 12-well plates (3×10^6 cells/well), stimulated with 100 ng/mL LPS for 24 h. BMDCs were cultured with OVA, HO-20 and MHO-10 which were equally labeled with rhodamine for different times at 37℃. BMDCs were washed with PBS containing 2 mM EDTA, 10 mM HEPES and 2% FBS 2 times and stained dead cells with SYTOX™ Green (Thermo Fisher Scientific, MA, USA). Mean fluorescence intensity (MFI) of rhodamine in BMDCs was analyzed by flow cytometry (CyroFLEX-S, Beckman Coulter Inc., IN, USA).

For florescence microscope observation, BMDCs were seeded in 96-well plates (5×10^4 cells/well), stimulated with 100 ng/mL LPS for 24 h. Then incubated with rhodamine labeled OVA, HO-20 and MHO-10 for different times at 37℃. BMDCs were fixed with 4% PFA, and stained with Hoechst. BMDCs were observed by florescence microscope (BZ-X800, KEYENCE, Osaka, Japan).

4.4.13 Bone marrow dendritic cells phenotype analysis

BMDCs were seeded in 12-well plates (3×10^6 cells/well), stimulated with 100 ng/mL LPS for 24 h, then treated with PBS, OVA, HO-20, MHO-10 and MHO-10-R for 24 h. BMDCs were collected and blocked non-specific binding of immunoglobulin to the Fc receptors by anti-mouse CD16/32 antibody. Then, BMDCs were stained with anti-mouse I-A^b-FITC, CD86-APC, CD80-BV421 and propidium iodide (PI) (Biolegend, CA, USA). Subsequent analysis was performed on flow cytometry.

4.4.14 MHC class II-restricted OVA presentation

BMDCs were seeded in 96-well plates (5×10^4 cells/well) and stimulated with 100 ng/mL LPS for 24 h. BMDCs were pulsed with PBS, OVA, HO-20 and MHO-10 for 3 h, respectively. Then co-culture BMDCs and OT-II $CD4^+$ T cells (2.5×10^5 cells/well) for 24 h. OT-II $CD4^+$ T cells were isolated from spleenocytes of OT-II mice with Mouse CD4 T Cell Isolation Kit (Biolegend, San Diego, CA, USA). IL-2 concentration in the culture medium was determined by IL-2 Mouse ELISA Kit (Thermo Fisher Scientific, CA, USA).

4.4.15 Anti-OVA antibodies reactivity with NPs

BALB/c mice were sensitized with10 μg of OVA and 1 mg of alum in 200 μL of PBS through intraperitoneal (i.p.) injection at day 0, 7 and 14. Mice were sacrificed 7 days after last sensitization and peripheral blood was collected. Serum was collected from blood for later measurement.

Briefly, 100 μL of OVA, HO-20 and MHO-10 (as 100 μg/mL of OVA) were coated on 96-well plate. The plate was washed and blocked with 200 μL of ELISA-ELISPOT diluent. Diluted serum was added to the plate to detect OVA. The plate was washed and biotin anti-mouse IgE antibody, biotin anti-mouse IgG1 antibody and

biotin anti-mouse IgG2a antibody was added, respectively. The plate was washed and streptavidin-HRP was added. After washing, TMB solution was added. Finally, the reaction was stopped by 1 M phosphoric acid. Optical density (OD) of each well were measured at 450 nm.

4.4.16 Statistical analysis

Statistical analyses were performed using GraphPad Prism 9 (GraphPad Software, La Jolla, CA, USA). One-way ANOVA was used to determine the significance of means from all groups. Then the Tukey's multiple comparisons was used to compare every mean to every other mean. *$P < 0.05$, **$P < 0.01$,***$P < 0.001$, ****$P < 0.0001$.

4.5 References

1. M. H. Shamji and S. R. Durham, *J Allergy Clin Immunol*, 2017, **140**, 1485-1498.
2. D. M. Smith, J. K. Simon and J. R. Baker Jr, *Nature Reviews Immunology*, 2013, **13**, 592-605.
3. J. J. Ryan, H. R. Bateman, A. Stover, G. Gomez, S. K. Norton, W. Zhao, L. B. Schwartz, R. Lenk and C. L. Kepley, *J Immunol*, 2007, **179**, 665-672.
4. S. Sirvent, I. Soria, C. Cirauqui, B. Cases, A. I. Manzano, C. M. Diez-Rivero, P. A. Reche, J. Lopez-Relano, E. Martinez-Naves, F. J. Canada, J. Jimenez-Barbero, J. Subiza, M. Casanovas, E. Fernandez-Caldas, J. L. Subiza and O. Palomares, *J Allergy Clin Immunol*, 2016, **138**, 558-567 e511.
5. P. J. Tacken, I. J. de Vries, R. Torensma and C. G. Figdor, *Nat Rev Immunol*, 2007, **7**, 790-802.
6. R. A. Maldonado, R. A. LaMothe, J. D. Ferrari, A. H. Zhang, R. J. Rossi, P. N. Kolte, A. P. Griset, C. O'Neil, D. H. Altreuter, E. Browning, L. Johnston, O. C. Farokhzad, R. Langer, D. W. Scott, U. H. von Andrian and T. K. Kishimoto, *Proc Natl Acad Sci U S A*, 2015, **112**, E156-165.
7. S. H. Kim, J. H. Moon, S. U. Jeong, H. H. Jung, C. S. Park, B. Y. Hwang and C. K. Lee, *Int J Nanomedicine*, 2019, **14**, 5229-5242.
8. W. W. Unger and Y. van Kooyk, *Curr Opin Immunol*, 2011, **23**, 131-137.
9. E. E. Weinberger, M. Himly, J. Myschik, M. Hauser, F. Altmann, A. Isakovic, S. Scheiblhofer, J. Thalhamer and R. Weiss, *J Control Release*, 2013, **165**, 101-109.
10. J. Qi, P. Yao, F. He, C. Yu and C. Huang, *Int J Pharm*, 2010, **393**, 176-184.
11. Y. Wen, H. Dong, K. Wang, Y. Li and Y. Li, *ACS Appl Mater Interfaces*, 2018, **10**, 11457-11466.
12. M. R. Green, G. M. Manikhas, S. Orlov, B. Afanasyev, A. M. Makhson, P. Bhar and M. J. Hawkins, *Ann Oncol*, 2006, **17**, 1263-1268.
13. A. O. Elzoghby, W. M. Samy and N. A. Elgindy, *J Control Release*, 2012, **157**, 168-182.

14. B. Arunachalam, U. T. Phan, H. J. Geuze and P. Cresswell, *Proceedings of the National Academy of Sciences*, 2000, **97**, 745-750.
15. S. Yu, P. Yao, M. Jiang and G. Zhang, *Biopolymers*, 2006, **83**, 148-158.
16. R. Wetzel, M. Becker, J. Behlke, H. Billwitz, S. Böhm, B. Ebert, H. Hamann, J. Krumbiegel and G. Lassmann, *Eur J Biochem*, 1980, **104**, 469-478.
17. F. Zhang, M. W. A. Skoda, R. M. J. Jacobs, R. A. Martin, C. M. Martin and F. Schreiber, *The Journal of Physical Chemistry B*, 2007, **111**, 251-259.
18. B. P. Chay Pak Ting, Y. Pouliot, S. F. Gauthier and Y. Mine, in *Separation, Extraction and Concentration Processes in the Food, Beverage and Nutraceutical Industries*, ed. S. S. H. Rizvi, Woodhead Publishing, 2013, DOI: https://doi.org/10.1533/9780857090751.2.595, pp. 595-618.
19. A. W. Vermeer and W. Norde, *Biophys J*, 2000, **78**, 394-404.
20. R. Aoki, A. Saito, M. Usui, H. Azakami and A. Kato, *J Agric Food Chem*, 2009, **57**, 4995-4999.
21. T. Weichhart, M. Hengstschläger and M. Linke, *Nature Reviews Immunology*, 2015, **15**, 599-614.
22. M. Usui, A. Saito, N. Taniguchi, N. Nishijima, H. Azakami and A. Kato, *Biosci Biotechnol Biochem*, 2003, **67**, 2425-2430.
23. G. L. Ellman, *Archives of Biochemistry and Biophysics*, 1959, **82**, 70-77.
24. M. DuBois, K. A. Gilles, J. K. Hamilton, P. A. Rebers and F. Smith, *Analytical Chemistry*, 1956, **28**, 350-356.
25. Z. Cui and R. J. Mumper, *J Control Release*, 2002, **81**, 173-184.

CHAPTER 5 Conclusions

5.1 General conclusions

In the intestine, containing around 10^{14} microorganisms that live in symbiosis with their hosts and maintain a dynamic balance with hosts. When the original intestinal homeostasis is disrupted, dysbiosis and some immune disorders, such as allergies, may occur. Thus, maintaining intestinal homeostasis is important for health. In this thesis, I developed a method to prevent antibiotic-induced dysbiosis and a method to treat allergy via intestinal immune system.

In Chapter 2, I proposed an AER as a specific adsorbent of CEF *in vivo*. In this study, the AER showed higher affinity with CEF than sodium cholate due to π-π interactions. The AER was specific for CEF over biological molecules in the intestine, indicating better selective adsorption ability of the AER for CEF. This is important for specific adsorption of CEF in a complex *in vivo* environment and for reducing the risk of side effects associated with the adsorption of nutrients. Oral administration of the AER successfully protected the microbiota from destruction by CEF and maintained the signature of resistance toward *C. difficile* colonization. Thus, the AER will be a superior *in vivo* adsorbent of CEF because of its high specificity.

In Chapter 3, I developed an approach to prepare mannan-coated OVA NP that can target DCs without affecting OVA dissociation. Thermal aggregation of OVA and protein part of MAN formed core of NP and MAN presented on the surface of NP. Disulfide bonds that crosslinked OVA and MAN were dissociated in DCs and could be presented to T cells. MDO could target DCs and induce tolerogenic DCs. MDO showed high safety during administration to mice and preventive effect and therapeutic effect to allergic asthma through both oral and subcutaneous routes. Hence, I provided an effective and safe preventive and therapeutic strategy for allergy treatment.

In Chapter 4, I utilized HSA as a matrix to prepare MAN-coated antigen-HSA NPs based on the approach developed in Chapter 3. I found that cargo antigen requires a similar denaturation temperature similar with HSA and a low tendency to self-aggregate. Mannan coating enhanced endocytosis by DCs and showed potential to induce tolerogenic DCs, incorporation of immunosuppressant drug, rapamycin, in MHO induced tolerogenic DCs more effectively. Safety of MHO was confirmed. Hence, MAN-coated HSA NP is applicable to various antigens for efficient and safe AIT.

5.2 Perspective

In this thesis, I developed two kinds of materials to maintain immune homeostasis. The AER showed ability to prevent CEF-induced dysbiosis. MDO successfully induced tolerance to prevent and treat allergy. MHO also showed tolerance inducing efficiency *in vitro*. These findings will not only have the above mentioned applications, but will give us a wider application by improving the design of materials.

The AER is a commercial resin that can be used in medical applications. Even it showed better selectivity than AC, but it still a non-specific adsorbent. For specific adsorption, some natural antibiotic-specific ligand could be used to make NP, such as D-Ala-D-Ala-OH specifically binds to vancomycin.[1] For the antibiotics which do not have suitable ligand, synthetic ligands are also possible. Molecularly imprinted polymers have complementary cavities to the target molecules which provide high affinity and specificity.[2] Thus, molecularly imprinted polymers are potential candidates for prevention of antibiotics-induced dysbiosis.m

In Chapter 3, MDO induced tolerance and has therapeutic effect for allergy. Most importantly, although I have demonstrated that MDO can produce therapeutic efficiency to allergies, it still needs to be verified whether MDO treatment can produce memory T cells and maintain long-term duration for therapeutic effect. In mouse model, after immune tolerance has been established, mice can be challenged again with the

antigen 2-3 times over the following 1-12 months and evaluated the symptoms.[3] Furthermore, CTL receptors expressed on DCs are different in murine and human.[4] In order to apply MDO in the clinic, I need to confirm the induction of immune tolerance by MDO *in vitro* using human cells.[5] After *in vitro* confirmation of the ability of MDO to induce tolerance by using human cells, clinical comparisons of the efficacy of MDO versus conventional AIT should also be evaluated.

In Chapter 4, the universality of MAN-coated antigen HSA NPs was not fully demonstrated, and I need to evaluate whether NPs can incorporate a wider variety of antigens. MHO had been proved that could incorporate antigens and rapamycin. MHO-R had higher effect to induce tolerogenic DC *in vitro*. For different autoimmune diseases or allergies, I can change the antigen in MHO-R as well as the immunosuppressant (such as vitamin D3) to achieve the best therapeutic effect.[6] Therefore, I believe that MHO is a promising platform for the wide range of applications in the induction of immune tolerance.

5.3 References

1. K. Yuzuriha, K. Yakabe, H. Nagai, S. Li, T. Zendo, K. Zai, A. Kishimura, K. Hase, Y. G. Kim, T. Mori and Y. Katayama, *Biosci Microbiota Food Health*, 2020, **39**, 128-136.
2. J. J. BelBruno, *Chem Rev*, 2019, **119**, 94-119.
3. S. Tofukuji, K. Katayama, Y. Nakano, S. Ishida, J. Tsuchida, M. Tajiri, Y. Shimo, H. Tanaka and M. Shichijo, *J Allergy Clin Immunol*, 2018, **142**, 1977-1979 e1979.
4. P. J. Tacken, I. J. de Vries, R. Torensma and C. G. Figdor, *Nat Rev Immunol*, 2007, **7**, 790-802.
5. S. Sirvent, I. Soria, C. Cirauqui, B. Cases, A. I. Manzano, C. M. Diez-Rivero, P. A. Reche, J. Lopez-Relano, E. Martinez-Naves, F. J. Canada, J. Jimenez-Barbero, J. Subiza, M. Casanovas, E. Fernandez-Caldas, J. L. Subiza and O. Palomares, *J Allergy Clin Immunol*, 2016, **138**, 558-567 e511.
6. T. K. Kishimoto, J. D. Ferrari, R. A. LaMothe, P. N. Kolte, A. P. Griset, C. O'Neil, V. Chan, E. Browning, A. Chalishazar, W. Kuhlman, F. N. Fu, N. Viseux, D. H. Altreuter, L. Johnston and R. A. Maldonado, *Nat Nanotechnol*, 2016, **11**, 890-899.

Appendix

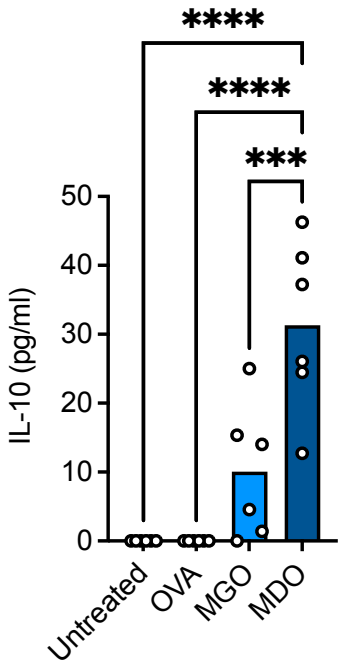

Fig. A1 IL-10 production from BMDCAs. BMDCs were isolated from C57BL/6J mouse as described in **3.4.9**. BMDCs were pulsed with PBS, OVA or NPs for 24 h then stimulated with 100 ng/mL LPS for 24 h. IL-10 concentration was determined by Mouse ELISA Kit. Data are expressed as the mean ± SEM (n = 6). *P < 0.05, **P < 0.01,***P < 0.001, ****P < 0.0001.

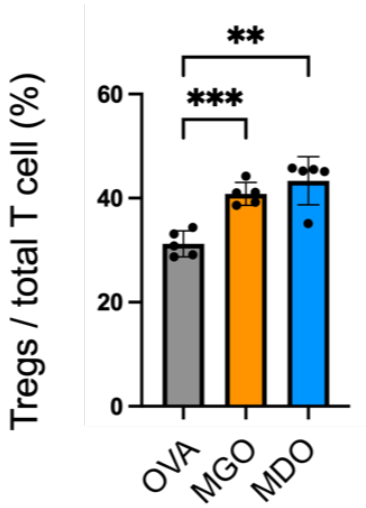

Fig. A2 Induction of T_{reg} cells. BMDCs were isolated from C57BL/6J mouse as described in **3.4.9**. BMDCs were pulsed with OVA, MGO and MDO for 24 h, respectively. Then stimulated with 100 ng/mL LPS for 24 h and co-cultured with $CD4^+$ naïve T cells. $CD4^+$ naïve T cells were isolated from OT-II Ly5.1/Ly5.1 $Foxp3^{hCD2}$ mouse. The proportion of T_{reg} cells in T cells was determined by flow cytometry. Data are expressed as the mean ± SEM (n = 5). *P < 0.05, **P < 0.01,***P < 0.001, ****P < 0.0001.

Achievement

List of publications

1. **Shunyi Li**, Kyosuke Yakabe, Khadijah Zai, Yiwei Liu, Akihiro Kishimura, Koji Hase, Yun-Gi Kim, Takeshi Mori, Yoshiki Katayama, Specific adsorption of a β-lactam antibiotic *in vivo* by an anion-exchange resin for protection of the intestinal microbiota, *Biomaterials Science*, 2021; **9**: 7219-7227.

2. **Shunyi Li**, Hiroki Toriumi, Daisuke Murakami, Daisuke Takahashi, Yiwei Liu, Jinting Li, Yoshiki Katayama, Koji Hase, Takeshi Mori, Mannan-coated antigen nanoparticles prepared by heat-induced self-assembly for oral allergen immunotherapy. (in preparation)

3. **Shunyi Li**, Hiroki Toriumi, Daisuke Murakami, Daisuke Takahashi, Yiwei Liu, Yoshiki Katayama, Koji Hase, Takeshi Mori, Preparation of mannan-coated antigen nanoparticles using human serum albumin as a non-antigenic proteinous matrix. (in preparation)

List of supplementary publications

4. Kazuki Yuzuriha, Kyosuke Yakabe, Haruka Nagai, **Shunyi Li**, Takeshi Zendo, Khadijah Zai, Akihiro Kishimura, Koji Hase, Yun-Gi Kim, Takeshi Mori, Yoshiki Katayama, Specific adsorption of a β-lactam antibiotic *in vivo* by an anion-exchange resin for protection of the intestinal microbiota, *Bioscience of Microbiota, Food and Health*, 2020; **39**: 128-136.

5. Kazuki Yuzuriha, Ayaka Yoshida, **Shunyi Li**, Akihiro Kishimura, Takeshi Mori, Yoshiki Katayama, Synthesis of peptide conjugates with vitamins for induction of antigen-specific immunotolerance, *Journal of Peptide Science*, 2020; **26**: e3275.

List of presentations

1. Protection of mice from *Clostridium difficile* infection by protecting gut microbiome with antibiotic capturing ion-exchange resin. The 24th Joint Seminar of the Kyushu Branch of the CSJ and the Busan Branch of KCS. Kumamoto, Japan, June, 2019. **(poster presentation)**

2. Antibiotics capturing ion-exchange resin to protect gut microbiome of mice. 56th the Annual Meeting of the Japan Society for Bioscience, Biotechnology, and Agrochemistry, Kyushu Branch. Kitakyushu, Japan, July, 2019. **(poster presentation)**

3. Microbiome protection to avoid *Clostridium difficile* infection by using antibiotic capturing ion-exchange resin. The 35th Annual Meeting of the Japan Society of Drug Delivery System. Yokohama, Japan, July, 2019. **(poster presentation)**

4. Gut microbiome protection by using antibiotic capturing ion-exchange resin. 2nd GLowing Polymer Symposium in KANTO. Tokyo, Japan, November, 2019. **(oral presentation)**

5. Microbiota protection from β-lactam antibiotic by using ion-exchange resin. The 37th Annual Meeting of the Japan Society of Drug Delivery System. Chiba, Japan, June, 2021. **(poster presentation)**

6. Gut microbiome protection by using antibiotic capturing ion-exchange resin. The 69th Annual Meeting of the Society of Polymer Science. Fukuoka, Japan, May, 2021. **(oral presentation, cancelled)**

7. Specific adsorption of a β-lactam antibiotic *in vivo* by an anion-exchange resin for protection of the intestinal microbiota. The 43rd Annual Meeting of the Japanese Society for Biomaterials & 8th Asian Biomaterials Congress. Nagoya, Japan, November, 2021. **(oral presentation)**

Acknowledgment

Before I started writing this thesis, I was happy that my doctoral career was finally coming to an end. But with the completion of thesis, I felt lost. On the one hand, part of the experiments are still in progress and the thesis is not presented in its fullest form, and on the other hand, this means that status is about to change. But the completion of the thesis is a happy thing, after all. This is a summary of my past work and some of my own thoughts, which I hope will be an inspiration to my fellow traveler and a reference for future researchers.

Looking back on the five and half years of studying and living at Kyushu University, I can say that studying abroad has indeed shown me something different. I think this experience will also shape me on conduct oneself.

Completion of this research and dissertation could not be achieved without the assistance, cooperation and understanding of multiple people.

First and foremost, I would like to express my gratitude to my supervisor, Professor Yoshiki Katayama for his continuous support. His insight and immense knowledge into the subject matter steered me through this research.

Associate Professor Takeshi Mori, who guided me throughout this project. Without his assistance and dedicated involvement in every step throughout the process, these papers would have never been accomplished. I would like to thank you very much for your support and understanding over these past five and half years.

I would like to express my thanks to Associate Professor Akihito Kishimura for his valuable advices during presentations.

I am deeply grateful for the collavorative assistance of Professor Yun-Gi Kim, Professor Koji Hase, Lecturer Daisuke Takahashi, Lecturer Daisuke Murakami, Mr. Kyosuke Yakabe and Mr. Hiroki Toriumi. They provided me with their knowledge and they supported me in cell and animal experiments. It was really influential in shaping my experiment methods and critiquing my results.

I am grateful to Professor Yoshihiro Baba for providing me with experimental mice, which played an important role in my research hypothesis.

I wish to extend my special thanks to my group members, Dr. Khadijah Zai, Dr. Kazuki Yuzuriha, Dr. Yunmei Mu, Dr. Yiwei Liu, Ms. Haruka Nagai, Ms. Matsuo Kurumi, Ms. Yee Ying Chuin, Mr. Takanatsu Hosokawa, especially thanks to Ms. Jinting Li for her experimental assistance. It is their kind help and support that have made my study and life in Kyushu University a wonderful time.

I am also grateful to Ms. Mari Miyazaki for her considerate guidance and support in office matters.

I would like to express my sincere thanks to my doctoral thesis committee members, Professor Masahiro Goto, Professor Yun-Gi Kim, Professor Yoshiki Katayama and Associate Professor Takeshi Mori for their time and invaluable advice on my thesis project.

I really appreciate to the Grant-in-Aid for Japan Society for the Promotion of Science (JSPS) Research Fellow and Grants-in-Aid for Scientific Research from the JSPS, which support me through my research and life at Kyushu University.

More importantly, I would like to thank my friends and family members who supported me. Thanks to my dog named Ray, who give me a lot of emotional comfort. Without their tremendous understanding and encouragement in the past few years, it would be impossible for me to complete my study.

Shunyi Li

Kyushu University

January, 2023